Environmental Research & Technology

YEAR : 2018 | VOLUME : 01 | ISSUE : 04

e-ISSN: 2636-8498

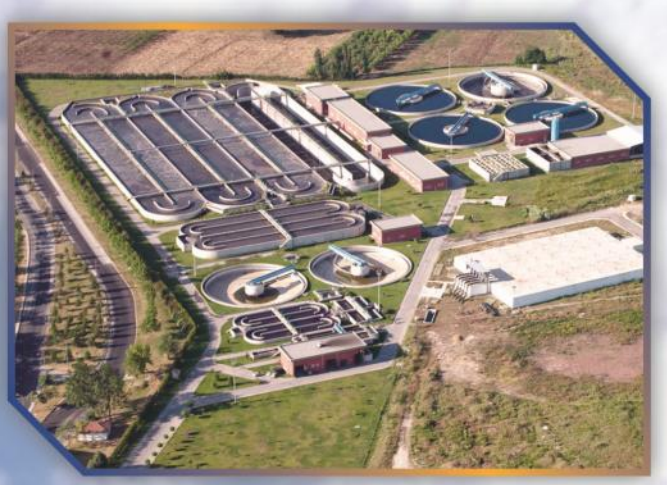

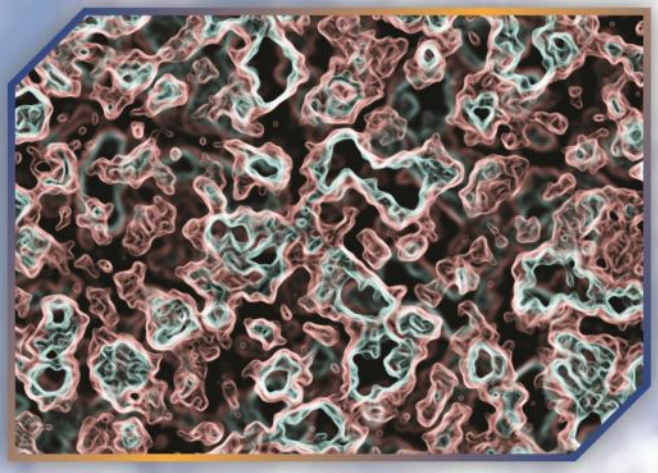

Environmental Research & Technology

http://dergipark.gov.tr/ert

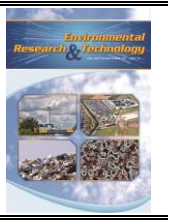

ACADEMIC ADVISORY BOARD

Prof. Dr. Adem Basturk

Prof. Dr. Mustafa Ozturk

Prof. Dr. Lutfi Akca

Prof. Dr. Oktay Tabasaran

Prof. Dr. Ahmet Demir

SCIENTIFIC DIRECTOR

Prof. Dr. Ahmet Demir (Yildiz Technical University)

EDITOR IN CHIEF

Prof. Dr. Mehmet Sinan Bilgili (Yildiz Technical University)

ASSISTANT EDITOR

Dr. Hanife Sari Erkan (Yildiz Technical University)

CONTACT

Yildiz Technical University
Environmental Engineering Department, 34220 Esenler
Istanbul – Turkiye
Web: http://dergipark.gov.tr/ert/
E-mail: ert@yildiz.edu.tr

Environmental Research & Technology

http://dergipark.gov.tr/ert

Environmental Research & Technology

http://dergipark.gov.tr/ert

Editorial Board

Environmental Research & Technology

http://dergipark.gov.tr/ert

TABLE OF CONTENTS

Title	*Pages*
Conference Papers	
Removal of Cu (II) from wastewater of metal coating process by borax sludge *Esma Burcu Rona, Meral Yildirim Ozen, Emek Moroydor Derun*	1-5
Decolorization of Reactive Orange 16 and Reactive Black 5 in aqueous solution by ozonation *Irem Onder, Okan Aydin, Afife Guvenc*	6-13
Comparative analysis on practical implications and evaluation of PVC geomembrane interfaces against particulate materials *Tanay Karademir*	14-21
Recycling posibilities of packaging wastes - the case of Kırıkkale *Oylum Gokkurt Baki, Ozan Parlak*	22-26
Characterization and optimization of palm industry ash waste (PIAW) derived zeolites using central composite cesign (CCD) *Said Nurdin, Syafiqah A. Khairuddin, Hajar Athirah M. Sukri, Chuah C. Wooi*	27-33
Life cycle assessment of an office: Carbon footprint of an office staff *Nilay Cambaz, E. Gamze Taskin, Ali Ruzgar*	34-39
Adsorption of Remazol Brilliant Blue R by raw and carbonized macroalgal wastes *Anil Tevfik Kocer, Benan Inan, Didem Ozcimen*	40-46
Pyrolysis of walnut shell biomass in fluidized bed reactor: Determination of optimum conditions for bio-char production *Zeynep Yildiz, Selim Ceylan*	47-51

Environmental Research & Technology, Vol. 1(4), pp. 1-5, 2018

Environmental Research & Technology

http://dergipark.gov.tr/ert

CONFERENCE PAPER

Removal of Cu (II) from wastewater of metal coating process by borax sludge

Esma Burcu Rona[1], Meral Yildirim[2], Emek Moroydor Derun[*,2]

[1]Istanbul Water and Sewerage Administration (ISKI) 34060 Eyup/Istanbul, TURKEY
[2]Yildiz Technical University Chemical Engineering Department, 34220 Esenler, Istanbul, TURKEY

ABSTRACT

The aim of this study is to determine the adsorption behavior of borax sludge for removal of copper from industrial wastewater. The borax sludge was generated during borax production and used for treatment of wastewater of metal coating process. The parameters of pH, concentration and contact time were investigated in batch experiments to determine the efficiency of adsorption. Inductively Coupled Plasma-Optical Emission Spectrometer (ICP-OES) was used to calculate the reduced amount of Cu (II). The results were applied to various kinetic models and adsorption isotherms. The pseudo second order model was successful to fit the adsorption process in the kinetic study because the regression coefficient values (R^2) were changed between 0.9995 and 0.9978. Langmuir (R^2=0.9985) and Temkin (R^2=0.9985) isotherms models were the best to explain the process.

Keywords: Adsorption, borax sludge, heavy metal, wastewater treatment

1. INTRODUCTION

Heavy metal ions in the exit water of different industries like electroplating, smelting, mining, petroleum and chemical industries cause soil and water related pollution effects to the environment. Even if they found in low amounts in the ecosystem, they cause severe damages [1]. In order to prevent industrial heavy metal contamination, the wastewater must be treated before being discharged to the receiving environment and the heavy metal concentrations contained in the contents must be reduced to the discharge limits specified in the laws and regulations. Heavy metal removal from industrial wastewater at high concentration levels is mainly carried out using purification methods such as chemical precipitation, reduction/oxidation, reverse osmosis, membrane filtration, ion exchange, neutralization, evaporation and adsorption [2-4].

Copper is one of the threatening heavy metal that excessive intake of it leads to serious toxicological consequences such as vomiting, cramps, convulsions and death in living bodies [5]. To remove of copper ions from aqueous solution effectively, precipitation [6], ion exchange [7], electrochemical separation [8] and adsorption methods [9] have been used. Compared to the other methods adsorption has many advantages that needs very low concentrations, easy handling and has continuous processes with the possibility of regeneration [10], while the others need excessive time requirements, high cost and high energy consumption [11].

In literature there are many studies about removal of copper from aqueous solutions among many low cost adsorbents like montmorillonite [12], kaolinite [13], illite [14], palygorskite, sepiolite [15], dolomite [16] and calcite [17].

As studies going on finding low cost adsorbents; using waste materials as adsorbents has also extra advantages on removal of heavy metals. For instance in Turkey 600.000 tons of boron waste causes an important waste problem [18]. As the consumption of boron increase, the waste boron amount will also increase in the future. Thus, using waste boron for waste removal is a unique approach. In published literature, boron waste has been used as an adsorbent in adsorption studies for dye, cadmium (II), zinc (II) [19-20] and chromium [18]. Although there are studies on copper adsorption with different

Corresponding Author: moroydor@yildiz.edu.tr (Emek Moroydor Derun)
Received 31 May 2018; Received in revised form 7 September 2018; Accepted 14 September 2018
Available Online 16 October 2018
Doi: ISSN: 2636-8498

This paper has been presented at EurAsia Waste Management Symposium 2018, Istanbul, Turkey

adsorbents, adsorption using boron waste has not been studied yet.

The aim of this work is to research the feasibility of using borax sludge as a low cost adsorbent for copper adsorption. The adsorption behavior of borax sludge was examined with various parameters such as pH, contact time and initial Cu (II) concentration and experimental data has been applied to different kinetic and isotherm models.

2. MATERIALS AND METHOD

2.1. Raw Material Preparation

Borax sludge was taken from Eti Mine Bandırma Boron Works (Balıkesir, Turkey). Before the sludge was used in experimental runs, in order to decrease the moisture content, it was dried at 105 °C for 2 hours in an incubator (Ecocell 111, Germany). The dried adsorbent was milled with an agate mortar and sieved with a vibrating screen- shaker (Fritsch, Germany) so its particle size was decreased below 90 µm. The XRD pattern of the borax sludge (Fig 1) showed the main components were dolomite ($CaMg(CO_3)_2$) and tincalconite ($Na_2B_4O_7{\cdot}5H_2O$) with powder diffraction file (pdf) numbers of 00-005-0622 and 00-008-0049.The BET surface area of borax sludge was 5.54 $m^2\ g^{-1}$ [18].

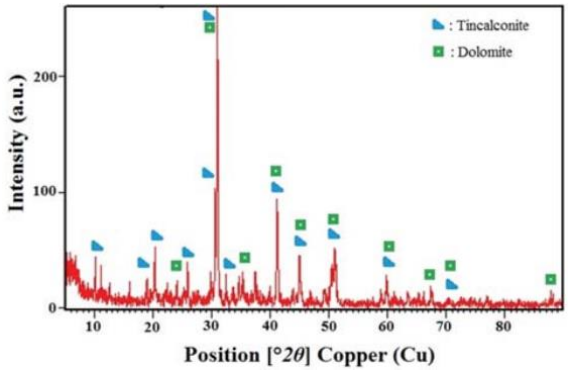

Fig 1. XRD pattern of borax sludge [18]

The wastewater was taken from the inlet water line of a wastewater treatment facility in the Ikitelli Organized Industrial Zone where wastewater from metal coating industries' is collected. The heavy metal content of the wastewater was Cu, Cr, Ni, Al, Cd, Zn, Pb etc. In this study, only removal of Cu was taken into account. Sodium hydroxide (NaOH), which was used to adjust the pH, was supplied Merck Chemicals.

2.1 Adsorption Experiments

The experiments were done with different pH values, initial Cu (II) concentrations and adsorption times at room temperature. Firstly, adsorption experiments were done with various pH values (pH 3, pH 5, pH 7 and pH 9) to determine the effect of pH on the adsorption.0.2 g borax sludge was added at each 100 mL wastewater and stirred with the speed of 200 rpm. After determination the optimum pH value, for the isotherm studies the same amount of borax sludge was added to the same amounts of wastewater with 3 different concentrations (75, 50 and 45 ppm Cu (II) containing) and the experiments were carried out for 6 different contact times (15-120 min). At the end of each adsorption period, the adsorbents were filtered through 110 mm Ø filter paper (Blue ribbon, Chmlab) and the residual Cu (II) concentration was analyzed by an Inductively Coupled Plasma-Optical Emission Spectrometer (ICP-OES) (Optima DV 2100, Perkin Elmer, USA).

Amount of Cu (II) removed from the solutions by the borax sludge was calculated from the decrease of metal concentration in the solutions by using the expression in Eq. 1:

$$q = \frac{C_i - C_f}{\mathrm{m}} \times \mathrm{V} \qquad (1)$$

where q is the removal capacity of the adsorbent at equilibrium (mg g^{-1}), V is the volume of the suspension (mL), m is the weight of adsorbents (g), C_i and C_f are the initial and final concentrations of Cu (II)(mg L^{-1}), respectively [18].

2.2. Kinetic Models

Parameters from two kinetic models, pseudo first-order (Eq. 2) and pseudo second-order (Eq. 3), were fitted to experimental data to examine the kinetics of copper uptake by the samples. The pseudo first-order model [18] equation is given as follow:

$$\mathrm{q_t} = \mathrm{q_e}\,(1 - \exp(-\mathrm{k_1\,t})) \qquad (2)$$

The pseudo-second-order model [21] equation is given as:

$$\mathrm{q_t} = \frac{\mathrm{k_2\,q_e^{\,2}\,t}}{1+\mathrm{k_2\,q_e t}} \qquad (3)$$

where, q_t is the removal capacities (mg g^{-1}) at time t, k_1 is the pseudo first-order model rate constant in min^{-1} and k_2 is the pseudo-second order adsorption rate constant in g mg^{-1} min^{-1}.

2.2 Isothermal Models

The Langmuir isotherm considers that the adsorption takes place on homogenous surfaces with negligible interaction between adsorbed molecules. The linear form of the Langmuir isotherm model [22] is described as (Eq. 4):

$$\frac{C_e}{q_e} = \frac{1}{q_m K_L} + \frac{C_e}{q_m} \qquad (4)$$

where q_e (mg g^{-1}) is the adsorbed Cu(II) per unit mass of adsorbent, q_{max} is the maximum adsorption capacity of adsorbent (mg g^{-1}), C_e is the equilibrium concentration of Cu(II) (mg L^{-1}) and K_L is the Langmuir constant related to the affinity of the binding sites.

The Temkin isotherm model (Eq. 5 and Eq. 6) that explains the influences of some indirect interactions between adsorbent and adsorbate is represented as;

$$\mathrm{q_e} = \mathrm{B_T ln A_T} + \mathrm{B_T ln C_e} \qquad (5)$$

$$\mathrm{B_T} = \frac{\mathrm{RT}}{\mathrm{b_T}} \qquad (6)$$

where B_T is the Temkin constant related to the heat of adsorption(Kj mol^{-1}), A_T is the equilibrium binding

constant, R is the gas constant (8.314 J mol^{-1} K^{-1}), T is the temperature (K) and b_T is the Temkin isotherm constant [18].

Harkins-Jura isotherm model explains the possibility of multilayer adsorption with the existence of heterogeneous pore distribution. The Harkins-Jura isotherm model can be expressed by Eq. (7) where B_H and A_H are the Harkins-Jura constants [23].

$$q_e = \sqrt{\frac{A_H}{\log C_e + B_H}} \quad (7)$$

3. RESULTS & DISCUSSION

The adsorption experiments were carried out with different pH values to decide the best pH value for the further experiments. Because pH directly affects the surface charge of the adsorbent. Results showed that the adsorption of Cu (II) ions onto borax sludge is pH dependent and suggested that highest removal efficiency was observed at pH range of 7-9 (Fig 2). Depend on the obtained results, pH=7 was chosen for all the experiments.

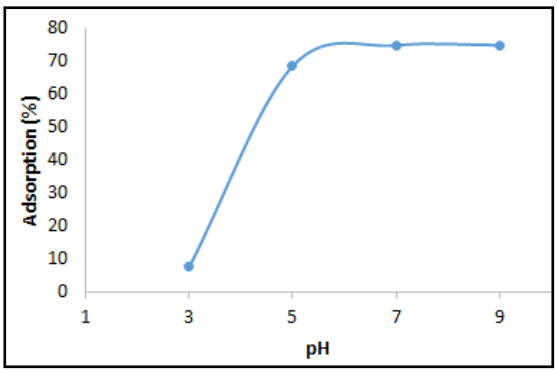

Fig 2. Adsorption percentage of Cu (II) ions for different pH values

Fig 3 shows the effects of contact time the adsorption of Cu (II) ions. As seen in the Fig 3, Cu (II) ions were adsorbed onto the borax sludge very rapidly within the first 15 min and the equilibrium was attained after 30 min.

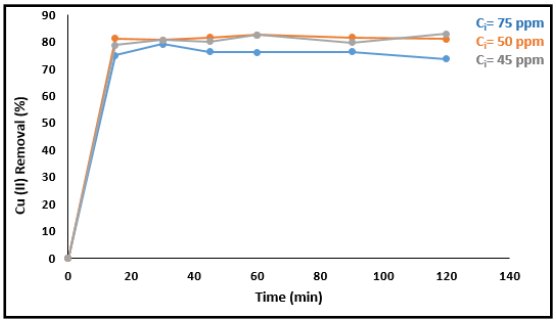

Fig 3. Removal percentage of Cu (II) ions for different contact times

Langmuir, Temkin and Harkins-Jura models were employed to describe the experimental data and results are revealed in Table 1. It is apparent from Table 1 that all the isotherms provide a good fit to the experimental results. The applicability of the all the applied isotherm models can be reasoned by the complex adsorption process between Cu (II) and borax sludge which can involve more than one mechanism.

Table 1. Isotherm parameters for Cu (II) removal by borax sludge

Isotherms	Parameters	R^2
Langmuir	K_L= 0.0337 q_{max}= 90.90 mg/g R_L= 0.2829	0.9985
Temkin	B_T= 24.528 A_T= 0.1131 b_T= 101.01	0.9985
Harkins-Jura	B_H= 1.3621 A_H= 172.414	0.9817

The essential characteristics of Langmuir isotherm can be explained by the constant separation factor (R_L) which was calculated according to Eq. (8).

$$R_L = \frac{1}{1+K_L C_i} \quad (8)$$

In the present study, R_L value was found as 0.2829 which was between $0<R_L<1$ and showed that adsorption process was favourable and borax sludge exhibited a good potential for Cu (II) removal. Also, the maximum Cu (II) adsorption capacity of borax sludge was found as 90.90 mg g^{-1}.

In Table 2, the comparison of maximum adsorption capacity (q_{max}) of Cu (II) for Langmuir model of previous studies in literature is given. As seen in Table 2, various low cost adsorbents and their activated forms were used for Cu (II) removal. When the borax sludge was compared with other adsorbents given in Table 2, it clearly seen that satisfying q_{max} value was obtained for borax sludge which was an industrial waste and not processed by an activation method.

Table 2. Previous studies using different adsorbents for removal of Cu (II)

Adsorbent	q_{max} (mg g^{-1})	References
CH_3COONa-intercalated halloysite	52.3	[24]
Chitosan-clay nanocomposites	181.5	[25]
Cationic surfactant modified bentonite	50.76	[26]
Sugarcane Bagasse (Citric Acid activated)	96.90	[27]
Bentonite	33.44	[28]
Acid activated bentonite	38.31	[28]
Borax sludge	90.90	present study

Different kinetic models were applied to the experimental data and the highest regression coefficients (R^2) were obtained for pseudo second

order kinetics which indicated the applicability of this kinetic model. Depend on the pseudo-second order kinetic equation, this adsorption is mainly controlled by the surface [18]. Fig 4 shows the pseudo second order plots for the experimental sets in which different initial Cu (II) concentrations were used. The pseudo-second-order rate constant (k_2), the calculated and experimental q_e values are given in Table 3. It was observed that the rate constant showed irregular change by increasing initial concentration. Also, the calculated and experimental qe values were showed similarity which indicated that the pseudo-second-order model can be applied to the Cu (II) removal by borax sludge [29].

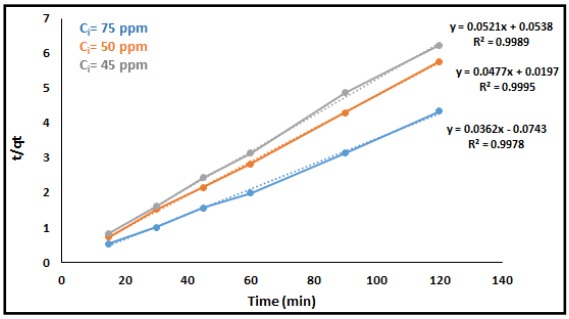

Fig 4. Adsorption kinetics of Cu (II) onto borax sludge for pseudo second-order kinetic model

Table 3. The second-order rate constants and q_e values

C_i (ppm)	q_e (mg g^{-1}) (experimental)	q_e (mg g^{-1}) (calculated)	k_2
75	30.14	27.62	0.01764
50	21.19	20.96	0.1155
45	19.14	19.19	0.0505

4. CONCLUSIONS

An industrial waste of borax sludge was used to remove Cu (II) ions from wastewater of metal coating process. Various experimental parameters such as pH, contact time and initial metal concentration were studied at a constant temperature of 25 °C. According to studies, the optimum pH was determined as 7. Many adsorption isotherms and kinetic models were applied to the obtained results. Experimental results are in good agreement with Langmuir, Temkin, and Harkins-Jura adsorption isotherm models. The adsorption of Cu (II) was fitted to pseudo-second order equation with good correlation. In conclusion, borax sludge can be an effective adsorbent for wastewater treatment with the Cu (II) adsorption capacity of 90.90 mg g-1.

ACKNOWLEDGEMENT

Authors thank to Istanbul Water and Sewerage Administration (ISKI) for ICP-OES analyses.

REFERENCES

[1]. K. G. Bhattacharyya and S. S. Gupta, "Removal of Cu (II) by natural and acid-activated clays: an insight of adsorption isotherm, kinetic and thermodynamics," *Desalination*, Vol. 272, 66–75, 2011.

[2]. O. Yavuz, Y. Altunkaynak and F. Guzel, "Removal of copper, nickel, cobalt and manganese from aqueous solution by kaolinite," *Water Research*, Vol. 37, 948–952, 2003.

[3]. N. G. Turan, S. Elevli and B. Mesci, "Adsorption of copper and zinc ions on illite: Determination of the optimal conditions by the statistical design of experiments," *Applied Clay Science*, Vol. 52, 392–399, 2011.

[4]. A. Sheikhhosseini, M. Shirvani and Shariatmadari, "Competitive sorption of nickel, cadmium, zinc and copper on palygorskite and sepiolite silicate clay minerals," *Geoderma*, Vol. 192, 249–253, 2013.

[5]. A. B. Albadarin, J. Mo, Y. Glocheux, S. Allen, G. Walker and C. Mangwandi, "Preliminary investigation of mixed adsorbents for the removal of copper and methylene blue from aqueous solutions," *Chemical Engineering Journal*, Vol. 255, 525–534, 2014.

[6]. Y. J. Lee, E. J. Elzinga and R.J. Reeder, "Cu(II) adsorption at the calcite–water interface in the presence of natural organic matter," *Geochimica et Cosmochimica Acta*, Vol. 69, 49–61, 2005.

[7]. F. T. Senberber, M. Yıldırım, N. Karamahmut Mermer and E. Derun, "Adsorption of Cr(III) from aqueous solution using borax sludge," *Acta Chimica Slovenica*, Vol. 64, 654-660, 2017.

[8]. A. Olgun and N. Atar, "Equilibrium and kinetic adsorption study of Basic Yellow 28 and Basic Red 46 by a boron industry waste," *Journal of Hazardous Materials*, Vol. 161, 148-156, 2009.

[9]. N. Atar, A. Olgun and S. Wang, "Adsorption of copper (II) and zinc (II) on boron enrichment process waste in aqueous solutions: Batch and fixed-bed system studies," *Chemical Engineering Journal*, Vol. 192, 1–7, 2012.

[10]. Y. S. Ho and G. McKay, "Pseudo-second order model for sorption processes," *Process Biochemistry*, Vol. 34, 451–465, 1999.

[11]. I. Langmuir, "The adsorption of gases on plane surfaces of glass, mica and platinum," *Journal of the American Chemical Society*, Vol. 40, 1361–1403, 1918.

[12]. R. Slimani, I. Ouahabi, A. Elmchaouri, B. Cagnon, S. Antri and S. Lazar, "Adsorption of copper (II) and zinc (II) onto calcined animal bone meal. Part I: Kinetic and thermodynamic parameters," *Chemical Data Collections*, Vol. 9, 184-196, 2017.

[13]. S. Mellouk, A. Belhakem, K. Marouf-Khelifa, .J. Schott and A. Khelifa, "Cu(II) adsorption by halloysites intercalated with sodium acetate," *Journal of Colloid and Interface Science*, Vol. 360, 716-724, 2011.

[14]. E. M.S. Azzam, Gh. Eshaq, A.M. Rabie, A.A. Bakr, A. A. Abd-Elaal, A.E. El Metwally and Salah M.

Tawfik, "Preparation and characterization of chitosan-clay nanocomposites for the removal of Cu(II) from aqueous solution," *International Journal of Biological Macromolecules*, Vol. 89, 507-517, 2016.

[15]. K. Tohdee, L. Kaewsichan and Asadullah, "Enhancement of adsorption efficiency of heavy metal Cu(II) and Zn(II) onto cationic surfactant modified bentonite," *Journal of Environmental Chemical Engineering*, Vol. 6, 2821-2828, 2018.

[16]. M. Gupta, H. Gupta and D.S. Kharat, "Adsorption of Cu(II) by low cost adsorbents and the cost analysis," *Environmental Technology & Innovation*, Vol. 10, 91-101, 2018.

[17]. H. Koyuncu and A. R. Kul, "An investigation of Cu(II) adsorption by native and activated bentonite: Kinetic, equilibrium and thermodynamic study," *Journal of Environmental Chemical Engineering*, Vol. 2, 1722-1730, 2014.

[18]. J. Lim, H. Kang, L. Kim, and S. Ko, "Removal of heavy metals by sawdust adsorption: Equilibrium and kinetic studies," *Environmental Engineering Research*, Vol. 13, 79-84, 2008.

Environmental Research & Technology, Vol. 1(4), pp. 6-13, 2018

Environmental Research & Technology

http://dergipark.gov.tr/ert

CONFERENCE PAPER

Decolorization of Reactive Orange 16 and Reactive Black 5 in aqueous solution by ozonation

Irem Onder[1], Okan Aydin[1], Afife Guvenc[1,*]

[1]Ankara University Chemical Engineering Department, 06100, Beşevler/Ankara, TURKEY

ABSTRACT

Textile industry is one of the most chemically intensive industries on Earth and the major polluter of potable water. There are many methods for dye removal in the textile industry. One of the most effective methods is colour removal by ozonation. The application of ozonation has increased in recent years. Preference of the ozonation method is the efficiency of colour removal and the short application time. In ozonation process, not only colour but also the toxicity caused by products of treated wastewater is important. So, suitable ozonation period must be obtained. The aim of this study is the removal of Reactive Black 5 (RB-5) and Reactive Orange 16 (RO-16) from the synthetic aqueous solution by ozonation. In this study, dye removal (%) and chemical oxygen demand (COD) removal (%) were determined and carried out by kinetic analyzing. The maximum dye removals were 99.9 % and 99 % at all pH values in initial dye concentration of 100 mg L^{-1} for RB-5 (40 min) and RO-16 (70 min), respectively. It was found that COD removal is 100 % for both dyes. Ozonation kinetics were studied and it was found that it agreed with the pseudo first order kinetics for two dyes. The highest pseudo first order kinetic constants are 0.1918 min^{-1} (R^2: 0.9978, pH:2) and 0.0794 min^{-1} (R^2: 0.9918, pH:6) for RB-5 and RO-16, respectively. The results obtained in this study showed that ozonation of reactive dyes at acidic or neutral pH was more suitable than that of alkaline pH.

Keywords: Ozonation, decolorization, chemical oxygen demand, Reactive Orange 16, Reactive Black 5

1. INTRODUCTION

The strong colour of textile effluent creates both environmental and aesthetic problems. It generates huge quantities of complex chemical substances as a part of unused materials including dyes in the form of wastewater during various stages of textile processing. The direct discharge of this wastewater into the water bodies like lakes, rivers etc. pollutes the water and affects the flora and fauna. Effluent from textile industries contains different types of dyes, which is because of high molecular weight and complex structures, shows very low biodegradability. The wastewater includes are both organic and inorganic structures after industrial processes. The dyestuffs used in the textile industry are generally azo dyes [1]. Azo dyes, which contain one or more azo bonds (-N=N-), are the most widely used synthetic dyes and generally are major pollutants in dyed wastewaters. Due to their toxicity and slow degradation, these dyes are classified as environmentally hazardous materials. Azo dyes are normally hazardous to the environment even if they are present at low concentration [2].

Ozonation is an oxidative process in which ozone (O_3) is used as an oxidizing agent. Interest in the use of ozone in wastewater treatment has increased considerably in recent years. Ozonation has excellent potential in decolorization as decolorization and degradation occur in one step; danger to humans is minimal; no sludge remains; all residual ozone can be decomposed easily into oxygen and water; little space is required and ozonation is easily performed [3].

The treatment methods of textile wastewater are divided into three basic section; physical treatments, chemical treatments, and biological treatments. In the adsorption method which is one of the physical methods there must be affinity between the dye and the adsorbent. Even if this method is successful, solid

Corresponding Author: guvenc@eng.ankara.edu.tr (Afife Guvenc)
Received 28 June 2018; Received in revised form 24 October 2018; Accepted 25 October 2018
Available Online 06 November 2018
Doi: ISSN: 2636-8498

This paper has been presented at EurAsia Waste Management Symposium 2018, Istanbul, Turkey

waste problem occurs in the solution. Among the physical methods membrane separation technique is effective, but expensive, for example. Besides, frequent occlusions happen in the system. Biological methods usually contain biodegradation (aerobic or anaerobic), biosorption and bioaccumulation. The biomass used for biodegradation must consume the dye as carbon source. Biosorption requires biomass-dye affinity as the adsorption. As a result, solid waste is formed again. This situation is also similar in bioaccumulation. The chemical treatment methods include electrolysis, coagulation and electrocoagulation methods. Electrolysis is an expensive method. The coagulation method causes solid waste formation. The electrocoagulation method is similar according to this point of view. The most effective method applied today in chemical methods is the advanced oxidation process (AOP). AOP is based on the generation of powerful oxidants such as hydroxyl radicals [4]. Photocatalytic, photo-fenton, fenton, photocatalytic fenton and ozonation are the AOP. Ozone can degrade the complex structure of dye in a short time. Because of this reason, ozonation is rather an attractive technique on dye removal in recent years.

The ozonation process has been postulated as a potential, alternative method for decolorization and improvement of biological treatment. In literature, Zakaria et al. [5] studied decolorization of RO-16 by electrochemical oxidation and adsorption methods. They compared the effectiveness of these treatments and evaluated the percentage of RO-16 decolorization and COD removal. Their results indicated that electrochemical is the most effective method. RO-16 was decolorized up to 98.5 % after by this method. Tizaoui and Grima [6] investigated ozonation of RO-16 at different conditions (25-100 mg L^{-1} dye; 20-80 g m^{-3}, NTP ozone gas, pH: 2, 7, 11). They achieved up to 90 % decolorization yield for the initial concentration of 90 mg L^{-1} between 20-80 g m^{-3} ozone gas concentration and 5-17 min ozonation time at pH 7. Also, they reported that degradation of the products are nitrosobenzene, nitrobenzene, benzene-1,4-diol, 1,4-benzoquinone, acetamide, phthalic, maleic, oxalic, acetic, formic acids. Şahinkaya [7] carried out the decolorization of RO-16 by ferrate (VI) oxidation assisted by sonication. It was found that dye removal efficiencies were 85 % by ferrate (VI) method and 91 % by sonoferrate (VI) method.

Venkatesh et al. [8] studied the effect of ozonation on decolorization and mineralization of azo dyes (Acid Red 14, Congo Red, Reactive Black 5) at 1500 mg L^{-1} initial dye concentration, 55.5 mg L^{-1} ozone concentration and pH 10. The results showed that the COD and dye removal are 50 % and 94 % at 25 min ozonation time for RB-5, respectively. Wang et al. [9] examined the effect of ozonation on the degradation process of the RB-5. They studied at different experimental conditions (20.5 mg L^{-1} ozone concentration, 2 g L^{-1} initial dye concentration and pH 6). They found that the COD, total organic carbon (TOC) reductions were about 40 % and 25 % for 6 h ozonation. Venkatesh et al. [10] investigated for RB-5 ozonation followed by anaerobic biodegradation using up flow anaerobic sludge blanket (UASB) reactor was carried out. Colour of dye solution declined exponentially with increase ozonation time at 1500 mg L^{-1} initial dye concentration, 5 g h^{-1} ozone flow rate, pH 10.13. It achieved around 70 % decolourization and 50 % COD reduction in 10 min. Decolourization efficiency was 94 % after 25 min of ozonation investigated in this study. The system of ozonation and anaerobic treatment by UASB reactor showed that the COD reduction has reached to about 90 % and dye removal 94 %, respectively.

Ozonation has been generally preferred for degradation of azo dyes due to the fact that ozone is highly reactive with azo double bond. Only one study [6] related to degradation of RO-16 by ozonation was found. A study of ozonation kinetic of RB-5 was not encountered in the literature. Also, it was observed that the COD removal for degradation of RB-5 was insufficient in the literature [8]-[10].

In the present study, in order to achieve high COD removal and colour removal for the effective degradation of RO-16 and RB-5, the effects of the ozonation time (0-150 min), the initial dye concentration (100-300 mg L^{-1}) and the initial pH (2-10) on the dye concentration and dye removal were investigated. The reason for the preference of Reactive Black 5 and Reactive Orange 16 (two types of azo dyes) is that they have complex chemical structures with various azo aromatic groups. Reactive Black 5 is a diazo dye and Reactive Orange 16 is a monoazo dye. The changing of pH of dye solutions with time were observed in the different initial dye concentrations. Also, the chemical oxygen demand (COD) removals were measured for 100, 200 and 300 mg L^{-1} initial dye concentrations and 2, 6, 10 initial pH of solutions at the end of ozonation. Furthermore, the kinetics of ozonation for two dyes were investigated at the different initial dye concentrations and pH values.

2. MATERIALS AND METHODS

2.1. Dyes

Reactive Black 5 and Reactive Orange 16 were purchased from Sigma Aldrich Company. In the preparation of the dye solutions, distilled water was used. Table 1 shows the chemical structure and properties of Reactive Black 5 and Reactive Orange 16 used in this study [11].

2.2. Experimental Procedure

The ozone was generated from dry air in a laboratory model ozone generator (BNP Ozone, Model: 5) with a maximum capacity of 5 g h^{-1}. Fig 1 shows the schematic diagram of ozonation apparatus. Ozonation experiments were carried out in 500 mL glass reactor with 250 mL volume of dye solution. All the experiments were performed at room temperature (25 ± 2 ºC), and in semi batch mode by sparging ozone continuously into the solution. Magnetic stirrer was used in the ozonation experiments. The chosen initial dye concentrations in the experiments were 100 mg L^{-1}, 200 mg L^{-1} and 300 mg L^{-1}. Ozonation

experiments at different pH values were conducted in order to observe the effects of acidic and basic pH values on the ozonation reactions and pH were adjusted with 1 M H_2SO_4 and 1 M NaOH. The samples were withdrawn from the reactor in every 10 minutes and the concentrations of dyes in their solutions were determined by spectrophotometric method (Shimadzu UV-1601 Spectrophotometer). The percentages of dye and COD removal was determined by using the following equation:

$$Dye\ removal\ (\%) = \frac{C_0 - C_t}{C_0} \times 100 \quad (1)$$

$$COD\ removal\ (\%) = \frac{COD_0 - COD_t}{COD_0} \times 100 \quad (2)$$

In equation (1), C_0 and C_t are the dye concentrations (mg L^{-1}) at the beginning and t time (every 10 minute) of ozonation, respectively. In equation (2), $(COD)_0$ and $(COD)_t$ are the chemical oxygen demand values at the beginning and end of ozonation, respectively.

Table 1. Structure and properties of Reactive Black 5 and Reactive Orange 16 [11]

Product Name	Structure	Formula	Molecular weight (g mol^{-1})	λmax (nm)
Reactive Black 5	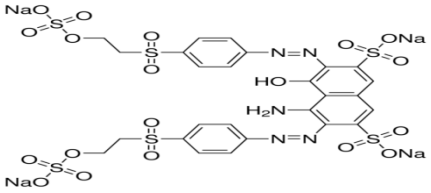	$C_{26}H_{21}N_5Na_4O_{19}S_6$	991.82	597
Reactive Orange 16	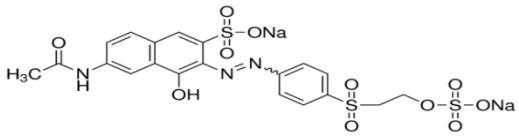	$C_{20}H_{17}N_3Na_2O_{11}S_3$	617.54	494

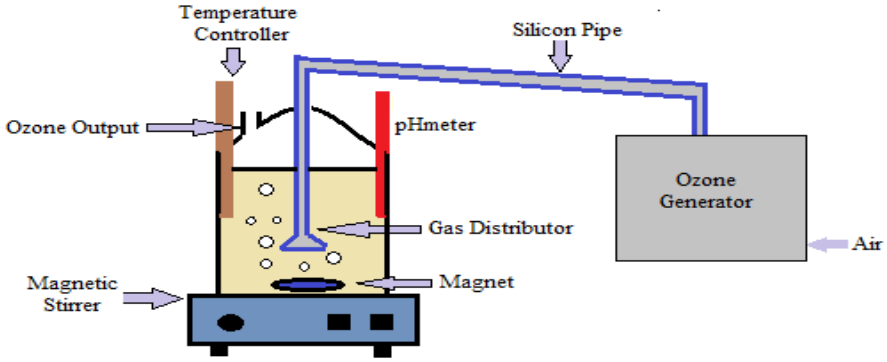

Fig1. Diagram of ozonation system

2.3. Analytical Methods

The samples were diluted with distilled water when required and the absorbance value was measured on the UV device. UV-VIS spectra of dye solution were recorded between 400 and 800 nm using double beam equipped with 2 mL plastic cuvette. The wavelengths of maximum absorbance (λ_{max}) were 597, 494 nm for RB-5 and RO-16, respectively. Chemical oxygen demands (COD) of the samples were measured by adding 2 mL of the sample solution into a glass vial containing 3 mL of COD standard solution and digesting the sample in a Lovibond Thermoreactor RD 125 for 2 h at 150 °C according to the standard methods (APHA 5220 COD) [12]. After the sample was cooled, its COD value was determined directly by a Lovibond Water Testing Tintometer Group MD 200. pH was measured by pH analyzer (Isolab Model 616.01.001 microprocessor-based waterproof pH/mV/Temp).

3. RESULTS & DISCUSSION

The decomposition reactions of ozone in pure water were reported in the literature [10], [13]-[18]. The reactions of decomposition mechanism of ozone in aqueous solution has been described by Hoigne, Staehelin and Bader (HSB model). Related reactions were given in following:

$O_3 + OH^- \rightarrow HO_2^\bullet + {}^\bullet O_2^-$ (3)

$HO_2^\bullet \leftrightarrow H^+ + O_2^-$ (fast) (4)

$O_3 + {}^\bullet O_2^- \rightarrow O_2 + {}^\bullet O_3^-$ (5)

${}^\bullet O_3^- + H^+ \rightarrow HO_3^\bullet$ (6)

$HO_3^\bullet \rightarrow OH^\bullet + O_2$ (7)

${}^\bullet OH + O_3 \leftrightarrow O_3OH$ (8)

$O_3OH \rightarrow HO_2^\bullet + O_2$ (9)

$O_3OH + HO_2^\bullet \rightarrow O_3 + O_2 + HO_2$ (10)

The reactions of organic molecule, M (M is dye in this study), with ozone in aqueous solution were given as explained with HSB model in literature:

$OH^{\bullet} + M \rightarrow Ø$ (11)
$OH^{\bullet} + M \rightarrow R^{\bullet}$ (12)
$R^{\bullet} + O_2 \rightarrow ROO^{\bullet}$ (13)
$ROO^{\bullet} \rightarrow M^{\bullet}_{oxid} + HO_2^{\bullet}$ (14)
$O_3 + M \rightarrow M_{oxid}$ (15)
$O_3 + M \rightarrow M^{+} + {}^{\bullet}O_3^{-}$ (16)

As it is shown in above equations, the radicals as $HO_2^{\bullet}$, $HO_3^{\bullet}$, $OH^{\bullet}$ and radicals ions ${}^{\bullet}O_2^{-}$, ${}^{\bullet}O_3^{-}$ or active spice as O_3OH were produced in this medium. Thus, it is too hard to explain the decomposition of organic molecule by ozone in textile wastewater. The effects of different parameters on dye removal and COD removal were investigated in order to facilitate the understandability of dye decomposition.

3.1. The Effect of Initial Dye Concentration on Dye Removal

The effect of initial dye concentrations and initial pH values on dye removal for RB-5 and RO-16 were investigated. Change of dye removal with ozonation time for two dyes were given in Fig 2 and Fig 3 (a,b,c). It was observed that dye removal increased with time in all cases of dye samples. For RB-5; it was observed that the ozonation time of 40 min is sufficient for maximum dye removal (99.9 %) at all pH values in low initial dye concentration (C_0: 100 mg L^{-1}). However, ozonation time increased more 20 min (total 60 min) at high initial dye concentrations (200-300 mg L^{-1}) at all pH values (Fig 2-a,b,c).

For RO-16; maximum dye removal (99 %) was observed at 70 min in low initial dye concentration (C_0: 100 mg $L^{-1}$and at all pH values. Also, in initial dye concentrations of 200 and 300 mg L^{-1}maximum dye removal (99 %) was observed at the end of 90 min for pH values of 2 and 10. This removal was obtained at the end of 150 min for pH value of 6 (Fig 3-a,b,c). According to Shu and Huang [19] and Muthukumar et al., [20] the time taken for complete decolorization of dyes by ozone increases with number of azo groups, while it decreases with increase number of sulfonic acid groups in the dye structure.

3.2. Changing pH of the Reaction Medium with Ozonation Time

In this section, changing pH of medium during ozonation was investigated. Related experimental results were given in Fig 4-a,b. As it is shown in this figure, while initial value pH of dye solutions was about 6 at all initial dye concentrations for RB-5 and RO-16, they reached acidic pH values (about 2) at the end of ozonation. We thought that it happened due to formation of molecules which have acidic structure at the end of ozonation.

Data in literature guides this hypothesis. The products of decomposition of RB-5 was reported as 5-aminonaphthalene-1,4 diol, 2,2'–Biphenyl-4,4'-diyldiacetic acid, N-formylformamide, (4-Nitrosophenyl) acetaldehyde, Muconic acid, (2Z)-pent-2-enedioic acid, Maleic acid by He et al. [4] Also, the products of decomposition of RO-16 was reported as nitrosobenzene, nitrobenzene, benzene-1,4-diol, 1,4-benzoquinone, acetamide, phthalic, maleic, oxalic, acetic, formic acids. As it is shown that by-products have generally acidic structure. High colour removal is achieved at low pH. In acidic solution, the dye ozonation is performed by the direct mechanism. The degree of decolorization is favored by direct ozone attack, at low pH, since molecular ozone selectively attacks chromophore groups [17]. Also, in the study, it was observed that pH of dye solutions decreased (from 6 to 2) and dye removal increased (99.9 %) during ozonation (Fig 2 and 3). Moreover, similar results were obtained by Venkatesh et al. [8], [10].

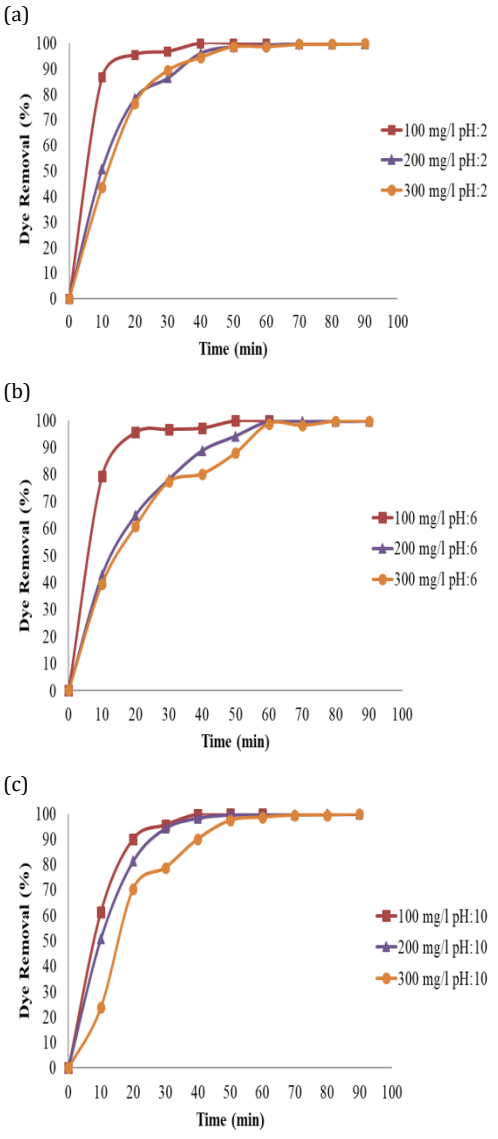

Fig 2. The changing of dye (RB-5) removal with ozonation time at different initial dye concentrations and pH (Q_{O3}=5g h^{-1}, T=25±2 °C) (a) pH:2 ; (b) pH:6 ; (c) pH:10

3.3. The Effect of Initial Dye Concentrations on COD Removal

COD values were measured at different initial dye concentrations and their ozonation time at pH values of 2, 6, 10 for RB-5 and RO-16 and COD removal values (%) were calculated. All the data of COD and COD removal were given at Table 2 and Fig 5-a,b.

In the study, COD removals are independently satisfactory (35-100 %) initial dye concentrations at neutral and acidic pH values for two dyes. On the other hand, it was observed that COD removals are low (30-70 %) at high pH values for dyes examined. Both RB-5 and RO-16 provided the highest COD removal (99, 100 %) at initial dye concentration of 200 mg L^{-1} at neutral pH values. If changing COD removal with ozonation time is investigated, it is seen that there is an increase first and decrease later. It was thought that it happened due to small organic molecules which are not completely degradable under the oxidative conditions. It could be said that high ozone flow rate (5 g h^{-1}) may cause the reduction of COD. Similar results were encountered in literature [8], [10].

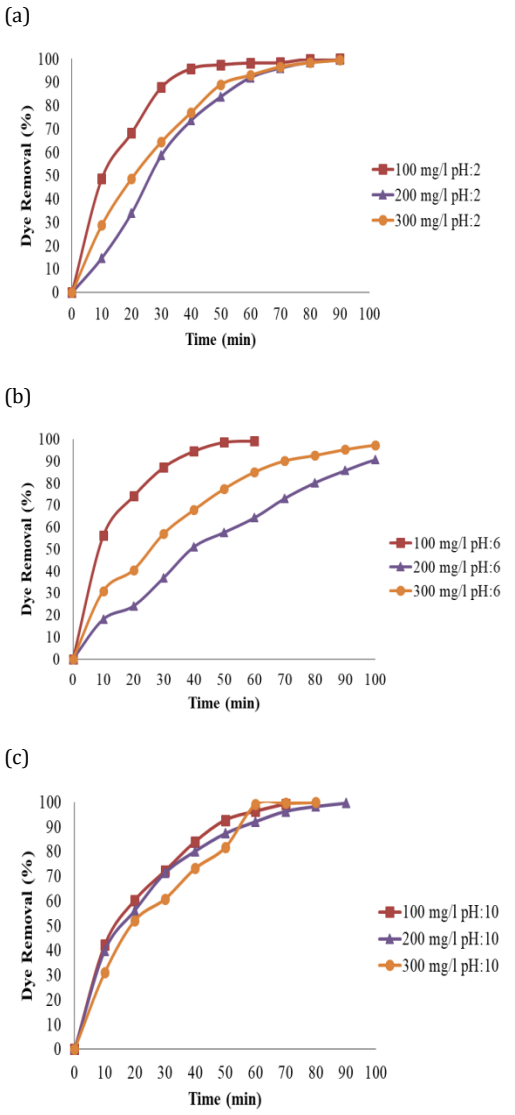

Fig 3. The changing of dye (RO-16) removal with ozonation time at different initial dye concentrations and pH (Q_{O3}=5g h^{-1}, T=25±2 ºC) (a) pH:2 ; (b) pH:6 ; (c) pH:10

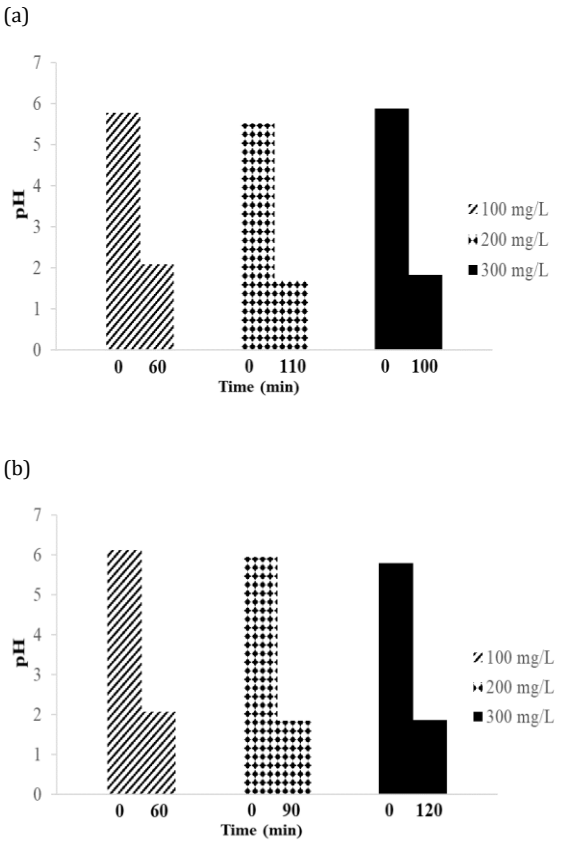

Fig 4. Changing pH at 25 °C with ozonation time for initial dye concentration:100, 200, 300 mg L^{-1} (a) RB-5 and (b) RO-16

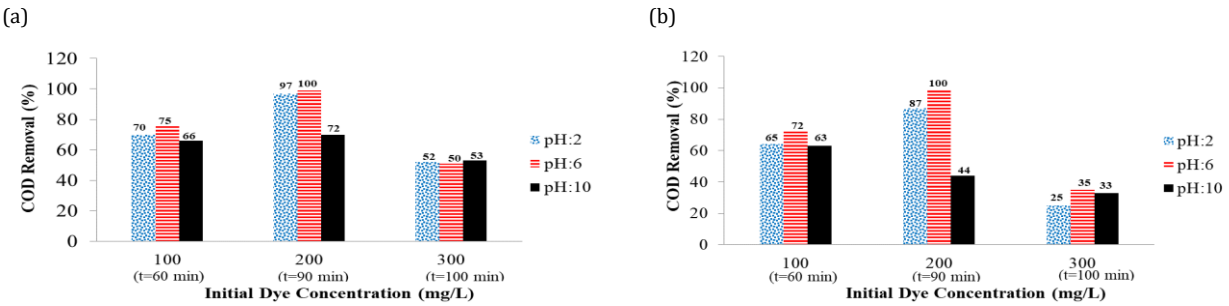

Fig 5. The efficiency of COD removal end of the ozonation for different initial dye concentration (100, 200, 300 mg L^{-1}) and initial pH values (2, 6, 10) (a)RB-5 (b)RO-16

Table 2. The influent and effluent concentrations of COD and COD removals for RB-5 and RO-16 at the different initial dye concentrations and pH values

RB-5					RO-16				
Initial Dye Concentrations (mg L^{-1})	pH	COD (influent)	COD (effluent)	COD % Removal	Initial Dye Concentrations (mg L^{-1})	pH	COD (influent)	COD (effluent)	COD % Removal
100	2	94	28	70	100	2	74	26	65
	6	53	13	75		6	60	17	72
	10	105	36	66		10	64	24	63
200	2	81	2	97	200	2	258	32	87
	6	167	0	100		6	207	0	100
	10	130	36	72		10	170	95	44
300	2	161	77	52	300	2	204	153	25
	6	129	64	50		6	200	130	35
	10	130	61	53		10	219	146	33

Table 3. Pseudo-first-order kinetic constants of RB-5 and RO-16 at different pH and different initial dye concentration

		pH: 2		pH: 6		pH: 10	
Dye Concentration (mg L^{-1})		RB-5	RO-16	RB-5	RO-16	RB-5	RO-16
100	R^2	0.9978	0.9827	0.9765	0.9818	0.9801	0.9783
	k	0.1918	0.0710	0.1314	0.0794	0.1481	0.0510
200	R^2	0.9854	0.9368	0.9703	0.9522	0.9691	0.9778
	k	0.0847	0.0366	0.0618	0.0215	0.0838	0.0457
300	R^2	0.9836	0.9679	0.9490	0.9846	0.9490	0.9328
	k	0.0739	0.0440	0.0519	0.0332	0.0519	0.0414

3.4. Ozonation Kinetics of RB-5 and RO-16

The process of ozonation happens because of oxidation by ozone molecules and by generation of hydroxyl radicals, which react with initial compound and intermediates. When the amount of ozone is excess or when the ozone concentration is assumed to reach a stationary state at the interface, the oxidation rate follows a pseudo-first-order kinetics with respect to the concentration of the organic substance in terms of degradation and the rate equation is as follows [21]:

$$C_{A\,(aq)} + O_3 \rightarrow \text{products} \quad (17)$$

where the rate constant k' can be determined by

$$\frac{-d[C_A]}{d_t} = k'[C_A][O_3] \quad (18)$$

Eq. (18) can be simplified and k takes the form of an apparent pseudo first-order constant k if we assume that the concentration of very reactive O_3 radicals takes on a steady-state value during the process:

$$\frac{-d[C_A]}{d_t} = k[C_A] \quad (19)$$

where k is pseudo-first-order rate constant and C_A is concentration of organic substance. On integration, the above equation is as follows:

$$\ln(C_A/C_{A0}) = -kt \quad (20)$$

The plot of $\ln(C_A/C_{A0})$ with reaction time (t), for decolorization of RB-5 and RO-16 during ozonation in Fig 6 was given. The reaction kinetics of ozonation at pH 2, 6 and 10 were investigated for RB-5 and RO-16, respectively. $\ln(C_A/C_{A0})$ versus time (t) curves (Fig 6-a,b,c) were found to be linear indicating a pseudo-first-order reaction at the equilibrium concentration of ozone in the aqueous phase for each pH (for pH range studied) and for both of the dyes. Oxidizing ability of ozone comes from either molecular ozone or hydroxyl free radical. The correlation coefficients (R^2) obtained were between 0.93 and 0.99.

(a)

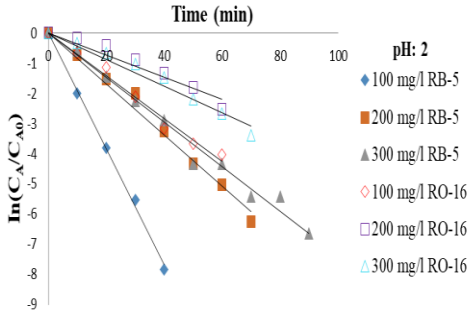

(b)

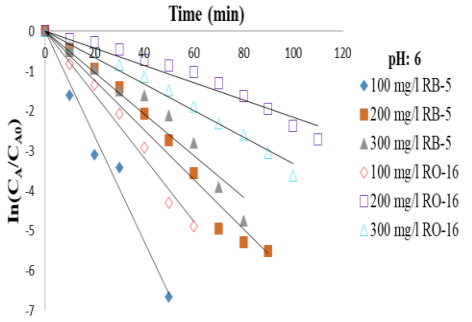

(c)

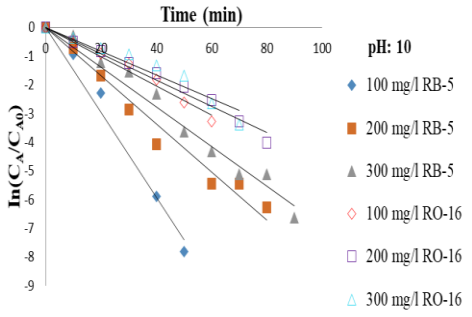

Fig 6. Linear transforms: $\ln(C_A/C_{A0})$ versus time for decolorization of RB-5 and RO-16 during ozonation (a)pH:2 (b)pH:6 (c)pH:10 (Q_{O3}=5 g h^{-1}, T=25±2 ºC)

Pseudo-first-order kinetic constants obtained by Fig 6 were given in Table 3 for RB-5 and RO-16 at different pH and different initial dye concentrations. It was found that the highest kinetics constants and correlation coefficients are in initial dye concentration of 100 mg L^{-1} at all pH values for RB-5 and RO-16. Ozonation rate of RO-16 was slower than that of RB-5. As it is shown in Fig 2 and Fig 3, ozonation time of RO-16 was longer than that of RB-5. The highest pseudo-first-order kinetic constants are 0.1918 min^{-1} (R^2: 0.9978, pH:2) and 0.0794 min^{-1} (R^2: 0.9818, pH:6) for RB-5 and RO-16, respectively.

He et al. [4] investigated decolorization of RB-5 by combined sonolysis and ozonation. They found that ozonation kinetic agreed with pseudo-first-order kinetic. Rate constants obtained by them are 1.21 min^{-1}, 0.744 min^{-1} and 0.636 min^{-1} at pH value of 11 and 35 °C for initial dye concentration of 100, 200, 300 mg L^{-1}, respectively.

The studies investigating ozone kinetics of RO-16 in wastewaters are insufficient in literature. The only one is the study of Tizaoui and Grima [6]. They carried out ozone oxidation RO-16 in aqueous solution. They reported that the reaction was assumed in the second order and Danckwerts model was used to determine the values of its rate constants.

4. CONCLUSIONS

The high volume of coloured wastewater in textile finishing industry demands a special treatment and evaluation of the ecotoxic effects of the process effluents released into the environment. Ozone treatment proves to be very effective for complete removal of colour, but provides only partial reduction of COD. Generally, ozonation is a potential technique for decolorization and COD removal of wastewater containing reactive dyes. In ozonation processes, not only colour but also the toxicity caused by products of treated wastewater is important. So, suitable ozonation period must be obtained.

In this study ozonations of Reactive Black 5 and Reactive Orange 16 were studied at initial dye concentrations of 100-300 mg L^{-1}, pH values of 2, 6, 10, ozone flow rate 5 g h^{-1}, temperature 25±2 °C. It was observed that dye concentration decreased and dye removal (%) increased with ozonation time at all experimental conditions. The maximum dye removals were 99.9 % and 99 % at all pH values in initial dye concentration of 100 mg L^{-1} for RB-5 (40 min) and RO-16 (70 min), respectively. It was found that COD removal is about 100 % for both dyes. The length of ozonation time and the high flow rate ozone caused the mineralization. Ozonation kinetics were studied and it was found that it agreed with the pseudo-first-order kinetics for two dyes. Removal of RB-5 by ozonation is faster than that of RO-16 according to obtained rate constants. The results obtained in this study showed that ozonation of reacitve dyes at acidic or neutral pH was more suitable than that of alkaline pH. The results illustrated that high colour and COD removal were achieved at initial dye concentration of 200 mg L^{-1} and acidic/neutral pH and quite short ozonation time. Reactive dye required low energy for

decolorization and mineralization compared to other dyes. The conclusions of the present study have clearly revealed that ozonation has been proved to be a viable technique for the treatment of highly recalcitrant azo dyes containing wastewater.

REFERENCES

[1]. K. Pazdzior, J. Wrebiak and A. Klepacz-Smolka, "Influence of ozonation and biodegradation on toxicity of industrial textile wastewater," *Journal of Environmental Management*, Vol.195, pp. 166-173, 2017.

[2]. Q. Zheng, Y. Dai and X. Han, "Decolorization of azo dye C.I Reactive Black 5 by ozonation in aqueous solution: influencing factors, degradation products, reaction pathway and toxicity assessment," *Water Science & Technology*, Vol.73.7, pp. 1500-1510, 2016.

[3]. E. Brillas and C.A. Martinez-Huitle, "Decontamination of wastewaters containing synthetic organic dyes by electrochemical methods. An updated review," *Science Direct*, Vol.166-167, pp. 603-643, 2015.

[4]. H. Zhiqiao, S. Shuang, Z. Huamin, Y. Haiping and C. Jianmeng, "C.I. Reactive Black 5 decolorization by combined sonolysis and ozonation," *Ultrasonics Sonochemistry*, Vol.14, pp. 298–304, 2007.

[5]. Z. Zakaria, W.Y.W. Ahmad, M.R. Yusop and M.R. Othman, "COD and color removal of Reactive Orange 16 dye solution by electrochemical oxidation and adsorption method," in AIP Conference Proceedings, 1678, 050007, 1-6, 2015.

[6]. C. Tizaoui and N. Grima, "Kinetics of the ozone oxidation of Reactive Orange 16 azo-dye in aqueous solution," *Chemical Engineering Journal*, Vol.173, pp. 463-473, 2011.

[7]. S. Şahinkaya, "Decolorization of reactive orange 16 via ferrate(VI) oxidation assisted by sonication," *Turkish Journal of Chemistry*, Vol.41, pp. 577-586, 2017.

[8]. S. Venkatesh, A.R. Quaff, N.D. Pandey and K. Venkatesh, "Impact of ozonation on decolourization and mineralization of azo dyes: Biodegradability enhancement, by-products formation, required energy and cost," *Ozone: Science & Engineering*, Vol.37, pp. 420-430, 2015.

[9]. C. Wang, A. Yediler, D. Lienert, Z. Wang and A. Kettrup, "Ozonation of an azo dye C.I. Remazol Black 5 and toxicological assessment of its oxidation products," *Chemosphere*, Vol.52, pp. 1225-1232, 2003.

[10]. S. Venkatesh, K. Venkatesh and A.R. Quaff, "Dye decomposition by combined ozonation and anaerobic treatment: Cost effective technology," *Journal of Applied Research and Technology*, Vol.15, pp. 340-345, 2017.

[11]. htpps:/www.sigmaaldrich.com/. Available. (2018)

[12]. A.D. Eaton, L.S. Clesceri, E.W. Rice, A. E. Greenberg. Standard Methods for the Examination of Water & Wastewater, 21st Ed., [M. A. H. Franson (man. ed.)]. APHA 5220 COD, Washington, USA, 2005.

[13]. J. Staehelin, R.E. Bühler, and J.Hoigne, "Ozone decomposition in water studied by pulse radiolysis. 2. OH and HO4 as chain intermediates," *The Journal of Physical Chemistry*, Vol.88, pp. 5999-6004, 1984.

[14]. J. Staehelin and J.Hoigne, "Decomposition of ozone in water in the presence of organic solutes acting as promoters and inhibitors of radical chain reaction," *Environmental Science and Technol*ogy, Vol.19, pp. 1206-1213, 1985.

[15]. H. Tomiyasu, H. Fukutomi and G. Gordon, "Kinetics and mechanism of ozone decomposition in basic aqueous solution," *Inorganic Chemistry*, Vol.24, pp. 2962-2966, 1985.

[16]. A.Ö. Yıldırım, " Investigation of the degradation of some reactive dyes by using advanced oxidation techniques," PhD Thesis, University of Çukurova, Adana, Turkey, 2009.

[17]. B. Langlais, D.A. Reckhow and D.R. Brink. Ozone in Water Treatment Application and Engineering, Lewis Publishers, New York, USA, 1991.

[18]. H. Selçuk, "Decolorization and detoxification of textile wastewater by ozonation and coagulation processes," *Dyes and Pigments*, Vol.64, pp. 217-222, 2005.

[19]. H. Y. Shu andC.R. Huang, "Degradation of commercial azo dyes in water using ozonation and UV enhanced ozonation process," *Chemosphere*, Vol.31, pp. 3813-3825, 1995.

[20]. M. Muthukumar, D. Sargunamani and N. Selvakumar, "Statistical analysis of the effect of aromatic, azo and sulfonic acid groups on decolorization of aciddye effluents using advanced oxidation processes," *Dyes Pigments*, Vol.65, pp. 151-158, 2005.

[21]. T. Kabdaşlı, T. Ölmez and O. Tünay, "Factors affecting color removal from reactive dye bath by ozonation," *Water Science Technology*, Vol.45, pp. 261-270, 2002.

Environmental Research & Technology, Vol. 1(4), pp. 14-21, 2018

Environmental Research & Technology

http://dergipark.gov.tr/ert

CONFERENCE PAPER

Comparative analysis on practical implications and evaluation of PVC geomembrane interfaces against particulate materials

Tanay Karademir[1]

[1] Istanbul Bilgi University, Civil Engineering Department, Santral Campus, 34060 Eyup, Istanbul, TURKIYE

ABSTRACT

An experimental research study including a series of laboratory large displacement interface shear tests between different particulate materials (rounded, angular sands) and smooth PVC geomembranes, and additionally, a series of Shore D Hardness measurements were conducted. The aim of this study is to investigate an easy and quick means of predicting shear resistance/strength of sand-polymer interfaces indirectly from the hardness of the continuum material (i.e. PVC geomembrane) at the interface to establish a comparative analysis between direct test results and indirect practical evaluation through hardness property based on an important interface shear property; friction angle, (δ) at peak and residual states measured directly from interface shear tests performed in the laboratory as well as computed indirectly from empirical models developed in the study for the case of different normal loading conditions (i.e. normal stress levels:25, 100, 400 kPa). The results and analysis will be presented throughout the paper demonstrate that the mobilized shear response and the resulting frictional resistance of sand (rounded, angular) – PVC geomembrane interface systems are highly dependent on a combination of loading conditions, geomembrane physical material properties (i.e. hardness) and particulate shape (i.e. angularity/roundness). For direct and indirect assessment of the resultant [δ_{Peak}] and [$\delta_{Residual}$] values, the comparative analysis showed that a reasonable similarity between the laboratory test results and the indirect analytical assessment analysis is evident from the analogicalness of the experimentally measured values at the predetermined normal stress levels (25, 100 and 400 kPa) to the computed values from the proposed empirical correlation equations proposed in the paper.

Keywords: Geosynthetic layereds, landfill design, particulate materials, PVC geomembranes

1. INTRODUCTION AND LITERATURE REVIEW

The design and development of geoenvironmental systems (i.e: composite structural systems at landfill base liners and side slopes) where soil (i.e. sand) is in contact with construction materials such as polymer (i.e. geosynthetics) is widespread. The placement of these dis-similar materials adjacent to one another creates interfaces which can lead to relatively weak shear strengths compared to the frictional strength of the soil mass itself. As such, particulate versus continuum interfaces (e.g. soil-geomembrane) governs the behavior of many geoenviroenmental structures including synthetic impervious liners in municipal waste containment facilities. They are generally used as composite systems rather than as stand-alone solutions in practice due to their complimentary advantages. The resisting forces at soil versus these construction material interfaces are mobilized due to relative movements between counterface materials [1]. As such, the interaction between these materials and soil plays a critical role in governing the integrity of such critical structures. To this end, numerous research efforts have been undertaken to evaluate the interface shear properties of polymers with the intention of establishing a general range for interface shear characteristics for these materials. The experimental studies of [1-5] amongst others, can be considered as important research work on the interface shear resistance of polymeric materials. These experimental studies, in addition to developing a database, also provide designers and engineering agencies with information

Corresponding Author: tanay.karademir@bilgi.edu.tr (Tanay Karademir)
Received 23 June 2018; Received in revised form 10 October 2018; Accepted 12 October 2018
Available Online 19 October 2018
Doi: ISSN: 2636-8498

This paper has been presented at EurAsia Waste Management Symposium 2018, Istanbul, Turkey

for estimating the likely range of frictional performance of geosynthetic interfaces in geoenvironmental applications.

Moreover, geomembranes are continuum materials and produced from polymeric material resins (i.e. Polyvinylchloride - PVC) for which the mechanical engineering properties (i.e. shear, tension, compression) are dependent on an important physical property such as hardness. The magnitude of surface hardness of the geomembrane liners, in general, can be associated and linked with the alteration of the material stiffness that is one of the most important visco-elastic and plastic properties of polymeric materials. A change in hardness such that a reduction in surface resistance of polymeric geomembrane liner sheet against indentation can be reflected by the alteration in Shore hardness index value. Furthermore, the stiffness of a polymer principally defines its state on the "softness" through "rigidity" scale as well as governs and is related to its surface hardness. In light of this, it is noted that the primary influence of surface hardness on sand – geomembrane interface shear response and resistance is thought to be related to the alteration of physical and mechanical properties of the geomembrane liner and are not necessarily due to changes in the sand properties. In this perspective, the use of surface hardness to indirectly evaluate the frictional performance of geosynthetic interfaces could be of importance. In this regard, the surface hardness tests of which the purpose is to measure the "resistance" of these polymeric materials developed through their physical properties to withstand an indentation force generated by a sharp object attempting to penetrate into their surfaces could provide a quick and practical mean of indirect evaluaition of frictional properties of those geosynthetics. Since the indentation hardness is inversely related to the penetration and dependent on elasticity, ductility, plasticity, strain, strength, stiffness, toughness, viscoelasticity, and viscosity properties of the polymeric materials that also could govern their interface frictional shear response and strength [6]. To this end, this study has been intended to extend the understanding on shear displacement behavior of granular material (sand) – geomembrane interfaces as numerous man-made polymer-based construction materials (i.e. geomembranes) are being routinely used in conjunction with particulate soils (i.e. sand) in various geoenvironmetal applications (i.e. landfills) and the demand for such composite soil – synthetic material systems has continuously been increasing owing to recent advancements in infrastructural construction technology. In this regard, the effects of distinct geo-material combinations at the interface on the friction properties of particulate versus geomembrane interfaces, investigated based on surface hardness measurements, will be presented. The goal of this experimental research study is to examine: i) the detection of geomembrane hardness; and, ii) develop empirical correlations between hardness and an engineering interface strength property (δ); and iii) compare results of empirically predicted interface frictional strength at peak as well as residual states based on hardness measurements with those of direct evaluation for sand – geomembrane interfaces obtained through direct interface shear tests in the laboratory.

2. MATERIALS AND EXPERIMENTAL METHODS

2.1. Granular Material

Granular materials including Ottawa 20-30 sand and Blasting sand were selected to be used to investigate the frictional properties of sand – PVC geomembrane interfaces. Both sand is poorly graded and has a similar mean grain size (D_{50} = 0.72 mm) while Ottawa 20-30 is composed of rounded quartz sand grains; however Blasting sand is comprised of angular quartz sand particles.

2.2. PVC Geomembrane

Geomembranes, in general, are used in a wide variety of waste containment related applications such as landfill liners (primary and secondary containment), landfill caps/closures. The PVC geomembranes produced with polyvinylchloride as the principal polymer resin are selected for use in infrastructure projects which require more flexibility in three dimensional performance as well as having less hardness of the geomembrane itself which can lead to enhancement of interfacial properties for combined and layered applications consisting of different material types. The benefits of PVC geomembranes are as follows: (i) Flexibility for three dimensional performance; (ii) larger panels (up to 80% less field seams); (iii) long-term survivability.

2.3. Characterization of Surface Hardness of Geomembranes

Shore Hardness is one of the most common methods of determining surface hardness of rubber and plastic materials (i.e. polymeric materials such as geomembranes). In particular, two types of Shore hardness scales are specifically utilized for polymeric/plastic materials: Shore A (H_A) scale is generally preferred for relatively "softer" plastics; while Shore D (H_D) is used for relatively "harder" plastics (e.g. geosynthetics) to obtain an index value of surface hardness.

2.4. Shore D Hardness Measurements: Testing Equipment and Procedure

The geomembrane continuum sheets produced from a base polymer PVC are categorized in the class of relatively hard plastics. Shore D hardness scale, (H_D) ranging from 1 to 100 on Type D durometer gauge was an appropriate technique to attain a scale for surface hardness of the PVC geomembranes in a consistent manner for the purpose of quantitatively assessing such important physical property of those geomembrane liners employed in geoenvironmental applications (landfills). Shore D Hardness, (H_D) measurements, which are conducted in accordance with [7] using a durometer with constant loader test stand (Fig 1), provide an index value of the material

surface hardness which can then be used in evaluating the interface frictional characteristics of geosynthetic materials counterfaced by granular soils.

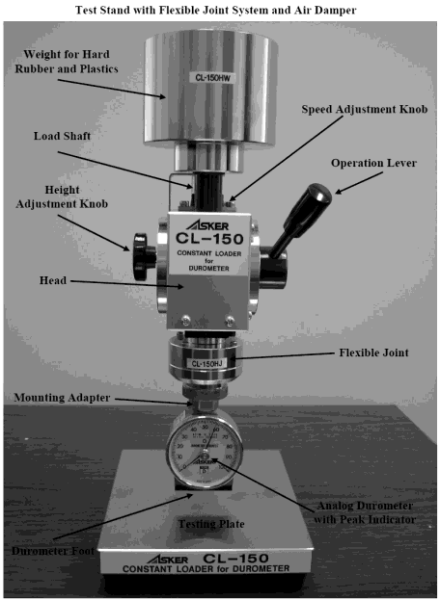

Fig 1. Durometer with constant loader test setup: Flexible joint system and air damper

The continuum material (polyvinylchloride (PVC) geomembrane liner) used throughout this study were neither corrugated nor textured and had clean smooth surfaces. The PVC geomembrane specimens were composed of plied pieces to obtain the minimum thickness with the intention of accurate determination of hardness with the durometer as required by [7]. Hardness measurements were taken at various locations of each specimen to reduce error in measurements by following a random pattern, to observe the variability in surface hardness of intact solid continua (geomembrane) and to investigate the variation in readings across the bulk. Further, for precise surface hardness measurements of polymeric plastic materials, there is a fundamental and important criteria required to be in consideration primarily which is the repeatability/steadiness and consistency of the implementation of durometer measurements. To this end, the constant loader test stand with an adjustable damping system as shown in Fig 1 was selected to ensure a constant speed of downward movement of the load shaft provided reliable and dependable results. This type of constant load stand maximizes repeatability of hardness tests by providing a variable speed control and a flexible joint on the load shaft to ensure complete contact with the sample material as well as to ensure consistent measurements by applying a consistent force throughout all the measurements.

2.5. Detection and Determination of Frictional Properties of PVC Geomembrane Interfaces

The frictional properties of geomembrane interfaces counterfaced with granular materials (i.e. sand) can physically be simulated (modeled) and assessed by performing interface shear tests in the laboratory environment. In this type of performance tests preferred by the engineers for evaluating one of the most important mechanical property (i.e. shear strength) of composite layered systems such that one component of counterface is maintained stationary (no motion) by fixing onto an immobile compartment; and other component of counterface is allowed for displacement relative to the stationary counterface component.

2.6. Interface Shear Strength Measurements: Testing Device and Methodolgy

The interface shear tests involving the particulate material (i.e. sand) and a continuum planar surface material (i.e. geomembrane) were performed by utilizing a Teflon shear box connected to the large displacement interface direct shear device. The box was laterally displaced on the upper surface of the geomembrane specimen that was fastened by clamping metal strips with bolts on a heavy metal block testing platform (Fig 2).

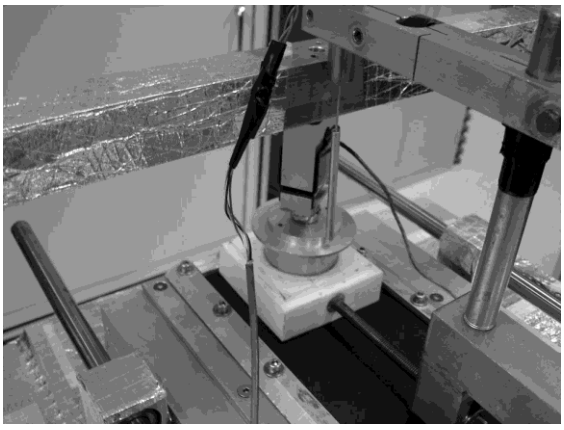

Fig 2. Sand – Geomembrane Interface Shear Testing Equipment

The normal load was applied on the sand specimen contained in the Teflon shear box through a metal cross beam by pressurizing the pneumatic cylinder. A metal round top cap was placed on top of the specimen and at the bottom of the load cell used to measure normal force. In addition, a steel ball was placed in between the normal load cell and the round top cap to prevent moment or eccentric forces from occurring during the test. Lateral and vertical displacements were measured by using a horizontally mounted LVDT attached on a moving metal frame connected to the lateral loading shaft and a vertically located LVDT on the round top cap over the sand specimen, respectively. The normal force and shear force were monitored by the normal load cell located under the loading cross beam and the shear load cell mounted on the lateral loading shaft that moved horizontally during the experiments.

3. RESULTS AND DISCUSSIONS

The shear resistance with respect to slope stability along various geosynthetic component interfaces (i.e. sand – geomembrane) is an important design issue for multi-layered composite systems. A number of case histories by [8-10] revealed that a geomembrane can create a problematic interface due to low frictional

resistance between it and soil or another geosynthetic component. To this end, the experimental results of this study that will be presented will enable deeper insight and further understanding on mutual mechanical performance (strength) of composite layered systems employed in various geoenvironmental applications. Since the mobilized frictional strength and the developed interface shear behavior at particulate material (sand) – continua (geomembrane) interfaces are strongly influenced by the surface hardness of the geomembranes. Therefore, the measured index value of hardness of the geomembrane based on a particular scale (i.e. Shore D) will provide a useful quantitative value to indirectly evaluate the magnitude of shear resistance being generated at the interface between granular soil and geosynthetic. Therefore, it is noted that the amount of shear resistance developed at the interface is mainly attributed to geomembrane surface pliability governed by the material hardness.

3.1. PVC Geomembrane Surface Hardness and the Variability in Measurement Data

A total of 30 measurements (Fig 3) were performed on PVC geomembrane plied samples stacked on top of each other making sure there was no air between the layers. In order to maintain consistency in measurements and to obtain accurate test results, it is required to conduct all the hardness measurements with the same speed for all the materials tested. It is recommended as good practice to take several readings and average the results by showing the variability in measurement data. The readings, in general, indicated that the variability in measurements was consistent for all the samples tested and the 30 repeat measurements were more than sufficient to constitute a sample population to evaluate the surface hardness of PVC geomembrane liners. Additionally, the variability in the measurement data and some statistical results on the Shore D surface hardness measurements are listed in Table 1.

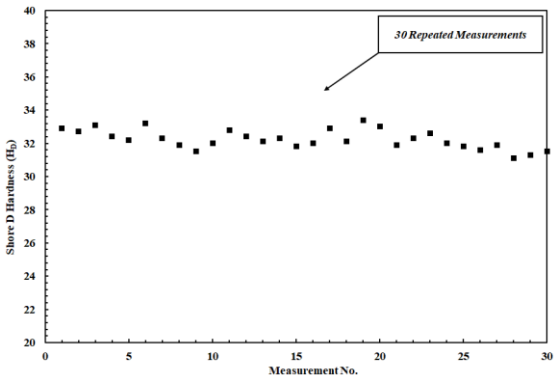

Fig 3. The overall shore D, (H_D) hardness measurements on the material surface of PVC geomembrane samples

As evident from Fig 3 and Table 1, the consistency in measurements on relatively soft and flexible geomembranes produced from PVC could be a beneficial advantage of this polymeric material in the field because of it possessing more consistent global material properties in terms of predicting a general index value by performing measurements on a limited portion of the material over a restricted region for estimating the durability properties of this polymeric geomembrane liner employed in situ over a very large area where probable variations in ambient conditions influencing material endurance characteristics may exist in large areal extent geoenvironmental projects.

Table 1. Variability in measurement data and some statistical results for PVC geomembrane

Specimen Material	Mean	Standard Deviation	Range
PVC	32.2	0.582	2.3

3.2. Interface Friction Angle and Hardness

The general model previously proposed by [5] for predicting frictional resistance of granular soil-polymeric material interfaces is as follows (Equation 1):

$$\frac{\delta}{\varphi'_{ds}} = -0.0088 \times H_D + 1.15 \quad (1)$$

Where;
δ: Interface Friction Angle
φ'_{ds}: Soil Direct Shear Friction Angle
H_D: Polymeric Material Shore D Hardness

This general model was based on a correlation by assessing interface peak friction angle with the knowledge of soil internal friction angle whereby the ratio of interface angle of shear resistance, (δ) to direct shear angle of soil friction (φ'_{ds}) was related to Shore D Hardness (H_D) index of the polymeric materials. The results of experimental data from laboratory testing programs conducted to explore direct shear angles of Ottawa 20/30 and Blasting sands as tabulated in Table 2 were utilized and a new model has been developed in this study by substituting direct shear angle of soil friction (φ'_{ds}) into the interface property (δ/φ'_{ds}) – hardness relationship to establish a direct correlation between interface friction angle (i.e. peak and residual states of interface shear response) and surface hardness for Ottawa 20-30 Sand – PVC Geomembrane and Blasting Sand – PVC Geomembrane interfaces as given in Equations 2 and 3, respectively. In this way, interface friction angle (i.e. either peak or residual) of sand-geomembrane interfaces can be evaluated with respect to hardness change.

Table 2. Peak and residual direct shear angles for ottawa 20/30 and blasting sands

	$\varphi'ds$ [Peak]	$\varphi'ds$ [Residual]
Ottawa 20-30 Sand	39°	28°
Blasting Sand	43°	35°

$$\delta_{peak} = -0.3432 x H_D + 44.85 \quad (2a)$$

$$\delta_{residual} = -0.2464 x H_D + 32.20 \quad (2b)$$

$$\delta_{peak} = -0.3784 x H_D + 49.45 \quad (3a)$$

$$\delta_{residual} = -0.3080 x H_D + 40.25 \quad (3b)$$

Using the developed empirical relationships (Equations 2 and 3), the peak and residual friction angles (δ_{peak}, $\delta_{residual}$) for Ottawa 20-30 Sand – PVC Geomembrane and Blasting Sand – PVC Geomembrane interfaces have indirectly been calculated based on Shore D surface hardness measurements as presented in the previous section and the computed values of δ_{peak} and $\delta_{residual}$ for those two interface systems are listed in Table 3.

Table 3. The Indirectly Computed Peak and Residual Interface Friction Angles for Ottawa 20/30 Sand – PVC Geomembrane and Blasting Sand – PVC Geomembrane Interfaces

	δpeak	δresidual
Ottawa 20-30 Sand – PVC Geomembrane	33.8°	24.3°
Blasting Sand – PVC Geomembrane	37.3°	30.3°

The preceding empirical models (Equations 2 and 3) between peak or residual interface friction angles (δ_{peak}, $\delta_{residual}$) and surface hardness were developed by interrelating/linking the corresponding frictional resistance parameters for engineering design in the relationships described based on the results of durometer hardness measurements on PVC geomembrane samples. They could be utilized as a mathematical correlation to rapidly evaluate the effects of the change in hardness of the materials at the interface in which both δ_{peak} and $\delta_{residual}$ values follows a inverse linear pattern with increasing hardness for only the geomembrane liners manufactured from PVC base polymer resins. For the other geomembrane types produced from different resins (i.e. HDPE, MDPE, LLDPE or VFPE), the mathematical relation and variational trend between δ and HD will likely be different.

3.3. Results of Interface Shear Tests on Particulate versus Smooth Continua

Ottawa 20-30 Sand – Smooth PVC Geomembrane Interface Systems

A series of interface shear tests involving Ottawa 20-30 sand (rounded grains) and smooth PVC geomembranes were performed at a range of normal stress levels from 25 kPa up to 400 kPa. Stress – displacement curves are presented in Fig 4. A rapid increase in shear stress up to peak stage within 1–2 mm of displacement was observed. This was followed by a reduction to some lower residual shear stress condition with continued loss in frictional resistance as shearing displacement progressed until the termination of the test at 60 mm horizontal displacement. Further, the increase in normal stress from 25 kPa up to 400 kPa resulted in an increase in the displacement to peak.

Blasting Sand – Smooth PVC Geomembrane Interface Systems

Shear stress – horizontal displacement failure curves at different normal stresses ranging from 25 kPa to 400 kPa for smooth PVC geomembrane sheared against Blasting sand (angular grains) are presented in Fig 5. The interface direct shear tests performed using angular sand resulted in higher peak and residual (post-peak) strengths at all loading conditions as compared to rounded Ottawa 20-30 sand. One interesting aspect of the plots is the relative shape of the different curves such that the stress-displacement curves corresponding to the low normal stress condition (25 kPa) resulted in an initial rise immediately in stress at very small displacements with a slight reduction in frictional resistance after the peak strength state was mobilized. However, as the magnitude of applied normal stress increased to higher stress levels (100 kPa and 400 kPa), the stress-displacement curves for the angular sand exhibited well-defined peak state that was followed by a decrease to a residual state.

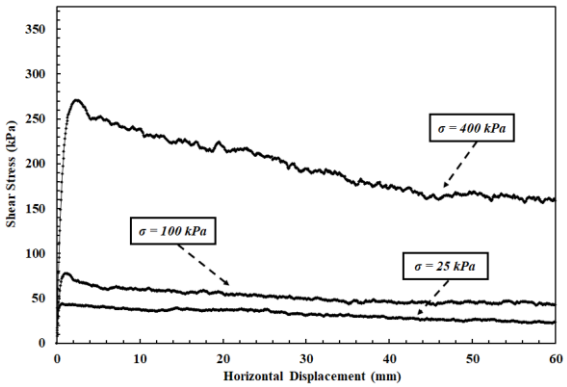

Fig 4. Shear stress – displacement curves at various normal loading conditions including: 25, 100, 400 kPa for ottawa 20-30 sand – smooth PVC geomembrane interface

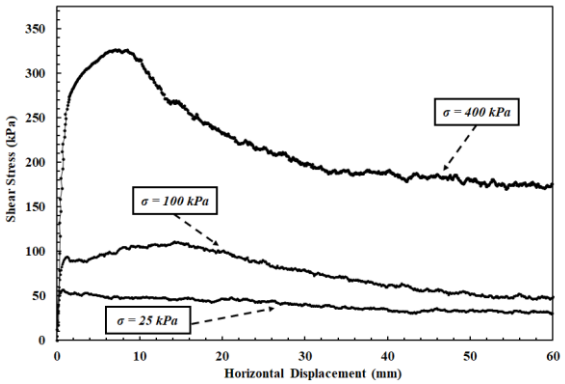

Fig 5. Shear stress–displacement curves at various normal loading conditions including: 25, 100, 400 kPa for blasting sand – smooth PVC geomembrane interface

4. FURTHER DISCUSSIONS ON THE EXPERIMENTAL FINDINGS

In light of the results of the experimental program, it was found that the mobilized frictional strength at granular material – geomembrane interfaces at different normal loading conditions is primarily influenced by the surface hardness of the counterface geomembrane. On this aspect, the measured index value of hardness of the geomembrane surface based on a standard scale (i.e. Shore D in this case) provided a useful quantitative value to evaluate and gauge the magnitude of shear resistance generating at the interface of granular soil – geosynthetic material.

Therefore, it was accomplished that the influence of a physical property of a polymeric geomembrane liners (i.e. hardness) on the mobilized interface shear strength at different loading conditions can indirectly be assessed through the use of the proportional value of δ/φ'ds which applies both for particulate material characteristics and continuum material surface properties. This normalized quantity provides a more comprehensive approach for evaluating shear properties of granular versus polymeric continuum material interfaces.

The peak and residual strengths increased with the use of angular sand instead of rounded sand at all loading conditions, the direct shear tests were performed, such that the angular sand system showed substantially higher interface strength characteristics regardless of normal stress level, and required larger horizontal displacements to reach both peak and residual state. This phenomenon is principally attributed to the amount of sand particle rearrangement occurring during shearing process as the Blasting sand is an angular material and possesses higher internal friction as being more interlocked and hence, more resistant to shear displacement. As a result, the particles on the interface surface are less likely to be rearranged during the course of shear displacement unless the applied shear stress on the interface is sufficiently large to overcome the internal friction of the particulate material itself compared to the Ottawa 20-30 sand consisting of rounded particles in which the rounded particles can easily rolling over each other and rearranging during shearing. As such, the rearrangement of the particles near the contact surface occurs with ease as the smoother rounded nature of Ottawa 20-30 sand grains. Additionally, owing to Blasting sand grains possessing relatively rough surface characteristics as compared to Ottawa 20-30 grains, angular sand – smooth PVC geomembrane system mobilized significantly higher peak and substantially larger residual shear strengths than rounded sands with increasing normal load.

5. COMPARATIVE ANALYSIS BETWEEN DIRECT TEST RESULTS AND INDIRECT PRACTICAL EVALUATION

Fig 6 shows peak interface friction angle (δ_{peak}) and residual interface friction angle ($\delta_{residual}$) plotted as a function of normal stress level for smooth PVC geomembrane interfaces sheared against rounded Ottawa 20-30 sand and angular Blasting sand, respectively, to make a comparative analysis between direct measurement test results (i.e. experimentally evaluated) and indirect assessment values (i.e. computationally evaluated) analytically calculated using empirical correlations. Reasonable similarity between the laboratory test results and the indirect analytical assessment analysis is evident from the proximity of the experimentally measured values at the predetermined normal loading conditions to the empirically computed values. The indirect assessment values from empirical equations generally concur with the direct measurement results from interface shear tests performed in the laboratory with particularly an exception of the 25 kPa normal stress level for the rounded Ottawa 20-30 sand and the angular Blasting sand granular material interfaces both of which counterfaced by the PVC geomembrane liners that shows a notable substantial difference. This is attributed to the occurrence of sand dilation during the course of shear displacement. As such the sand structure dilated which resulted in the development of higher frictional resistances and obtaining greater magnitude of the interface strength values in terms of δ at low normal loading condition of 25 kPa stress level owing to smaller magnitude of confinement applied on the interface.

Furthermore, it is noted that the dilation initiates from the sand grains existing at the contact surface and adjacent to the interface and progresses through the other sand grains beyond the contact surface and positioned within the volume of the sand sample [1]. These particles are relatively free to rearrange their contacts (interlocking between the grains), and thus dilate. As seen in the comparison plots for both δpeak and δresidual frictional properties presented in Figure 6, the response of the two different interface systems (Ottawa 20-30, Blasting) at other loading conditions including 100 kPa and 400 kPa normal stress levels, the test results from experimental direct measurements are similar to the resultant indirectly computed values using the proposed empirical relationships previously presented in the paper.

Additionally, the experimental data in Figure 6 show that both the peak and the post-peak interface friction angle (δpeak, δresidual) decreased with an increase in the normal stress. This relationship concurs with Archard's Theory on elastic deformation friction [11]. The rate of this reduction depends on the shape (i.e.: angularity) of the sand particles, and most importantly, the hardness of the counterface geomembrane which is strongly influenced by the geomembrane liner core material type (i.e. PVC). As such, the friction angle for the tested sand (rounded, angular) – smooth geomembrane (PVC) interfaces decreased with normal stress at low normal stress levels up to ~100 that is consistent with Hertzian contact theory [12]. Under higher normal stresses, the coefficient of friction became constant or continued to decrease slightly with normal stress. This is considered to be the influence of the plowing effect that often occurs at a granular material/planar surface interface as previously noted by [1].

Moreover, the indirect assessment results predicted through the developed empirical equations are marginally higher than that of the direct shear tests for particularly the greatest normal stress level of 400 kPa (Fig 6) in which the sand specimen exhibited larger amount of contraction during shearing. This is further demonstrated in Fig 7 that the percentage error in indirectly evaluated peak and residual friction angles obtained through the developed empirical relationships with respect to the direct measurement test results are negative and notable, in particular, for angular Blastind sand interface system. Two compensating effects occur simultaneously during shear displacement. The sand specimen tends to dilate in order to generate a larger internal frictional strength due to the increased shear resistance mobilized at the interface resulting from the deeper

sand particle penetration. At the same time, the sand specimen is subject to volumetric contraction due to highly increased confinement effect of loading at the magnitude of 400 kPa. As such, the dilation in the sand structure was significantly prevented due to compressing and contracting impact of the larger loading conditions (400 kPa) applied on the sand specimen in such a way that a larger volumetric contraction compared to that at low normal stresses was exhibited as a result of the higher confinement of the interface.

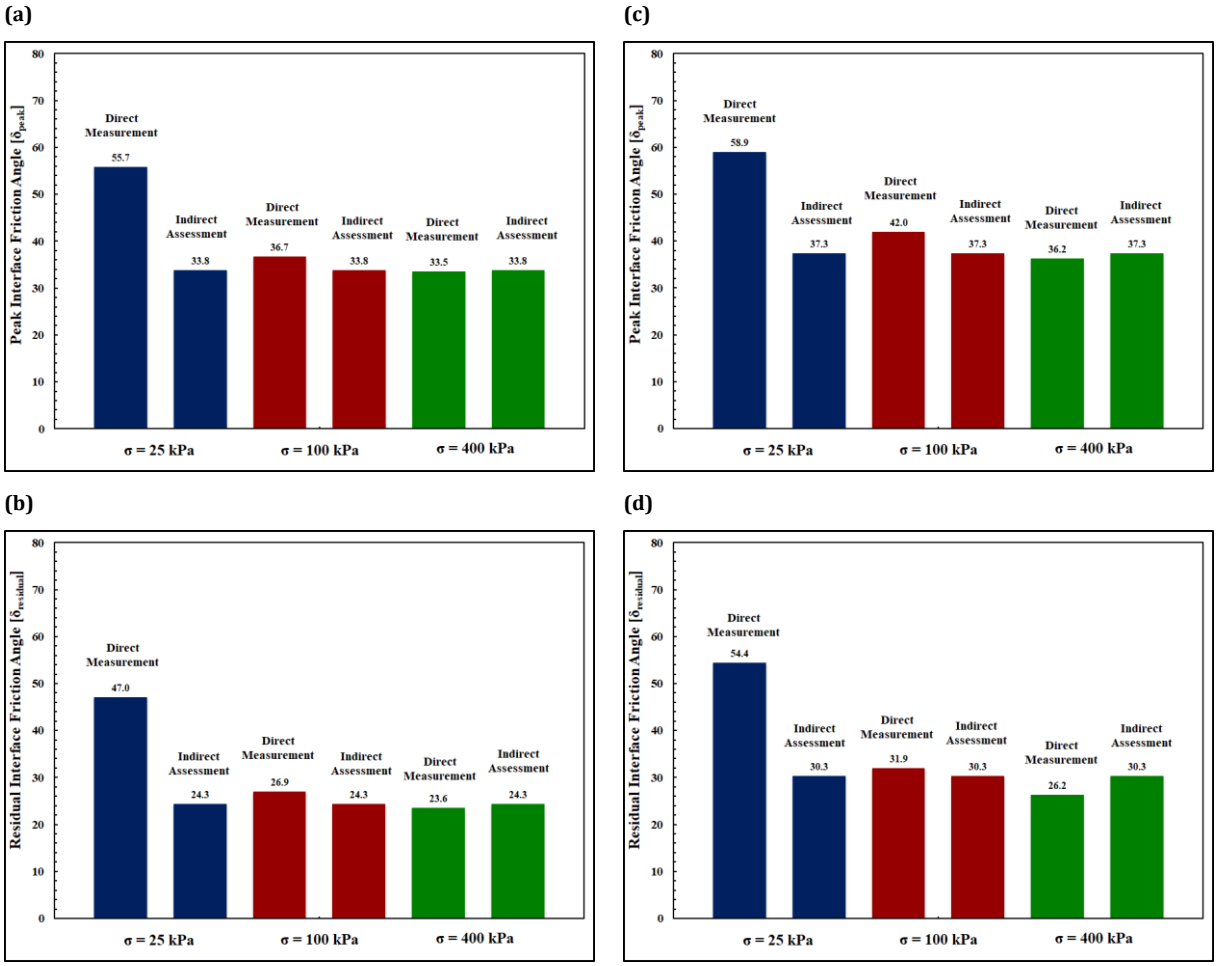

Fig 6. Comparison between direct test results of interface shear tests and indirect evaluation using the developed empirical relationships: Ottawa 20-30 sand–PVC geomembrane (a), (b) and blasting sand–PVC geomembrane (c), (d)

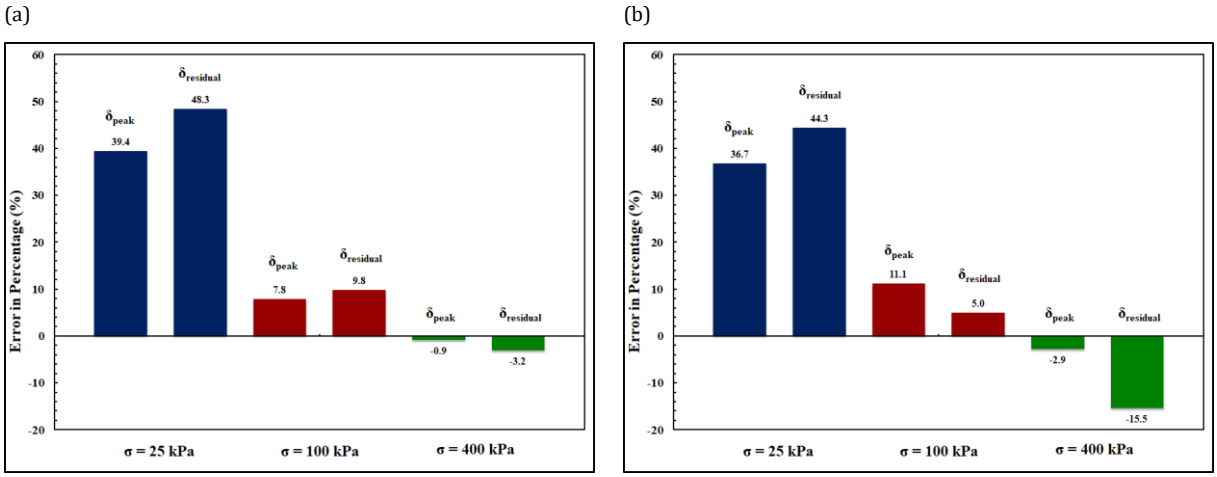

Fig 7. Percentage error in indirectly evaluated peak and residual friction angles computed using the developed empirical equations with respect to direct measurement test results: Ottawa 20-30 sand–PVC geomembrane (a); blasting sand–PVC geomembrane (b)

6. CONCLUSION

The results and analysis presented herein demonstrate that the mobilized shear response and the resulting frictional resistance of sand (rounded, angular) – PVC geomembrane interface combinations are highly dependent on a combination of loading conditions, geomembrane physical material properties (i.e. hardness) and particulate shape (i.e. angularity/roundness). For direct and indirect assessment of the resultant [δPeak] and [δResidual] values, the comparative analysis plots were presented in Fig 6 and Fig 7 and a reasonable similarity between the laboratory test results and the indirect analytical assessment analysis is evident from the proximity of the experimentally measured values at the predetermined normal stress levels (25, 100 and 400 kPa) to the computed values from the proposed empirical correlation equations proposed in the paper. Consequently, the practical implication of this study is that the empirical relationships proposed in light of experimental findings as a result of the laboratory testing program could be utilized for quick, indirect evaluation of frictional properties and shear characteristics of granular soil – geomembrane interfaces.

Moreover, the magnitude of the change in geosynthetic interface response and resistance is, in particular, critical and important when short-term perspectives of the structure are in consideration during design. For example, the design considerations for landfill side slopes for which interface shear resistance between geosynthetic components is crucial and designates the performance and stability of the entire infrastructure application. The practical significance of the results presented in the paper provide a rapid and simple means of estimating the interface design engineering parameters simply from measuring Shore D Hardness, HD of the geosynthetic materials practically in situ; thus, the indirect assessment of the expected mobilized frictional resistance of particulate material – geosynthetic interfaces could be rendered possible quickly in the field in place without laboratory testing by creating the necessary ambience in the lab to imitate real field conditions; or, through a developed numerical simulation analysis. As such, the findings and results of this experimental research study showed the importance of counterface material surface hardness on interface shear response of geosynthetic layered composite systems in addition to providing a rapid and simple evaluation analysis methodology for interface friction properties. Based on the correlations and experimental data on a geosynthetic liner produced from PVC core material, the Shore D Hardness, HD was found to be one of the fundamental factors in controlling frictional resistance. Finally, to sum up, as the frictional shear resistance of geosynthetic interfaces is product dependent and project specific, the discussions on the test results herein are aimed to provide comparative analyses on overall interface shear behavior and relative change (i.e. increment versus decrement) of strength parameters (δ_{peak}, $\delta_{residual}$) as a function of normal loading rather than providing specific shear strength values for use in design applications.

REFERENCES

[1]. J. E. Dove and J. D. Frost, "Peak Friction Behavior of Smooth Geomembrane- Particle Interfaces," Journal of Geotechnical and Geoenvironmental Engineering, ASCE, Vol. 125 (7), pp. 544-555, 1999.

[2]. J. P. Martin and R. M. Koerner, and J. E. Whitty, "Experimental friction evaluation of slippage between geomembranes, geotextiles and soils,". In: Proceedings of International conference on Geomembranes, IFAI, Denver, CO, June 20-23, pp. 191–196, 1984.

[3]. R. M. Koerner, J. P. Martin, and G. R. Koerner, "Shear Strength Parameters between Geomembranes and Cohesive Soils", Geotextiles and Geomembranes, Vol. 4(1), pp. 21-30, 1986.

[4]. J. K. Mitchell, R.B. Seed, and H. B. Seed, "Kettleman Hills Waste Landfill Slope Failure. I: Liner System Properties," Journal of Geotechnical Engineering, Vol. 116(4), pp. 647-668, 1990.

[5]. T. D. O'Rourke, S. J. Druschel, and A. N. Netravali, "Shear strength characteristics of sand-polymer interfaces." Journal of Geotechnical Engineering, ASCE, Vol. 116(3), pp. 451–469, 1990.

[6]. P. Haasen. Physical Metallurgy, 3rd Edition, Cambridge University Press, Cambridge, p. 420, 1996.

[7]. ASTM D2240-05, Standard Test Method for Rubber Property - Durometer Hardness, ASTM International, West Conshohocken, PA, USA, 2005.

[8]. R. B. Seed, J. K. Mitchell, and H. B. Seed, "Kettleman Hills Waste Ladnfill Slope Failure. II: Stability Analysis," Journal of Geotechnical Engineering, Vol. 116(4), pp. 669-690, 1990.

[9]. R. B. Seed and R. W. Boulanger, "Smooth HDPE-clay liner interface shear strengths: compaction effects," Journal of Geotechnical Engineering, Vol. 117 (4), pp. 686–693, 1991.

[10]. R. Byrne, J. Kendall, and S. Brown. Cause and Mechanism of Failure, Kettleman Hills Facility, Kettleman City, California, Report Prepared for Chemical Waste Management, Inc. by Geosyntec Consultants, Atlanta, Georgia, 1992.

[11]. J. F. Archard, "Elastic Deformation And The Laws Of Friction," Proceedings of the Royal Society of London, Series A, Mathematical and Physical Sciences, Vol. 243, Issue 1233, pp. 190-205, 1957.

[12]. K. L. Johnson, "One hundred years of hertz contact,". Proceedings of the Institution of Mechanical Engineers, Vol. 196, pp. 363–378, 1982.

Environmental Research & Technology, Vol. 1(4), pp. 22-26, 2018

Environmental Research & Technology

http://dergipark.gov.tr/ert

CONFERENCE PAPER

Recycling posibilities of packaging wastes-the case of Kırıkkale

Oylum Gokkurt Baki[1], Ozan Parlak[2]

[1] Sinop University Engineering and Architecture Faculty Environmental Engineering Department, Sinop, TURKEY
[2] Sinop University Institue of Science Interdisciplinary Environmental Health Programme, Sinop, TURKEY

ABSTRACT

Packaging wastes arise as a result of the use of packaging materials, which are natural resources. Packaging wastes have an important share in solid wastes. For this reason, it is necessary to address the issue with a sustainable waste management plan, to promote recycling activities and to prevent pollution. Another important issue is the data logging system of packaging wastes. The fact that collection activities originating from scavengers can not be recorded, therefore, a proper waste management plan can not be created and it is not known exactly where the raw materials are recycled. Collection and recycling of packaging waste is important and necessary in order to ensure the continuity of sustainable development.

In this study, the process of collecting, sorting and recycling packaging wastes on 31 stations in Kırıkkale province was examined. Stations include markets and shopping areas. The study was conducted by taking daily data for January, February, March and April 2017. The collection process was carried out for every 2-3 days with 2 workers who were working in packing waste collecting-sorting and plastic breaking production facility. The collected packaging wastes are separated according to their composition. Wastes collected by vehicles were brought into service and weighed.

Paper packaging and PE plastic types wastes are sent to facilities that have a recycling license by pressing. PP plastic packages were turned into burrs and sent to licensed recycling plants. Packing waste outside of paper cardboard and plastic types is not collected because it is not a receiver unit in the vicinity.

In the study, recycling of packaging wastes management with environmental and economical aspects, management components, importation, exports and so on are evaluated. As a result of the study, the management of packaging waste in Kırıkkale was examined and the composition and quantity distributions of the collected wastes were evaluated. In addition, the effects of application of the recycling of packaging waste in Kırıkkale have been evaluated with obtained results.

Keywords: Recovery, recycle, waste management, packaging wastes

1. INTRODUCTION

In parallel with an increase in population in the world and Turkey, the amount of solid waste is increasing day by day and the recovery of solid waste is becoming significantly important. Due to the recovery of packaging waste, natural resources are conserved, energy is saved, the amount of waste is reduced, the requirement for storage area is reduced, the load intensity of the collection system decreases and foreign dependency is reduced if the raw materials required for production are imported [1]. Everyday increasing in the life standarts with increasing daily population causes changes in both waste volume and waste composition. An integrated waste management is a prerequisite for the reduction and disposal of this amount of waste. Today, the first two important steps in integrated waste management hierarchy are: waste prevention and waste reduction. The others are respectively; re-use, recycling, recovery and finally as final disposal [3].

The most important share among solid wastes is packaging wastes. Packaging wastes are recyclable because they are manufactured from materials, such as glass, plastic, metal, paper and composite. Recycled

Corresponding Author: oylumbaki@gmail.com (Oylum Gokkurt Baki)
Received 28 June 2018; Received in revised form 28 September 2018; Accepted 8 October 2018
Available Online 18 October 2018
Doi: ISSN: 2636-8498

This paper has been presented at EurAsia Waste Management Symposium 2018, Istanbul, Turkey

packaging wastes are often used as secondary raw materials by incorporating them in the production. In order to recycle packaging wastes, it is necessary to collect them separately from garbage in the same way as in developed countries and deliver them to the recycling industry in a clean way.

The largest proportion of recoverable waste is paper and cardboard with 45.5%, glass with 18.5%, and packaging waste with petroleum origin with 22.7% [4].

2006 in Turkey on Packaging and Packaging waste recovery rate in the total solid waste according to the statistical result is given as 33% [5].

Thus, it is necessary to collect packaging wastes by the waste producer in a separate bag or box in a clean and healthy way. The works including the collection of wastes separately from the landfill in a clean and organized way, the transport to the separating plant and the delivery to the relevant recycling industry after separation according to types are called "*separate collection at source application*". Packaging wastes can be collected in a separate, clean, efficient, healthy and hygienic way with separate collection at source applications [2]. Separate collection at source is the most accurate way of collecting packaging wastes, but there are few applications of this in Turkey. As in this study, packaging wastes are collected in a mixed way and then separated according to their composition in the related plants. In study, the management this and importance of packaging waste were examined with a pilot study.

2. MATERIALS AND METHOD

The study was carried out in a facility located in Kırıkkale, which has a total area of 5252 m^2 and operates in packaging waste collection, separation and non-hazardous waste recycling activities. The process started with the collection of packaging wastes from thirty one stations. The red dots on the map indicate A-group supermarket chain while blue dots indicate B-group supermarket chain (Fig 1).

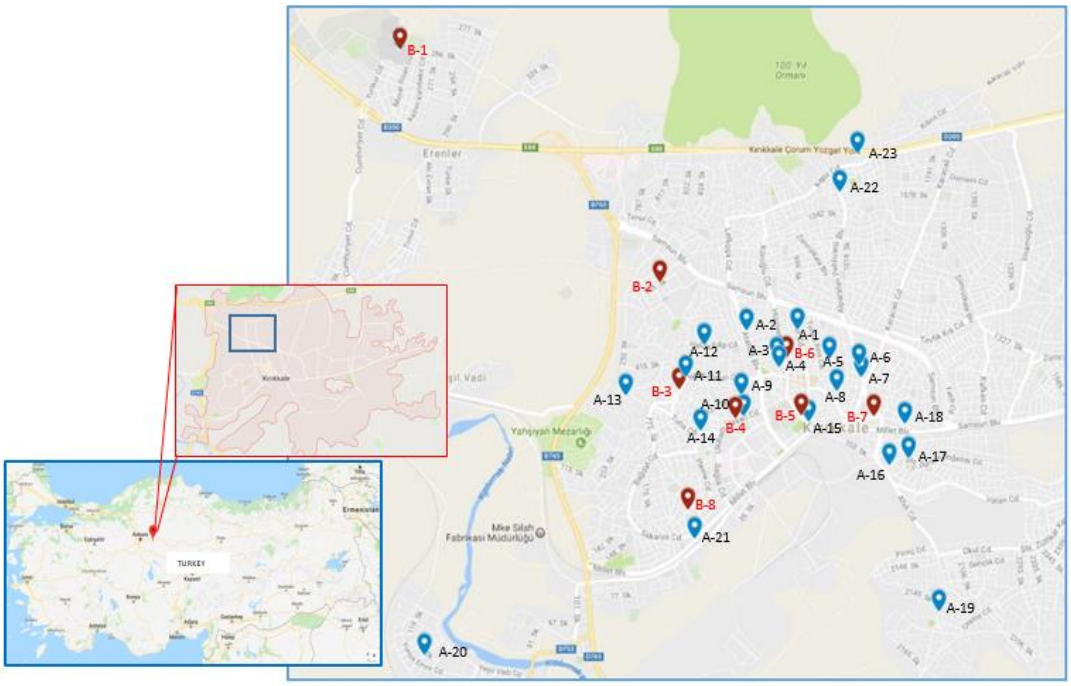

Fig 1. The location of Kırıkkale in Turkey and study area and sampling stations

The collection was carried out in January, February, March and April of 2017. The collection of wastes was done by two workers.

Data were obtained from a total of 32 stations. These stations are markets where packaging waste is concentrated. The collection was carried out every 2 to 3 days within the specified 4 months. The packaging collection tools (PP, PE and paper-cardboard) were collected from the stations together with the package collection tool and 2 personnel. Then, the collected packaging wastes were stored in the mixed storage area and the wastes in the separation unit were separated according to their types. During this process both types of wastes were determined and their quantities were determined.

After this process, the pressing packages were pressed and shipped for re-use.

The packaging wastes were brought to the separation plant and separated into four basic groups: paper, glass, metal and plastic. The wastes brought to the plant as mixed were taken to the separation band and then the staff responsible for separating each material group completed the separation process on two sides of the band. The separation staff separated packaging wastes passing over the band according to their type. The separated packaging wastes, which were accumulated in the sections on the band, were taken to the pressing unit and the pressed wastes were stacked according to their types and stored for the delivery to the relevant recycling facilities.

The whole process in the plant is as follows: the collection of packaging wastes from the market, the storage of them in the mixed storage area, the separation of wastes according to their types in the separation unit, the pressing of packaging wastes and the delivery of pressed packaging wastes.

The packaging waste collection and sorting activity unit of the plant includes mixed warehouse area, metal warehouse area, paper-cardboard warehouse area, plastic warehouse area, pressing areas. The packaging waste collected from the market in this unit is separated and transported to the vehicles by pressing. In the press machine, the packaging waste that has been separated into the facilities is pressed and made ready for shipment. 100 tons of paper-cardboard packaging and 50 tons of metal packaging are pressed daily in the press machine.

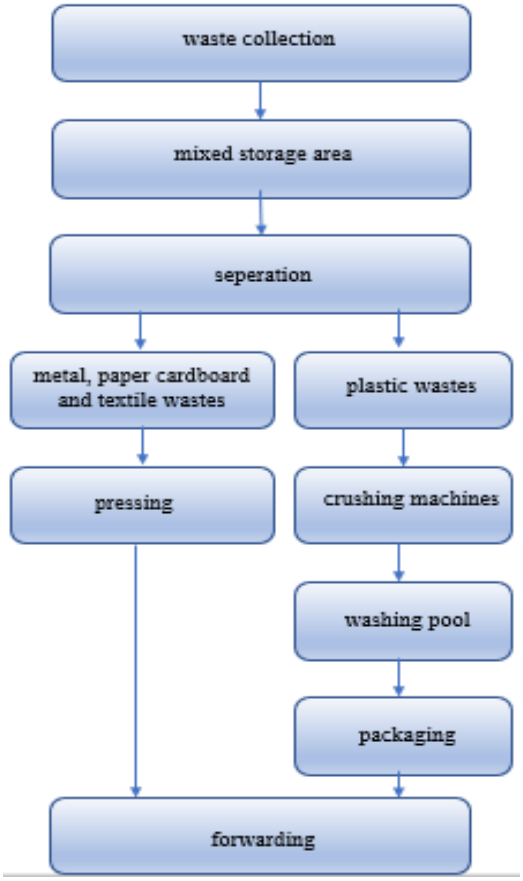

Fig 2. Packaging waste collection - separation activity management scheme

3. RESULTS AND DISCUSSION

The packaging wastes were stored in the cages in the storage area of the shop. It was determined that the cages had a waste collection capacity between 20 and 40 kg. According to the workload of the shops located in stations, it was determined that the shops used one to four cages per day. It was found out that the wastes coming from the stores consist of three groups: PP, PE and paper cardboard. Fig 3 shows the compressed waste papers and plastic wastes in the plant.

The waste types and quantities of the stations in January, February, March and April of 2017 are given in Table 1. As seen in Table 1, two of A stations group and only one of B stations group are not active stations In general, waste compositions and their quantities are increasing or decreasing according to their capacities.

Fig 3. Waste paper in the form of compressed and sent to the recycling of plastic waste before processing

Paper packaging and PE plastics were pressed and delivered to the facilities having a recycling license while PP plastic packages were turned into burrs and sent to license recycling facilities. Fig 4 and Fig 5 shows the overall composition distribution for January, February, March and April of 2017.

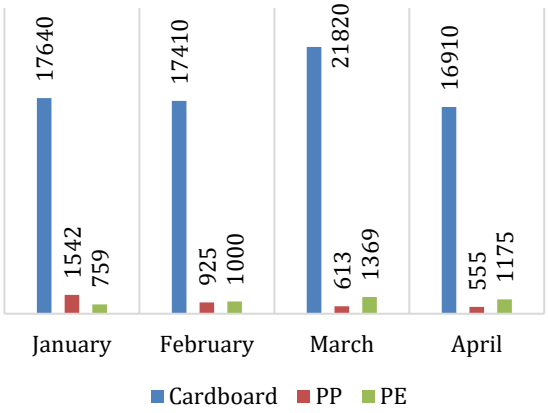

Fig 4. Packaging wastes amounts of January, February, March and April 2017

Table 1. Amount and composition of the stations for January, February, March and April 2017

Stations	January	February	March	April
A-1	870	785	820	885
A-2	545	578	610	570
A-3	705	710	703	700
A-4	920	899	902	900
A-5	515	450	425	415
A-6	355	368	295	370
A-7	360	350	366	375
A-8	470	485	550	560
A-9	240	195	230	185
A-10	515	493	412	415
A-11	365	352	380	365
A-12	1065	950	882	600
A-13	445	550	772	940
A-14	temporarily non-active station			
A-15	350	287	292	260
A-16	160	155	164	130
A-17	615	555	512	490
A-18	130	155	169	185
A-19	540	552	541	580
A-20	temporarily non-active station			
A-21	395	412	420	430
A-22	730	698	725	690
A-23	160	156	125	130
B-1	945	987	953	915
B-2	785	775	730	720
B-3	temporarily non-nactive station			
B-4	150	175	180	200
B-5	160	183	195	200
B-6	185	170	150	130
B-7	270	263	255	285
B-8	155	190	185	230
Total	13,100	12,878	12,943	12,855

Paper, cardboard and other types of packaging waste other than plastic types are not collected because they are not the receiving units in the vicinity. In the plant process, appropriate process change for waste reduction is being investigated. For the moment, there is no change to waste reduction in proce- dures. Wastes that are accepted for processing plastic materials (except packaging), plastic and rubber, paper and cardboard packaging, plastic packaging, wooden packaging, metallic packaging, composite packaging and glass packaging waste recycling and also used again in the administrative office waste and the waste printing tiles containing dangerous substances are replenished and refilled. Edible liquids and fats resulting from the food prepared for the crew are deposited in the licensed company's waste collection bin and given to the licensed company. Mixed municipal wastes of the facility are taken with the municipal waste collection vehicles of Kırıkkale Municipality and forwarded to the regular landfill site. Alkaline batteries originating from the administrative office were collected from 2017 and collected by the Portable Battery Manufacturers (Tap) Association. In addition, hazardous wastes generated during operation are subjected to recycling.

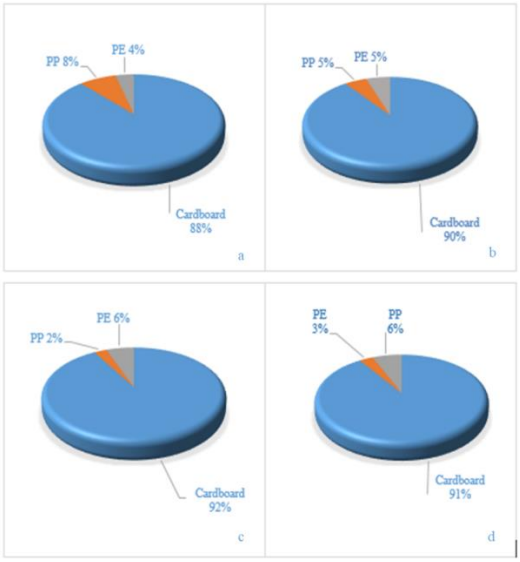

Fig 5. Packaging wastes distribution of (a) January, (b) February, (c) March and (d) April 2017

4. CONCLUSION

Collection waste at source is a time consuming, costly work that requires manpower. A healthy and productive recovery work is possible with a system that will be realized by a coordinated work of all parties. In order to efficiently operate the packaging waste management system and satisfy the public, it is necessary to operate the collection system effectively as planned.

In Turkey, the amount of solid waste and its composition has changed in parallel with population growth, changing living standards and the developments in technology and the recovery of

packaging waste, which has high volume in solid wastes, has gained great importance.

In order for the packaging waste management system to be operated efficiently, it is necessary to operate the collection system effectively as sustainable planned. For this reason, the collection system is very important part of the management and should be easily accustomed and applicable in accordance with the social, economic and environmental perspective of the society.

At the end of the study, only paper cardboard and plastic types were obtained. The delivery of collected packaging wastes to the relevant recycling facilities is the last step in the process. Because there are no facilities around Kırıkkale for delivering packaging wastes other than plastic and paper cardboard wastes, packaging waste types except these wastes cannot be collected. In this regard, appropriate process changes for waste reduction in the plant process have been investigated.

A fact that emerged in the process of study, in order to collect the packaging wastes separately at the source, it has been obliged to collect the packaging wastes from the houses and the packaging waste enterprises by acting together with the municipalities, licensed companies and authorized organizations. The collection process is the most costly part of the management system as our study. And also as the collection of waste at the source is time consuming and laborious. The municipalities have very serious duties.

ACKNOWLEDGMENT

This study was presented as a poster presentation in the Eurasia 2018 Waste Management Symposium.

REFERENCES

[1]. N. P. Karamangil. Characterization of the recovery and disposal of packaging waste in Turkey, M.Sc., Gebze Institute of Technology, Institute of Science and Technology, Gebze. 2008.

[2]. A. Çoban and S. Kılıç. “Policies for the environment of local governments in Turkey: Konya Selçuk Municipality,” SELKAP Example. Selcuk University Journal of Social Sciences Institute, 22/2009.

[3]. M. N. Alpaslan. “Solid Waste Management ", Chamber of Environmental Engineers, Ankara, 6-33, 2005.

[4]. MEF. Ministry of Environment and Forestry, "Packaging and packaging waste statistics 2006," Packaging Bulletin Specification: 3, 2009.

[5]. S. Maden. Establishment of packaging waste collection and separation facilities, cost analysis and operation. Master Thesis, Yıldız Technical University Institute of Science, Istanbul, 131 p. 2014.

Environmental Research & Technology, Vol. 1(4), pp. 27-33, 2018

Environmental Research & Technology

http://dergipark.gov.tr/ert

CONFERENCE PAPER

Characterization and optimization of palm industry ash waste (PIAW) derived zeolites using central composite design (CCD)

Said Nurdin[1,*], Syafiqah A. Khairuddin[1], Hajar Athirah M. Sukri[1], Chuah C. Wooi[2]

[1] Faculty of Chemical & Natural Resources Engineering, Universiti Malaysia Pahang (UMP), Lebuhraya Tun Razak, 26300 Gambang, Kuantan, Pahang, MALAYSIA
[2] CH Biotech Sdn Bhd, Kancil str. 3&4, 36400 Hutan Melintang, Teluk Intan, Perak, MALAYSIA

ABSTRACT

The prodigious ashes from power electricity generation plants were devastated as solid waste by palm industries into environment. PIAW, mostly Palm Oil Fuel Ash (POFA) comprising silica and alumina was discarded as non-profit oriented products, thus this work is about PIAW, essentially POFA derived zeolites using ultrasound irradiation. Performance of POFA was characterized, and process optimization was done by employing CCD. Pre-treated POFA as feedstock and formed zeolites were designated and analyzed using X-Ray Fluorescence (X-RF), Scanning Electron Microscopy (SEM) images, Fourier Transform Infrared (FTIR) spectrum and X-Ray Diffraction (XRD) diagram. Alkaline concentration (0.6 M-1.4M), irradiation time (140 min-160 min) and KOH/POFA (1.5:1-2.5:1) were examined as non-constant variables. Otherwise, ultrasonic power (600W), temperature (80°C) and silica alumina ratio were justified as constant and response variables. An optimal synthesized zeolites as ratio of SiO_2 and Al_2O_3 (10.60) was found from surface plot based on quadratic typical at KOH=1 M, KOH/POFA=2 and time=150 min. Presence of A, P, X and irregular shape structures zeolites are commensurable to another resources, mainly fly ash. These findings are also important for waste reduction, recycling and zeolites synthesis from material under economic value.

Keywords: Quadratic model, ultrasound irradiation, alkaline, waste recycling, silica

1. INTRODUCTION

Palm industry ash waste (PIAW) is a by-product from palm oil mills, resulted from combustion of palm shell and bunches for steam generation. PIAW which is palm oil fuel ash (POFA) was devastated as solid waste by palm oil industries. There have been certain ways of the PIAW abundant utilization and treatment such as act as fuel sources in oil palm mill and dumped in landfill. Unfortunately, the PIAW usage for electricity generation via combustion process does not enough due to dispose of approximately 0.25 million tons in landfills [1]. Efforts for PIAW utilization via production of value-added materials have been being done i.e. additive in concrete and cement [4], [5], masonry building blocks [6], adsorbent [7] and filler in natural rubber [8] etc. Alternatively, conversion of PIAW to zeolite could be processed, and it enables the industries to develop the under economic value waste to powerful materials. Previous researchers related with solid waste zeolites from various resources and techniques have been being developed [9], [10].

Zeolites are one of micro-porous materials that commercially used as catalysts and adsorbents like gas separation, etc. Framework of zeolite comprises of three-dimensional connection of SiO_4 and AlO_4 tetrahedra through shared oxygen atoms forming many regular arrangements resulted to an open crystal lattice. As the substitution of an AlO_4 tetrahedron for a SiO_4 tetrahedron, negative charge was created [11]. The crystalline aluminosilicate material has an intense acid strength and a regular molecular sized-pore structure of hydrocarbons [12]. There are several forms of zeolites such as limonite, X-type, Y-type, sodalite and calcium aluminosilicate. Zeolites are commonly synthesized using hydrothermal approach at 200 °C in an alkaline

Corresponding Author: snurdin2@gmail.com (Said Nurdin)
Received 11 July 2018; Received in revised form 21 October 2018; Accepted 21 October 2018
Available Online 31 October 2018
Doi: ISSN: 2636-8498

This paper has been presented at EurAsia Waste Management Symposium 2018, Istanbul, Turkey

medium condition. At similar conditions, different types of zeolites from various sources can be produced. Moreover, the zeolites synthesis were also conducted at temperature range of 90°C-200°C [13], [14]. However, the hydrothermal methods required energy-intensive and time-consuming. Ultrasonic approach could be used to minimize the supplied energy and erforced time [15]. The application of ultrasound for chemical reactions and processes is termed as sonochemistry. Presence of ultrasound during crystallization may affect the physicochemical phenomena which connected to nucleation and crystal growth. The sonification plays crystallization time and temperature reduction many roles, and it can increase the degree of zeolites crystallinity [16]. This paper reported about characterization and optimization of zeolite synthesis from PIAW, mostly POFA using CCD. Effects of KOH/POFA ratio, irradiation time and alkaline-KOH concentration as non-constant variables were investigated.

2. MATERIALS AND METHODS

2.1. *Materials*

The PIAW, mostly POFA was supplied by CH Biotech Sdn Bhd, Teluk Intan, Perak, Malaysia. Potassium hydroxide was ordered by Permula Sdn Bhd, Kuantan, Malaysia. The commercialized zeolites was provided by Gelanggang Kencana, Sdn Bhd, Malaysia.

2.2. Methods

2.2.1. Pre-treatment and performance of PIAW

The PIAW, principally POFA was dried and sieved for foreign and uncombusted palm fibres separation. Next, the used samples were ground for pozzolanic reaction enhancement. Calcination of PIAW was conducted by using a muffle furnace at 800°C for 2 hours. This treatment was subjected to remove unburnt carbon, volatiles matters and others impurities removal. The POFA performance was then identified using X-Ray Flourescence (XRF), Fourier Transform Infrared (FTIR) and Scanning Electron Microscopy (SEM) for composition, infrawave and morphological identification.

2.2.2. Experimental procedure

In mixing steps, potassium hydroxide (analytical grade) was agitated with deionized water. Then, the POFA and KOH were mixed in supersonic device with specification of adjustable Crest Ultrasonic P1800D, like power and temperature (Fig 1). The temperature was set up constant by heater and controller. Frequency and ultrasonic wave power of 45 kHz and 600 W were arranged respectively. Irradiation time (140 min-160 min), alkaline concentration (0.6 M-1.4 M) and KOH/POFA ratio (1.5:1-2.5:1) were preferred as altered variables. Ultrasonic power (600 W), operation temperature (80°C) and silica alumina ratio were substantiated as constant and response variables. The mixture was then filtered to obtain solids of synthesized zeolites and washed until neutral. Obtained filtrate was dried, grinded and stored in desiccator prior to use. The resulted zeolites were then characterized and analyzed.

Fig 1. Crest Ultrasonics P1800D for PIAW derived zeolites optimization

2.2.3. Zeolites characterization

Zeolites characterization was carried out based on obtained optimal process parameters. Morphology, infrared spectra, and X-ray diffraction of synthesized zeolites were recognized and compared with others. Zeolites types, texture and phases were also discovered. Silica and alumina ratio was subjected to ascertain the resulted zeolites interpretation.

2.2.4. CCD optimization

CCD via Design Expert 7 program comprising 15 runs was employed for analysis of optimal synthesized zeolites. The lay out from CCD was tabulated by test run, KOH/PIAW ratio, ultrasonic exposure time and KOH concentration. Five levels with five replicates at the central point, and these set points for each variables with low (coded value: -2) and high value (coded value: +2) were applied , as shown in Table 1.

Response of the experiments was analyzed based on SiO_2/Al_2O_3. The highest silica per alumina ratio was selected as the best condition from PIAW conversion to zeolites. Validated three times of experimental results were approved for process parameter optimization. In front of the terms, positive sign attributed to synergistic effects on the silica-alumina ratio as synthesized zeolites.

Error analysis was calculated between predicted and experimental values as given in the following equation 1.

$$Experimental\ error\ (\%) = \frac{Experimental - Predicted}{Experimental} \times 100\% \quad (1)$$

Effect of the chosen variables and the interaction with each other by obtained silica-alumina ratio as zeolites was illustrated in three-dimensional surface diagram. The results of the CCD were identified and interpreted

by analysis of variance (ANOVA), and coefficient R^2 and R^2 adjusted determination were run by Design Expert 7. Empirical equation was determined by the Fisher variance ratio (the F-test value) for examination of created model. The CCD has also been being widely applied in various adsorption, separation, etc. for optimization [17], [18].

Table 1. The manipulated optimization variables using CCD

	Coded factor levels				
Optimized variables	-2	-1	0	+1	+2
A: KOH/POFA	1.5:1	1.75:1	2:1	2.25:1	2.5:1
B: Irradiation time, min	140	145	150	155	160
C: KOH concentration (M)	0.6	0.8	1	1.2	1.4

3. RESULTS AND DISCUSSION

3.1. Materialization of PIAW

Materialization of PIAW, mainly POFA for zeolites was related on performance analysis. Morphological structure of POFA was distinguished using scanning electron microscopy (Fig 2). The scanning electron diagnosis of POFA shows less fibrous form than cubic structure. Poros characteristics and cubic structure of the PIAW have been found by the SEM image of x 1000. Textures images of POFA revealed diffused melt phase. The POFA has also covered an aluminosilicate glass phase. Absorption band characteristics of POFA were presented by FTIR analysis in Fig 4. Silanol group, Si-OH was reflected by stretch band at 3447.80 cm-1. This band was reported which present in range of 3200-3750 cm^{-1}. The unique characteristics were also found around 1300-1400 cm^{-1} that belongs to alcohol and phenol on adsorbent surface. Al_2O_3 also included in this adsorption band at 550 -875 cm^{-1}. XRD diagram of POFA was illustrated in Fig 5, which it predominantly consisted of aluminosilicate-glass, quartz and mullilite. These structures were almost similar with fly ash. Broad hump around 20^o-22^o and 15^o - 40^o stipulated the amorphous identity of POFA [19]. X-RF analysis of POFA could be exhibited with chemical compounds. The chemical contents of POFA were SiO_2 (50.29%), CaO (18,16%), K_2O (7.10%), Al_2O_3 (6.53%), MgO (6.48%), P_2O_5 (5.62%), Fe_2O_3 (4.02%), TiO_2 (0.37%), Na_2O (0.29%), MnO (0.13%) and ignition loss (1.01%). The POFA constituents of SiO_2, CaO, Al_2O_3 etc. have also been reported by another researchers [20], but the dissimilar composition and characteristics were caused by various operation methods, feedstocks and palm oil plantation areas.

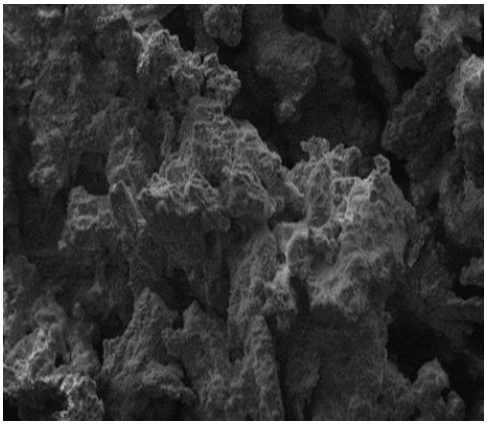

Fig 2. SEM images of POFA at 1000 x magnification

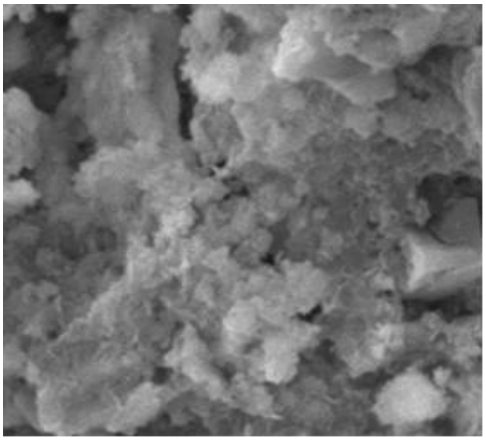

Fig 3. SEM images of zeolites at 1000 x magnification

3.2. Zeolites improvization

Zeolites improvization was also conducted by elemental, X-ray diffraction, morphology and infrared. The infrared analysis results of zeolites were displayed in Fig 4. Characteristic bands were commonly stated to spectra of zeolites. The peaks region 650-720 cm^{-1} attributed to internal tetrahedral: symmetric stretch, 750-820 cm^{-1} corresponded to external tetrahedra: symmetric stretch, and 950-1250 cm^{-1} related to internal tetrahedral: asymmetric stretch [21].

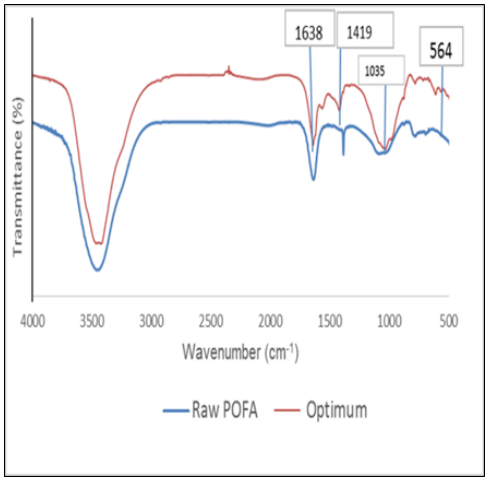

Fig 4. FTIR spectrum of POFA and zeolites (optimum)

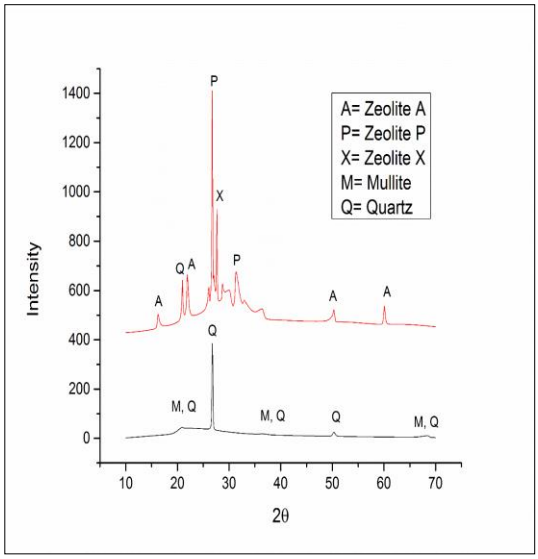

Fig 5. XRD diagram of POFA and zeolites (optimum)

For justification of zeolites presence, there was characteristic peaks within region 420-1200 cm^{-1}, it was IR character of zeolites A [22]. Presence of zeolites A was also supported by characteristic band at 1035 cm^{-1} [23]. Peak at 564 cm^{-1} indicated zeolite X as reported by previous reports [24]. Bands closed to 1419 cm^{-1}, it designated carbonate stretching vibration that facilitated nucleation and zeolites crystallization [25]. The peak at 1638 cm^{-1} was associated with zeolites P [26]. Elemental analysis of zeolites was also governed by SiO_2, CaO, Al_2O_3, etc. The SiO_2/ Al_2O_3 ratio > 5, it reflected the PIAW, typically POFA conversion with high silica zeolites. Morphology of zeolites was identified by scanning electron microscope with 1000 x magnitudes (Fig 3). The image almost match zeolites A and P as obtained by precursory discoveries [27], [28]. Surface morphology and structural were irregular, rough and different compared raw material. Estimated, it was caused by alkali activation and cavitation bubbles from ultrasonic irradiation. Next, zeolites recognition was also examined using X-ray diffraction (Fig 5). The image indicated presence of zeolite A, P and X. Amorphous phase and high intensity peak obtained were virtually similar to former data [29].

3.3. CCD optimization model

3.3.1. Factorial design and quadratic model

Three factorial design: KOH/POFA ratio (A), ultrasonic time (B) and KOH concentration (C) have been optimized by Response Surface Model (RSM) using CCD. The list of experiments designed by CCD is shown in Table 2. Regression analysis was performed to fit the response variable. The results of the CCD were identified and interpreted by analysis of variance (ANOVA), and the final empirical model is presented as:

$$Y = 10.44 + 0.29A - 0.12B - 0.13C - 0.045AB + 0.045AC + 0.13BC - 0.24A^2 - 0.19B^2 - 0.17C^2 \quad (2)$$

where Y is predicted silica per alumina ratio, A is KOH/POFA ratio, B is irradiation time and C is KOH concentration. In front of the terms, positive sign attributed to synergistic effects on the silica per alumina ratio of the synthesized zeolites. The importance of the empirical model was determined by the Fisher variance ratio (the F-test value). Statistically evaluation was subjected to approve the eligibility of used empirical model based on data variations. The model adequacy was elucidated with ANOVA as presented in Table 3.

Regression parameters of the predicted response surface quadratic model were exhibited. Higher F-value is unity, the more certain of the empirical model is described sufficiently, the data variation and the predicted significant terms of the synthesized zeolites are real. With 95% confidence level, the tested model was significant, and the reflected model F-value was 25.28. Obtained R-square was 0.9785, and the found value of 97.9% from total variation in the silica per alumina responses.

Table 2. Experimental layout from CCD

Test Run	KOH/POFA Ratio	Ultrasonic irradiation time (min)	KOH Concentration (M)
1	2.25	155.00	0.80
2	2.25	145.00	1.20
3	1.75	155.00	1.20
4	1.75	145.00	0.80
5	1.50	150.00	1.00
6	2.50	150.00	1.00
7	2.00	140.00	1.00
8	2.00	160.00	1.00
9	2.00	150.00	0.60
10	2.00	150.00	1.40
11	2.00	150.00	1.00
12	2.00	150.00	1.00
13	2.00	150.00	1.00
14	2.00	150.00	1.00
15	2.00	150.00	1.00

The error analysis of actual compared prediction model was < 10%. There are only a 0.12 % chance that a "Model F-value" was large, it could be occured due to noise. The obtained value enables the reliable model in estimating the silica per alumina ratio. Significance model was stated with Probability (Prob)>F less than 0.05. Analysis of variance has also been examined for rapid synthesis of zeolites NaA using microwave with a low probability value (P>F<0) and the model value F = 27.88 exceeded the table value F=2.72 [30]. Both results fitted well and specified the model terms were impressive.

3.3.2. Effects of model components

Effects of the chosen variables interactions with silica per alumina ratio as synthesized zeolites were illustrated in three-dimensional surface plot diagram (Fig 6). At ultrasonic exposure time (145-150 min) and KOH/POFA ratio (2.0 – 2.25), it might be achieved the maximum silica per alumina ratio. The silica per alumina ratio increased up to 10.60, with enlarged KOH/POFA ratio and exposure time. In addition, when KOH concentration, KOH/POFA ratio and irradiation time were extended up to peak, the obtained silica alumina ratio verified optimum value. A good interactions of the two variables within the three-dimensional surface diagram was also assigned by the elliptical shape [31].

3.3.3. Model verification

The CCD model generated during RSM was verified by experiments run for an obsessed optimal medium setting. A KOH concentration of 1 M was found SiO_2 and Al_2O_3 ratio of 10.60 as measured zeolites parameters, at KOH/POFA ratio of 2:1 and irradiation time of 150 min. The experiment was carried out depended on these relevant modes to justify the actual value. The validation data were arrayed in Table 4. Laboratory results revealed SiO_2 and Al_2O_3 of 10.32, which are almost and fitted well with the optimized value using CCD generated by the RSM tool.

Table 3. ANOVA and adequacy of the quadratic model

Source	Sum of squares	Degree of freedom	Mean square	F value	p-value Prob > F
Model	3.08	9	0.34	25.28	0.0012
A	0.68	1	0.68	50.49	0.0009
B	0.11	1	0.11	8.15	0.0356
C	0.14	1	0.14	10.36	0.0235
AB	5.4 E-003	1	5.4 E-003	0.40	0.5557
AC	5.4 E-003	1	5.4 E-003	0.40	0.5557
BC	0.045	1	0.045	3.32	0.1279
A^2	1.31	1	1.31	96.55	0.0002
B^2	0.88	1	0.88	64.98	0.0005
C^2	0.69	1	0.69	50.79	0.0008
Residual	0.068	5	0.014		
Lack of fit	0.014	1	0.014		
Pure error	0.054	4	0.014	1.01	0.3719
Cor total	3.15	14			

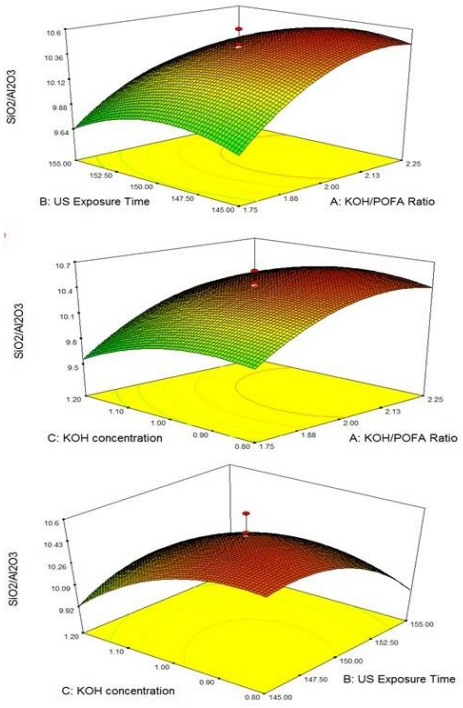

Fig 6. CCD generated response surface plot for PIAW derived zeolites as SiO_2/Al_2O_3

Table 4. Optimization results of PIAW derived zeolites as SiO_2/Al_2O_3

Optimum validation	Experimental/ Actual	Predicted by RSM Using CCD	% Error
1	10.32	10.60	2.64
2	10.03	10.60	5.38
3	10.14	10.60	4.34

4. CONCLUSIONS

Characterization and optimization of PIAW derived zeolites have been exhibited to be efficacious within 150 min of irradiation time at 80°C. The formed zeolites were found at KOH/POFA ratio (1.5:1 – 2.5:1) and alkaline concentration (0.6 M-1.4 M) at ultrasonic power of 600 W. Zeolites performance and treated PIAW were assessed, which showed that the different morphology, chemical substituent, diffraction, infrared and phases are strictly controlled by synthesis operation parameters. Appearance of A, P and X zeolites and asymmetrical structures are comparable with diversified zeolites waste sources. Effects of used variables and its interactions were tested by analysis of variance. Statistically examinations were significant ($p < 0.05$), and some correlations among each other were disclosed. Experimental results (SiO_2/Al_2O_3 = 10.32) acquired were well matched with the optimized value given by the CCD (SiO_2/Al_2O_3 = 10.60). The resulted zeolites as SiO_2/Al_2O_3 from PIAW substantially POFA could be also optimized using additional statistical methods, like Taguchi, etc.

ACKNOWLEDGMENT

The authors are grateful for sponsorship by the Ministry of Higher Education, Malaysia under Grants FRGS-RDU 160126 & RDU 141005, PRGS 160321&160354, CH Biotechs Sdn Bhd for materials providing, Research & Innovation Dept. and Faculty of Chemical & Natural Resources Engineering Laboratory Staff-UMP for technical supports.

REFERENCES

[1]. A. Kongnoo, S. Tontisirin, P. Worathanakul and C. Phalakornkule, "Surface characteristics and CO2 adsorption capacities of acid- activated zeolite 13X prepared from palm oil mill fly ash," *Fuel*, Vol.193, 385–394, 2017.

[2]. Z. Y. Lai and S. M. Goh, "Mechanical strength of binary oil palm kernel shell and HZSM-5 zeolite fuel pellets," *Fuel*, Vol.150, 378–385, 2015.

[3]. N. H. A. S. Lim, M. A. Ismail, H. S. Lee, M. W. Hussin, A. R. M. Sam and M. Samadi, "The effects of high volume nano palm oil fuel ash on microstructure properties and hydration temperature of mortar," *Construction and Building Materials*, Vol.93, 29–34, 2015.

[4]. M. M. U. Islam, K. H. Mo, U. J. Alengaram and M. Z. Jumaat, "Mechanical and fresh properties of sustainable oil palm shell lightweight concrete incorporating palm oil fuel ash," *Journal of Cleaner Production*, Vol.115, 307–314, 2015.

[5]. M. Safiuddin, M. Abdus Salam and M. Z. Jumaat, "Utilization of Palm Oil Fuel Ash in Concrete: A Review," *Journal of Civil Engineering and Management*, Vol.17(2), 234–247, 2011.

[6]. M. E. Rahman, A. L. Boon, A. S. Muntohar, M. N. H. Tanim and V. Pakrashi, "Performance of masonry blocks incorporating Palm Oil Fuel Ash," *Journal of Cleaner Production*, Vol.78, 195–201, 2014.

[7]. C. Acquah, L. S. Yon, Z. Tuah, N. L. Ngee and M. K. Danquah, "Synthesis and performance analysis of oil palm ash (OPA) based adsorbent as a palm oil bleaching material," *Journal of Cleaner Production*, Vol.139, 1098–1104, 2016.

[8]. Z. X. Ooi, H. Ismail and A. Abu Bakar, "Characterization of oil palm ash (OPA) and thermal properties of OPA-filled natural rubber compounds," *Journal of Elastomers and Plastics*, Vol.47(1), 13–27, 2015.

[9]. A. Á. B Maia, R. F. Neves, Rô. S. Angélica and H. Pöllmann, "Synthesis, optimisation and characterisation of the zeolite NaA using kaolin waste from the Amazon Region: Production of zeolites KA, MgA and CaA," *Applied Clay Science*, Vol.108, 55–60, 2015.

[10]. L. Deng, Q. Xu and H. Wu, "Science Direct Synthesis of zeolite-like material by hydrothermal and fusion methods using municipal solid waste fly ash," *Procedia Environmental Sciences*, Vol.31, 662–667, 2016.

[11]. N. Al-Jammal, Z. Al-Hamamre and M. Alnaief, "Manufacturing of zeolites based catalyst from

zeolites tuft for biodiesel production from waste sunflower oil," *Renewable Energy*, Vol.93, 449–459, 2016.

[12]. G. Watanabe, Y. Nakasaka, T. Taniguchi, T. Yoshikawa, T. Tago and T. Masuda, "Kinetic studies on high-pressure methylation of 2-methylnaphthalene over MTW-type zeolites with different crystal sizes," *Chemical Engineering Journal*, Vol.312, 288–295, 2017.

[13]. J. C. Kim, M. Choi, H. J. Song, J. E. Park, J. H. Yoon, K. S. Park and D. W. Kim, "Synthesis of uniform-sized zeolite from windshield waste," *Materials Chemistry and Physics*, Vol.166, 20–25, 2015.

[14]. P. Roy and N. Das, "Ultrasonic assisted synthesis of Bikitaite zeolites: A potential material for hydrogen storage application," Ultrasonics Sonochemistry, Vol.36, 466–473, 2017.

[15]. J. Behin, H. Kazemian and S. Rohani, "Sonochemical synthesis of zeolite NaP from clinoptilolite," *Ultrasonics Sonochemistry*, Vol.28, 400–408, 2015.

[16]. N. E. Gordina, V. Y. Prokof'Ev, Y. N. Kul'Pina, N. V. Petuhova, S. I. Gazahova and O. E. Hmylova, "Effect of ultrasound on the synthesis of low-modulus zeolites from a metakaolin," *Ultrasonics Sonochemistry*, Vol.33, 210–219, 2016.

[17]. B. Sadukhan, N. K. Montal and S. Chattoraj, "Optimization using central composite design and desirably function for sorption of methylene blue from aqueous solution onto Lemna major," *Karbala International Journal of Modern Science*, Vol.2(3), 145-155, 2016.

[18]. N. F. Ramandi, A. Ghassempous, N. M. Najafi and E. Gashemi, "Optimization of ultrasonic assisted extraction of fatty acids from Borago officinalis L. flower by central composite design," *Arabian Journal of Chemistry*, Vol.10(1), S23-S57, 2017.

[19]. M. A. Salih, A. A. A. Ali and N. Farzadnia, "Characterization of mechanical and microstructural properties of palm oil fuel ash geopolymer cement paste," *Construction and Building Materials*, Vol.65, 592–603, 2014.

[20]. A. S. A. Aziz, L. A. Manaf, H. C. Man and N. S. Kumar, "Kinetic modeling and isotherm studies for copper (ii) adsorption onto Palm Oil Boiler Mill Fly Ash (POFA) as a natural low-cost adsorbents," *Bioresources*, Vol.9(1), 336–356, 2014.

[21]. N. M. Musyoka, L. F. Petrik, E. Hums, H. Baser and W. Schwieger, "In situ ultrasonic diagnostic of zeolite X crystallization with novel (hierarchical)," *Ultrasonics*, Vol.54(2), 537–543, 2014.

[22]. M. P. Moisés, C. T. P., Da Silva, J. G. Meneguin, E. M. Girotto and E. Radovanovic, "Synthesis of zeolite NaA from sugarcane bagasse ash," *Materials Letters*, Vol.108, 243–246, 2013.

[23]. M. Gougazeh and J. C. Buhl, "Synthesis and characterization of zeolite A by hydrothermal transformation of natural Jordanian kaolin," *Journal of the Association of Arab Universities for Basic and Applied Sciences*, Vol.15(1), 35–42, 2014.

[24]. C. Santasnachok, W. Kurniawan and H. Hinode, "The use of synthesized zeolites from power plant rice husk ash obtained from Thailand as adsorbent for cadmium contamination removal from zinc mining,'' *Journal of Environmental Chemical Engineering*, Vol.3(3), 2115–2126, 2015.

[25]. S. S. Bukhari, J. Behin, H. Kazemian and S. Rohani, "Conversion of coal fly ash to zeolite utilizing microwave and ultrasound energies: A review," *Fuel*, Vol.140, 250–266, 2015.

[26]. S. N. Azizi and N. Asemi, "The effect of ultrasonic and microwave-assisted aging on the synthesis of zeolite P from Iranian perlite using box-behnken experimental design," *Chemical Engineering Communications*, Vol.201(7), 909–925, 2014.

[27]. S. Bohra, D. Kundu and M. K. Naskar , "One-pot synthesis of NaA and NaP zeolite powders using agro-waste material and other low cost organic-free precursors," *Ceramics International*, Vol.40(1), 1229–1234, 2014.

[28]. T. V. Ojumu, P. W. Du Plessis and L. F. Petrik , "Synthesis of zeolite A from coal fly ash using ultrasonic treatment - A replacement for fusion step," *Ultrasonics Sonochemistry*, Vol.31, 342–349, 2016.

[29]. T. Aldahri, J. Behin, H. Kazemian and S. Rohani, "Synthesis of zeolite Na-P from coal fly ash by thermo-sonochemical treatment," *Fuel*, Vol.182, 494–501, 2016.

[30]. N. Sapawe, A. A. Jalil, S. Triwahyono, M. I. A. Shah, R. Jusoh, N. F. M. Salleh, B. H. Hameed and A. H. Karim, "Cost-effective microwave rapid synthesis of zeolite NaA for removal of methylene blue," *Chemical Engineering Journal*, Vol.229, 388-398, 2013.

[31]. E. A. Mohamed, A. Q. Selim, M. K. Seliem and M. R. Abukhadra, "Modeling and optimizations of phosphate removal from aqueous solutions using synthetic zeolite NaA," *Journal of Materials Science and Chemical Engineering*, Vol.3, 15-29, 2015.

Environmental Research & Technology, Vol. 1(4), pp. 34-39, 2018

Environmental Research & Technology

http://dergipark.gov.tr/ert

CONFERENCE PAPER

Life cycle assessment of an office: Carbon footprint of an office staff

Nilay Cambaz*[,1], E. Gamze Taskin[1], Ali Ruzgar[1]

[1]BUTEKOM-Bursa Technology Coordination and R&D Center, 16245, Osmangazi, Bursa, TURKEY

ABSTRACT

Environmental problems have become today's most emphasized issues due to the unconscious use of natural resources and the ongoing increase in consumption resulted in an increased level of environmental pollution. Offices, where most of the daily time is being consumed in today's modern world, generate the important amount of daily wastes and increase the environmental burden. In this respect, it is important to investigate and to reveal their environmental impacts. In this study, the Organizational Life Cycle Assessment (O-LCA) of an office has been conducted in order to investigate the environmental impacts caused by a typical office and to reveal carbon footprint of an office staff. The water and energy consumption (electricity and natural gas), transportation, and business travel data were obtained based on the real consumptions of the organization, while data required for the calculation of the waste amount (paper, cardboard, plastic etc.) were provided from literature. Afterwards, data obtained for office have been run into SimaPro Analyst 8.0.2 software in order to calculate carbon footprint and to analyze the environmental impacts. As a result of the calculations made, the carbon footprint of the office has been found as 10^5 kg CO_2-eq $year^{-1}$ and the carbon footprint of an office staff has been determined as 5263.16 kg CO_2- eq $year^{-1}$, accordingly. The obtained results have indicated that the highest share in terms of carbon dioxide emission is caused by electricity consumption, followed by transportation, business travel, office consumables, electronic devices, natural gas consumption, office wastes, water consumption, and electronic wastes, respectively.

Keywords: Carbon footprint, environment, life cycle assessment (LCA), office waste

1. INTRODUCTION

The ongoing increase in consumption and the increasing environmental problems (such as global warming) associated with population growth in the world are one of the most important discussed issues today. The actions which have been taken until today and what needs to be done further in order to solve these problems are also among the important issues on the agenda [1].

Buildings are one of the largest consumers of energy in any country with intense industry, and office buildings have a significant participation. As the transformation of the global economy towards the service industries intensifies, so too do investments in offices and other commercial buildings. Studying the energy and environmental effects of office buildings throughout their life cycle, therefore, is important [2].

According to a study carried out in the United Kingdom, waste generated from commercial sector represents 12% of all waste in the UK. The amount of waste which commercial offices occupied by large companies in the financial sector generally produce is around 500 kg per employee for each year and it comprises of 60% paper and cardboard. It also refers to a study carried in 2000, which has been found that almost 70% of all waste was disposed of to landfills [3].

The wastes and the emissions which offices generate are just the one part of the issue. The other part is the interaction with the environment during the life cycles of the products and services [1]. One of the best ways to make this interaction clear is the Life Cycle Assessment (LCA) approach, which provides a numerical output that identifies potential environmental impacts by examining the

Corresponding Author: nilaycambaz@gmail.com (Nilay Cambaz)
Received 30 May 2018; Received in revised form 20 September 2018; Accepted 20 September 2018
Available Online 17 October 2018
Doi: ISSN: 2636-8498

This paper has been presented at EurAsia Waste Management Symposium 2018, Istanbul, Turkey

environmental aspects of production, use, end-of-life evaluation, recycling and disposal stages of products and services throughout the entire life cycle [1], [4].

In response to the increase of offices' importance in terms of environmental burden, the environmental impacts of different types of office buildings have been investigated via LCA approach in some previous studies. In the LCA study of a 4-story commercial office building located in Southern Finland with 4,400 m^2 gross floor area and roughly 200 staff, the emissions related with the materials, construction, use, maintenance, and end-of-life phases have been investigated. It has been found that the use phase of the office has the highest share as 50-90% in all emissions (for CO_2, SO_2 NO_x, and PM_{10}) among the other phases. Use phase's contribution in the total CO_2 emission of the office has been found as 83%. When the use phase investigated in detail, it has been revealed that the highest impact with a range between 30-45% is caused by electricity consumption and heating process. On the other hand, it has been found that the use phase dominates the materials, construction, maintenance and end-of-life phases for a 5-story commercial office building located in Midwest U.S. with 4,400 m^2 area, in terms of all emissions except PM_{10} (particulate matter smaller than 10 μm). It has been found that the use phase has an important share which is not less than 46% among other phases in terms of all emission categories, and lighting and electricity consumption have been dominated in use phase [2]. In another study carried on in Thailand, it has been found that the life cycle distribution of environmental impacts is concentrated in the operational stage of the typical commercial office building. It has been stated that the operational phase was accounted for approximately 52% of the total global warming potential, about 66% of the total acidification potential, and about 71% of the total photo-oxidant formation potential, respectively. The results indicated that the main contribution to the impact categories during the operation phase was caused from emissions related to fossil fuel combustion, particularly for electricity production [5]. In reference [6], authors performed an economic input-output LCA and compared it to primary energy and CO_2 emissions of 10 office buildings with 40 years of service life in Japan. The study reported that the energy use and CO_2 emissions caused by the electrical energy utilization in the use phase of the office building contributed most of the environmental impacts in all 10 cases with an average percentage of 80%. The significance of the use phase in terms of environmental impacts has been further revealed in another LCA study of an 8-story office building located in Athens, Greece. Investigating the environmental impacts of raw material extraction, components manufacture, components transportation, construction of the office building, use, and demolition/waste management stages of the office building, it has been found that the use phase contributes by 91.94% to the total of the environmental score. Global warming potential is the environmental impact that corresponds to the highest portion as 78.35 % in the use phase. The environmental impact of the use phase was regarded to the energy consumption used for heating, cooling, and lighting of the building, which is attributed with fossil fuel use in energy production processes [7].

While revealing the most of the environmental impacts of offices are caused from the use phase, these studies have not investigated the use phase with an organizational approach exhaustively. In this respect, the Organizational Life Cycle Assessment (O – LCA) of an office located in Turkey has been conducted by means of this study. The LCA method was applied referring to ISO/TS 14072 standard which provides recommendations and requirements specifically for O-LCA to ensure a more effective application of ISO 14040 and ISO 14044 to organizations [8].

2. MATERIALS AND METHOD

2.1. Life Cycle Assessment Goal and Scope Definition

The goal of this study was to investigate the environmental impacts caused by a typical office and to reveal the carbon footprint of an office staff. In this study, Organizational Life Cycle Assessment of a 3-roomed, 160 m^2 typical office operating in a service sector with 19 staff located in a 6-story commercial office building in Nilüfer, Bursa was performed. The total carbon dioxide emission of the office has been calculated and the carbon footprint of an office staff has been determined. In addition, environmental impacts were investigated.

The system boundary of the study was determined as cradle-to-grave, which includes the energy consumption and emissions of the use phase of the office for a given reference period, and the end-of-life phase (i.e., waste disposal and recycling) of products used by the organization throughout the reference period. In other words, solely the use phase of the office for a given reference period has been investigated in cradle-to-grave boundary. The construction and demolition phases of the office have not been included in the study. Besides, the reference period of the study has been defined as one year, 2016.

2.2. Life Cycle Inventory

In order to create inventory analysis, the activities and materials have been categorized as follows:

2.2.1. Water and energy consumptions

In this category, monthly bills for 2016 served as a source for calculating the amount of water and energy consumption (for electricity and natural gas) of the office.

2.2.2. Transportation

Transportation data include the distance covered by each staff to come to the office in the reference period. In order to calculate emissions caused from transportation, the distances were determined

separately for shuttle service, individual car, and public transportation (subway).

2.2.3. Business travel

This activity includes travels made for purposes such as scheduled and unplanned visits of the customers on-site, project meetings, fairs, symposiums, conferences and so on. In this category, the intercity and overseas distances passed on for business travel in the reference period, 2016, were taken as a basis, and emissions have been calculated for car (taxi), train (intercity), airplane (separately for domestic and international flights), coach (intercity), and ferryboat, individually.

2.2.4. Office consumables

During the calculation of the emissions related to office consumables, the type and yearly consumption amount of consumables for a typical office have been determined from the literature [3]. Major ones were selected as whitepaper, cardboard, newspaper and magazine, glass, aluminum cans, and plastic cups. Since some types of the consumables are not possible to evaluate accurately, sections named other paper and other plastic were determined additionally.

2.2.5. Office wastes

In order to determine the carbon dioxide emission in office wastes category, the waste amount generated from office consumables in a year and recycling rates for each type have been obtained from literature [3], [9], [10].

2.2.6. Electronic devices

Electronic devices refer to desktop computer, portable computer, computer adaptor, cabled mouse, black and white printer, and colored printer. The total amount has been determined by taking as a basis the number and weight of each of these electronic devices within the organization. The operation and production phases were investigated separately for desktop and portable computers with taken into consideration the operation hours and working days in the reference period.

2.2.7. Electronic waste

To evaluate the emissions associated with this category, the amount of electronic waste was obtained from the organization's real consumptions, while the service life for each equipment was estimated based on the organization's experience. Besides, an assumption referred to the organization's attitude was made for recycling rates in terms of electronic devices. Service life has been assumed as 5 years for desktop computer, portable computer and computer adapter, 1 year for cabled mouse, 10 years for black and white printer and, 8 years for colored printer. On the other hand, it has been assumed that all the computers and printers are dispatched to be recycled, while computer adaptors and cabled mouses are disposed of to landfills after completing their service life.

2.2.8. Wastewater

Wastewater amount has been calculated by using the organization's real consumption data. All the wastewater goes to a treatment plant located in the industrial zone and there is no reuse of wastewater within the organization. Regrettably, the characterization of the wastewater could not be assessed and there is no information about its treatment process.

A summary of the data and the sources they are compiled from is shown in Table 1.

Table 1. Summary of data and their source

Data	Data Source	Recycling Rate Source
Electricity Consumption	Direct Measurement	-
Water Consumption	Direct Measurement	-
Natural Gas Consumption	Direct Measurement	-
Transportation (Shuttle Service, Subway, Car)	Direct Measurement	-
Business Travel (Taxi, Train, Airplane, Coach, Ferryboat)	Direct Measurement	-
Office Consumables (Whitepaper, cardboard, plastic cups, etc.)	[3]	-
Office Waste	[3]	[9, 10]
Electronic Devices	Direct Measurement	-
Electronic Waste (Desktop computer, portable computer, etc.)	Direct Measurement	Assumption referred to organization's attitude
Wastewater	Direct Measurement	-

2.3. Life Cycle Impact Assessment

The data obtained for office have been run into SimaPro Analyst 8.0.2 software and total carbon footprint of the office has been determined. In addition to global warming potential (which reveals the carbon footprint), several environmental impacts comprising;

- Abiotic depletion (Decrease in the natural availability of abiotic natural resources, including minerals [11].)
- Abiotic depletion (fossil fuels) (Decrease in the natural availability of abiotic natural resources, including fossil energy resources [11].)
- Ozone layer depletion (Depletion in the ozone layer that leads larger fraction of UV-B radiation to reach to earth surface, and may cause harmful effects on human health, animal health, terrestrial and aquatic ecosystems, and biochemical cycles [11].)
- Human toxicity (Effects of toxic substances on the human environment [11].)
- Freshwater aquatic ecotoxicity (Impact of the emissions of toxic substances to air, water, and soil on freshwater ecosystems [11].)
- Marine aquatic ecotoxicity (Impact of toxic substances to marine ecosystems [11].)
- Terrestrial ecotoxicity (Impact of toxic substances to terrestrial ecosystems [11].)
- Photochemical oxidation (The formation of reactive substances (mostly ozone) which are hazardous to human health and ecosystems [11].)
- Acidification (Impacts of acidifying substances on soil, groundwater, surface water, organisms, ecosystems, and materials (buildings) [11].) and,
- Eutrophication (Impacts of excessive levels of macro-nutrients in the environment related with emissions of nutrients to air, water, and soil [11].)

have been investigated. EcoInvent, the most comprehensive database available, and the CML-IA BaseLine 3.0 method have been used in terms of calculation of carbon dioxide equivalent emissions (global warming potential) and other environmental impacts throughout the study.

3. RESULTS & DISCUSSION

As a result of the analysis, the carbon footprint of the office was found to be 10^5 kg CO_2 –eq $year^{-1}$, and it is determined that an office staff's carbon footprint is 5263.16 kg CO_2-eq $year^{-1}$. The environmental impacts of the office have been revealed, and the contribution of each parameter was investigated.

In Fig 1, which is obtained from SimaPro Software, the characterization of the environmental impacts have been revealed. If the global warming potential (GWP) column in Figure 1 was examined in detail, it could be seen that 66% of the carbon footprint which an office staff generates in a year was caused from electricity consumption, 15% from transportation, 10.3% from business travel, 4.74% from office consumables and, 2.88% from electronic devices. The total rest of the share, 1.08%, which is too small hence it is not possible to visualize in the graph, is caused by natural gas consumption, office waste, water consumption, and electronic waste, respectively. The characterization of the wastewater plays a major role when assessing its impacts in an environmental point of view and it would also affect the selection of its treatment process. Since the software could calculate the exact emissions caused from wastewater only depending on its characterization, and wastewater's characterization could not be evaluated in this study, no environmental impact in terms of global warming potential caused from wastewater has occurred.

Fig 2 illustrates the network obtained from SimaPro Software in terms of global warming potential of the office which has been demonstrated that the highest carbon dioxide emission is caused from electricity consumption as $6.61 \bullet 10^4$ kg CO_2 – eq $year^{-1}$.

As the second highest share in carbon dioxide emission is caused from transportation, investigation of transportation type hereby gains importance. In Fig 3, the percentages of transportation types have been illustrated. It could be seen that the highest effect is caused from passenger car and subway, after shuttle service.

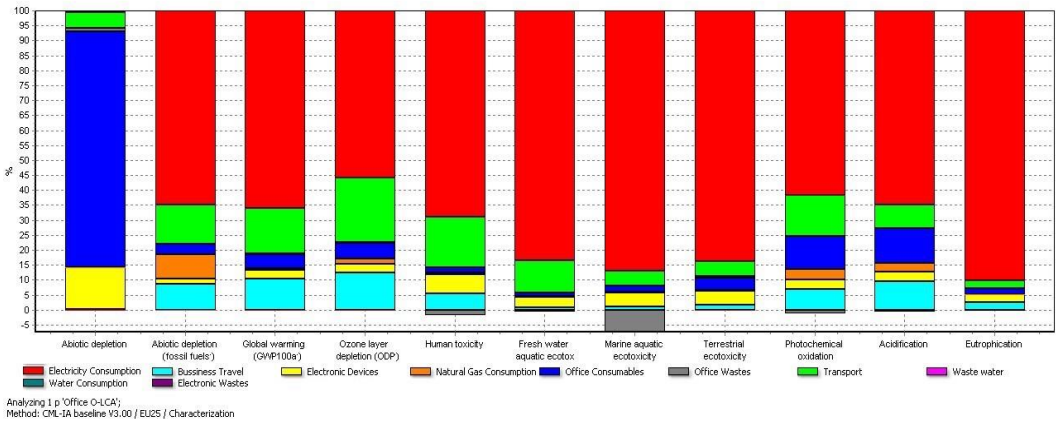

Fig 1. Characterization graph of the environmental impacts of the office

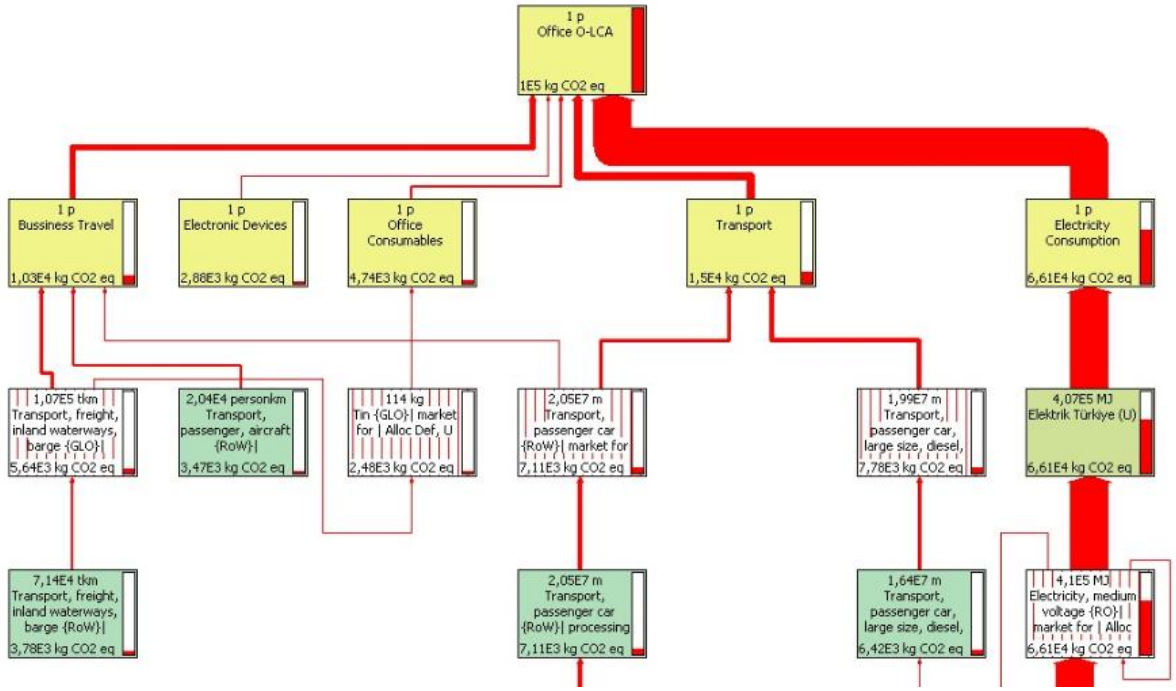

Fig 2. Global warming potential network

This result is related to the office's location which does not make it attractive for the staff to prefer subway to come to the office.

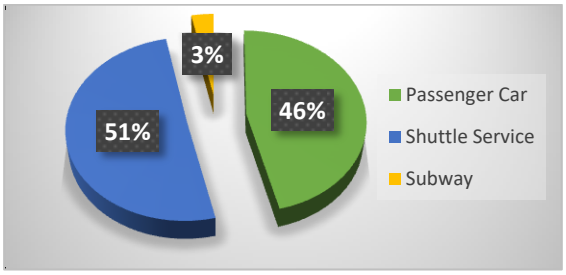

Fig 3. Percentages of transportation types in terms of GWP

Besides, business travel has a significant share, as 10.6%, in terms of global warming, and revealing the effects in a more detailed way, therefore, is important. The types of transportation used for business travel and their share have been illustrated in Fig 4. It has been found that the highest emission is generated from the ferryboat, followed by airplane (international flights), coach, airplane (domestic flights), train, and car, respectively. Although it has been found in the literature that the emission per person related with domestic flight is higher than international flight, and the emission caused from ferryboat is the smallest among both types of flights [12], such a result could be explained by the staff's attitude to prefer mostly ferryboat and coach in their domestic travels, and the numbers of travels abroad to be quite less compared to the domestic ones.

It is also important to investigate other environmental impacts besides the global warming potential. As it could be seen from Fig 1, electricity consumption dominates in terms of all environmental impacts except abiotic depletion. In the eutrophication category, it has been shown that the electricity consumption has an important proportion as 90%. On the other hand, it is clear that transportation has a significant share in each environmental impact category.

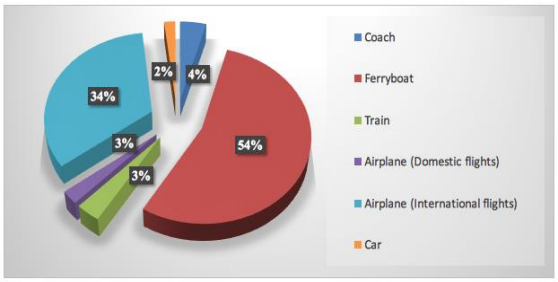

Fig 4. Percentages of transportation types in business travel in terms of GWP

Investigating all impact categories, it has been shown that the transportation has its biggest share in ozone layer depletion category as 23.5%. Besides, it has been demonstrated that office consumables have an important share as 78.7% in terms of abiotic depletion, while the second highest impact has been caused from electronic devices. The second and third highest impacts caused by office consumables have been found to be in acidification as 12% and in photochemical oxidation as 11%, respectively. It also could be seen that the recycling of some of the office wastes caused 7% improvement in terms of marine aquatic ecotoxicity, %2 in human toxicity and %1 in photochemical oxidation. In abiotic depletion (fossil fuels) category, natural gas consumption has a significant share as 8% after electricity consumption and transportation, respectively.

4. CONCLUSIONS AND RECOMMENDATIONS

In this study, the carbon footprint of one office staff for 2016 has been determined as 5263.16 kg CO_2-eq $year^{-1}$. Given that a large portion of this release (66%)

is due to the electricity consumption, it is evident how important energy source use habits are. In this case, it is clear that taking actions such as changing the bulbs with more efficient ones, giving more importance to the use type of electronic devices (computers, printers, etc.), and air conditioners would affect the total carbon footprint. Besides, such a result also matches up with the studies previously mentioned in the introduction section which have been stated that the electricity consumption has the highest impact in the use phase of the office.

On the other hand, the obtained results indicated that transportation has a significant contribution as 15% in terms of global warming. Considering the highest share is caused from shuttle service and individual car, it could be seen clearly how effective results switching to public transportation would reveal. Additionally, the emission associated with business travel should not be ignored since it has an important role in the total carbon footprint of an office staff. Choosing the transportation type with low emission where possible could be a good solution to achieve notable reductions in terms of environmental burdens.

Besides, it should not be ignored that recycling and reduction in the usage amount of typical office consumables such as whitepaper, cardboard, and plastic cup are also one of the major factors which have a direct effect in terms of reducing the carbon dioxide emission and environmental burdens. The awareness of the office staff hereby takes an important role. In this case, the separation and collection processes of recyclable and reusable materials would have a significant effect in terms of waste amount reduction. The recycling rate of the consumables in the office itself should be increased, and, if possible, the materials which are appropriate to reuse must be selected. In addition, promoting campaigns in order to increase the awareness in terms of reuse and recycling could be a good solution to reduce the waste amount and hence the environmental load. Besides, if reasonable purchasing policies and waste management practices are implemented, the amount of emission caused from wastes could be fairly small in the overall footprint.

Considering the electricity consumption dominates all the environmental impacts except abiotic depletion, it can be said that energy source use habits and attitude take an important role in the use phase of the office. On the other hand, it is explicit that one of the most important issues in terms of reducing the environmental load caused from the office appears to be the office staff's awareness. Since offices generate a significant amount of daily wastes, working towards the environmental impacts which these wastes reveal should be one of the issues that need to be emphasized. Besides, all the actions associated with reducing the total carbon footprint of an office staff should be carefully investigated and implemented. It is indisputable that knowing the energy profiles and expected emissions of the life cycle of offices could be useful in the matter of making informed decisions about the environment for future.

REFERENCES

[1]. A. Güngör, Y. İkiz, S. Palamutçu, G. Gören, G. Ağırbaş and O. Polat, "Life Cycle Assessment of Textile Products by an Environmentally Sensitive Perspective," (in Turkish), *Tübitak Project Result Report*, Project No: 104M376, Denizli, Turkey, 2007.

[2]. S. Junilla, A. Horvath and A. Guggemos, "Life cycle assessment of office buildings in Europe and the United States," *Journal of Infrastructure Systems*, Vol. 12(1), 10-17, USA, 2006.

[3]. D. Clark, "CO_2 emissions due to office waste," Information Paper-6, What Colour is Your Building, England, 2013.

[4]. International Organization for Standardization (ISO), "ISO 14044: Environmental management – Life cycle assessment –Requirements and guideline," Geneva, Switzerland, 2006.

[5]. O. F. Kofoworola and S. H. Gheewala, "Environmental Life Cycle Assessment of a Commercial Office Building in Thailand", *The International Journal of Life Cycle Assessment*, Vol. 13(6), 498, 2008.

[6]. M. Suzuki and T. Oka, "Estimation of life cycle energy consumption and CO_2 emission of office buildings in Japan", *Energy and Buildings*, Vol. 28(1), 33-41, 1998.

[7]. C. Koroneos, A. Dompros, and M. Loizidou, "Life cycle assessment of an office building in Greece," In *Proceedings of the 10th International Conference on Environmental Science and Technology. Kos Island, Greece* (pp. 5-7), 2007.

[8]. United Nations Environment Programme (UNEP), Society of Environmental Technology and Chemistry (SETAC) and Life Cycle Initiative, "Guidance on organizational life cycle assessment," 2015.

[9]. National Environment Agency, "Waste and Recycling Statistics for 2016," Available: http://www.nea.gov.sg/energy-waste/waste-management/waste-statistics-and-overall-recycling (accessed 18.09.2017).

[10]. European Aluminium, *Aluminium beverage can recycling at 73%*, Press release, Brussels, Nov. 2017. Available: https://www.european-aluminium.eu/media/1988/european-aluminium-press-release-2014-can-recycling-result-7nov2017_final.pdf (accessed 12.12.2017).

[11]. Pre, "SimaPro Database Manual- Methods Library," Version 4.1, California, USA, 2018.

[12]. K. Kumbaroğlu and Y. Arıkan, "Awareness and Making a Difference: CO_2 Emissions of Turkey," (in Turkish), *Açık Toplum Vakfı*, 2009.

Environmental Research & Technology, Vol. 1(4), pp. 40-46, 2018

Environmental Research & Technology

http://dergipark.gov.tr/ert

CONFERENCE PAPER

Adsorption of Remazol Brilliant Blue R by raw and carbonized macroalgal wastes

Anıl T. Kocer[1], Benan Inan[1], Didem Ozcimen*[1]

[1]Yildiz Technical University Bioengineering Department, 34220 Esenler, Istanbul, TURKIYE

ABSTRACT

In this study, adsorption of Remazol Brilliant Blue R (RBBR) dye was carried out using *Ulva lactuca*, *Codium fragile* and their carbonization products; adsorption kinetics and isotherms were determined. Carbonized adsorbents were produced in a tubular furnace at the heating rate of 20˚C min^{-1} and temperature of 500 ˚C with a nitrogen flow rate of 300 ml min^{-1}. Adsorption was carried out in a shaking water bath at the temperature of 25 ˚C and shaking speed of 200 rpm for 2 h. Carbonized adsorbents have been found to have greater adsorption capacity than raw biomass. It was seen that the adsorption lasted for 90 and 60 minutes for raw and carbonized adsorbents, respectively and then desorption begun. Maximum adsorption was achieved with the carbonized *Ulva lactuca* macroalgae (2.11 mg g^{-1}). It has been found that the most suitable kinetic model for all absorbents was the pseudo-second-order kinetic model. The best fit of equilibrium data for all adsorbents was described by the Langmuir model.

Keywords: Adsorption, carbonization, macroalgae, remazol brilliant blue R

1. INTRODUCTION

Water pollution is one of the most important problems which society is facing today. Recent environmental problems and the development of the industry have led to a gradual decline in the amount of potable water [1]. Especially the synthetic dyes used in the industry cause serious water pollution. Therefore, there are many studies in the literature regarding the removal of dyes from industrial wastewaters [2]. Today, there are many physical and chemical methods such as adsorption, chemical coagulation, precipitation, ultra-filtration and ionizing radiation which are effectively used to remove synthetic dyes. Among these methods, adsorption is considered as a superior technique comparatively with other techniques due to the availability of many adsorbents, easy design and operation and high efficiency [3-6].

The adsorption process takes place due to presence of unbalanced or residual forces at the solid surface that is termed the adsorbent. Adsorption is affected by the solid surface and dissolved gas or solute in the solvent. Adsorption is essentially a surface phenomenon. Adsorption process involves two components: Adsorbent and adsorbate. Adsorbent is the substance on the surface of which adsorption takes place. Adsorbate is the substance which is being adsorbed on the surface of adsorbent [7].

In general, adsorbents should have a high surface area for more efficient adsorption. Depending on the application, the surface may be hydrophobic or hydrophilic [7]. Different adsorbents such as carbon nanotubes (CNTs) have been conventionally used for the adsorption process, whereas activated carbon has been widely used in the recent past [2]. Activated carbon has been studied for the adsorption process not only at laboratory scales but also for the industrial applications and it has been seen that the obtained results are quite remarkable [8],[9]. However, usage of activated carbon is limited due to relatively expensive material and operation costs. Thus, researchers are studying to produce low-cost carbon-based adsorbents from alternative feedstocks such as agricultural wastes and algal wastes [2, 10].

This work focused on evaluation of the potential of different algal adsorbents (*Ulva lactuca*, *Codium fragile*, carbonized *U. lactuca* and carbonized *C. fragile*) for the removal of Remazol Brilliant Blue R

Corresponding Author: ozcimen@yildiz.edu.tr (Didem Ozcimen)
Received 5 June 2018; Received in revised form 7 September 2018; Accepted 14 September 2018
Available Online 19 October 2018
Doi: ISSN: 2636-8498

This paper has been presented at EurAsia Waste Management Symposium 2018, Istanbul, Turkey

(RBBR) from aqueous solution. The adsorbents were characterized by Fourier transform infrared spectroscopy (FT-IR) and proximate analysis. In the batch adsorption experiments, adsorption kinetic data were determined, pseudo-first-order and pseudo-second-order kinetic models were tested to fit these adsorption kinetic data. The equilibrium data were analyzed using Langmuir and Freundlich isotherm models.

2. MATERIALS AND METHOD

2.1 *Preparation and Characterization of the Adsorbents*

Ulva lactuca, Codium fragile and their carbonized products were used as adsorbent in this study. Macroalgae samples were collected from coastal areas of Marmara Sea and washed with distilled water to remove impurities such as shell and sand. These algae were dried at 70°C for a night and then powdered using a grinder. The obtained *Ulva lactuca* and *Codium fragile* were referred as UL and CF, respectively.

The production of carbonized adsorbents were conducted using the procedure described by Kocer et al. [11]. The carbonization process was performed in Protherm model split typed furnace. Obtained UL and CF powder were carbonized at the temperature of 500 ^{0}C, heating rate of 20°C min^{-1}, retention time of 30 min and with nitrogen flow rate of 300 mL min^{-1}. Before the experiments, inside of the furnace were swept with nitrogen gas for 15 minutes to provide an inert atmosphere. After the carbonization process, the furnace was cooled and the samples were placed in a desiccator for characterization and adsorption experiments. The obtained carbonized *Ulva lactuca* and *Codium fragile* were referred as CUL and CCF, respectively.

Proximate analyzes of the UL and CF were carried out using the thermogravimetric analyzer (TA Instrument, SDT Q600). In proximate analysis, moisture content, volatile matter content, fixed carbon content and ash content were determined according to Ozcimen [12]. The functional groups present at the surface of the UL, CF, CUL and CCF were identified by FT-IR in the range of 4000–600 cm^{-1} using a Thermoscientific Nicolet 6700 spectrophotometer.

2.2 Adsorption Experiments

The adsorption experiments were performed using the procedure described by Ozcimen and Salan [2]. In these experiments, UL, CF, CUL and CCF were used to remove Remazol Brilliant Blue R (RBBR) dye from aqueous solutions. Firstly, 1000 mg L^{-1} stock solution of RBBR was prepared and then this stock solution was diluted to standard concentrations of 20, 40, 60, 80 and 100 mg L^{-1}. The pH values of the standard solutions were adjusted to 3 in all cases with HCl/NaOH solutions due to provide increased interactions between the adsorbent and reactive azo dyes. At lower pH, the reactive azo dyes such as anthraquinonic RBBR dissolves and releases colored negatively charged dye anions into aqueous solution, which will exhibit electrostatic attraction towards positively charged surfaces. Moreover, at acidic pH values, some functional groups of adsorbent are also protonated. The dissociated anions of dye molecules are transferred from solution to the surface of adsorbent and adsorption occurs via the electrostatic interactions between the ions of negatively charged dye molecules and positively charged absorbent surface [2].

In the batch adsorption experiments, 40 mg adsorbent was thoroughly mixed with the 5 ml aqueous solution of dye (60 mg L^{-1}) in a sealed conical centrifuge tube placed into a tube rack. These experiments were carried out at a constant agitation speed of 200 rpm and temperature of 25 ^{0}C for 120 min. After each adsorption experiment was completed, residual concentration of RBBR was determined by spectrophotometric analysis (PG Instruments T60 UV-Visible Spectrophotometer) in the visible range at the wavelength of 593 nm (λ_{max}). The amount of the remained RBBR was determined from the calibration curve obtained according to concentration-absorbance chart of initial standard solutions. The adsorbed quantity was calculated using the following equation:

$$Q = \frac{(C_0 - C_e).V}{W} \quad (1)$$

where C_0 and C_e (mg L^{-1}) are the amount of initial and remaining RBBR in the solution at time of equilibrium respectively, V is the volume (L) of the solution, and W is the weight (g) of the adsorbent.

The kinetic data were fit by employing the pseudo-first-order [13] and pseudo-second-order [14] models, as expressed by Eq. (2) and Eq. (3) respectively:

Pseudo-first-order equation:

$$\ln(Q_e - Q_t) = \ln Q_e - (k_1.t) \quad (2)$$

Pseudo-second-order equation:

$$\frac{t}{Q_t} = \left(\frac{1}{Q_e^2.k_2}\right) + \frac{t}{Q_e} \quad (3)$$

where Q_e and Q_t are the amounts (mg g^{-1}) of RBBR adsorbed onto the adsorbents at the equilibrium and at the time of t, respectively, while k_1 and k_2 are the kinetic rate constants for the pseudo-first-order (1 min^{-1}) and the pseudo-second-order (g mg^{-1} min^{-1}) adsorption processes, respectively.

After determination of adsorption kinetics, the experimental data obtained for the equilibrium adsorption of RBBR onto the adsorbents were analyzed employing the Freundlich [15] and Langmuir [16] isotherm with Eq (4) and Eq (5) given below:

Freundlich isotherm equation:

$$\log Q_e = \frac{\log C_e}{n} + \log K_f \quad (4)$$

Langmuir isotherm equation:

$$\frac{1}{Q_e} = \left[\frac{1}{Q_{max}.b}\right].\frac{1}{C_e} + \frac{1}{Q_{max}} \quad (5)$$

where Q_e (mg g^{-1}) and C_e (mg L^{-1}) are the equilibrium concentrations of RBBR dye in the solid and liquid phases, respectively, while K_f [(mg g^{-1})/(mg L^{-1})$^{1/n}$]

and *n* are the Freundlich constants related to the adsorption capacity and intensity, respectively. Similarly, Q_{max} (mg g^{-1}) and *b* (L g^{-1}) are the Langmuir constants related to the adsorption capacity.

3. RESULTS & DISCUSSION

3.1 *Characterization of the Adsorbents*

The results of proximate analysis of the adsorbents were shown in Table 1. As it can be seen in Table 1, UL had maximum moisture content (12.29%), on the contrary, CF had minimum moisture content (9.04%). The reason for the high moisture content of all adsorbents was the moisture holding in the environment by these adsorbents. Therefore, adsorbents should be stocked in the desiccator prior to the adsorption process for increasing adsorption efficiency [17]. Due to the high carbohydrate content of macroalgae, the amount of volatile substances of raw macroalgal adsorbents were higher than volatile contents of carbonized adsorbents [18]. When the ash contents of all adsorbents were compared with each other, it was seen that the highest and the lowest value were belonged to CUL and CF, respectively. According to proximate analysis results, the data obtained from this study were in agreement with the literature [19].

Table 1. Proximate analysis of adsorbents

Adsorbents	Moisture Content (%)	Volatile Matter Content (%)	Fixed Carbon Content (%)	Ash Content (%)
UL	12.29	67.37	6.438	13.69
CF	9.04	66.44	12.65	11.87
CUL	10.26	23.22	29.82	36.70
CCF	10.12	22.03	38.70	29.15

The FTIR spectrums of the adsorbents were shown in Fig 1. As can be seen in Fig 1, O- and H- containing functional groups were not presented in CUL and CCF due to the formation of carbonized macroalgae at high temperatures. The absence of these functional groups in carbonized adsorbents indicates the emission of CO_2, CH_4 and H_2 [20]. The FTIR spectra of UL and CF showed a broad band present between 3600 and 3200 cm^{-1} which can be assigned to the O–H stretching groups which were hydroxyl containing compounds such as water. This band was broader in the FTIR spectrum of UL because UL has more water content than CF [21]. In the spectrums of UL and CF, the bands seen at 2950 cm^{-1} indicated symmetric and asymmetric C-H stretching vibrations originating from aliphatic hydrocarbons. Peaks between 1250 and 1300 cm^{-1} also indicated the aliphatic C-N stretching [22].

When the FTIR spectra of adsorbents were compared with each other, it was seen that the high temperature in the carbonization process causes the transition from aliphatic to aromatic structure, aromatic ring formation and H deformation. During the carbonization process, while the OH and CH_3 bonds decreased, the C = C structures increased [23]. Bands between 700-900 cm^{-1} indicated aromatic structure; bands between 1500-1600 cm^{-1} were due to the aromatic C = C vibration [24].

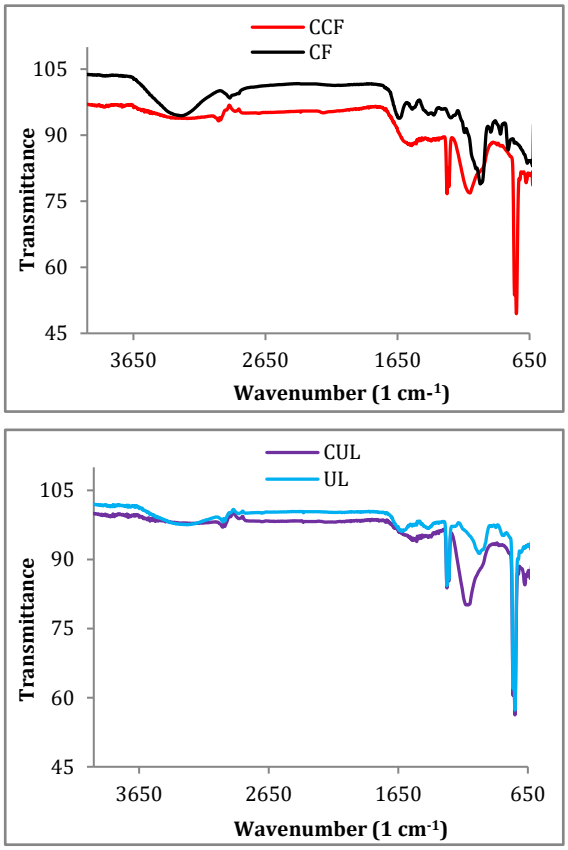

Fig 1. FTIR spectras of adsorbents

3.2 *Adsorption Kinetics*

In order to determine the optimum adsorption time, the effect of contact time on adsorption was evaluated at 25°C by using 60 mg L^{-1} dye solution and obtained results were shown in Fig 2. According to the Fig 2, the adsorption rate increased rapidly at the beginning of the process and it becomes slow with the increase in the contact time until equilibrium was reached. Furthermore, since the adsorbents were saturated with RBBR, the desorption process started after the equilibrium time [2, 25, 26]. The minimum contact times required for the equilibrium were found as 60 and 90 min for carbonized macroalgae and raw macroalgae, respectively.

As can be seen in Fig 2, the adsorption capacity of carbonized macroalgae was about two times higher than the raw macroalgae. This may be due to network pore structure of carbonized macroalgae and other factor that is generated during the carbonization process which exhibit high specific surface area [27]. CUL showed the best adsorption performance while CF showed worst performance among the four samples.

Pseudo-first-order kinetic model and Pseudo-second-order kinetic model have been investigated to

determine what kind of mechanism was carried out during adsorption. Parameters of the pseudo-first-order and pseudo-second-order models were calculated from Fig 2 and the obtained data and the correlation coefficients were given in Table 2.

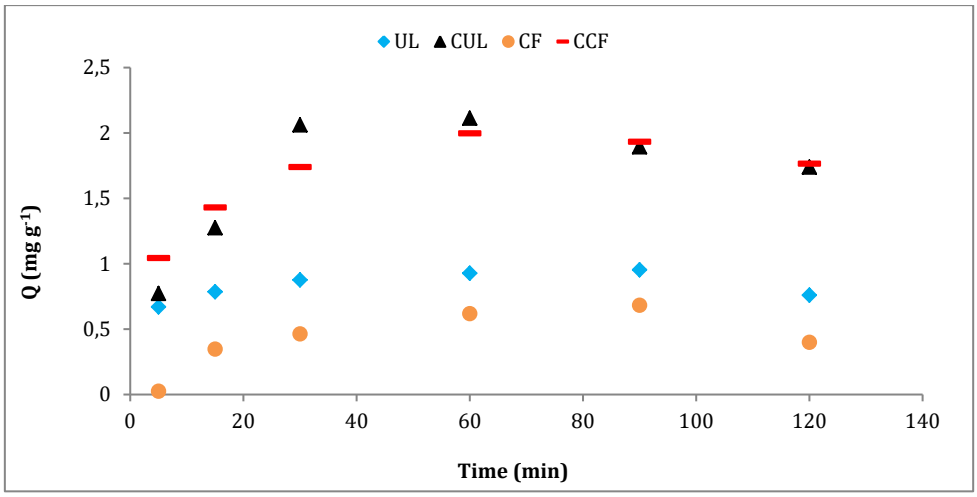

Fig 2. Adsorption capacities of RBBR onto the adsorbents

Table 2. Pseudo-first-order and Pseudo-second-order kinetic models

Adsorbent		Pseudo-First-Order			Pseudo-Second-Order		
	Q_{exp} (mg g^{-1})	k_1	Q_e (mg g^{-1})	R^2	k_2	Q_e (mg g^{-1})	R^2
UL	0.953	0.043	0.324	0.991	0.032	0.983	0.999
CF	0.683	0.023	0.446	0.871	0.049	0.859	0.998
CUL	2.113	0.013	3.652	0.926	0.075	2.129	0.979
CCF	1.997	0.030	0.885	0.959	0.087	2.084	0.997

As can be seen in Table 2, although the correlation coefficient was quite high, Q_e values of adsorbents from pseudo-first order kinetic model were not in agreement with experimental data. Thus, the adsorption process did not comply with this model. The values of Q_e were in agreement with the experimental data (Q_{exp}) for the pseudo-second order kinetic model. The correlation coefficients of pseudo-second-order kinetic model were also higher than that of the pseudo-first order kinetic model. Consequently, the adsorption can be estimated more appropriately by the pseudo-second-order kinetic model for all adsorbents [1, 2, 26].

3.3 Adsorption isotherms

Adsorption isotherms are important for the design of adsorption process because they show how the adsorbates are partitioned between the liquid and solid phases when the adsorption process reaches equilibrium conditions [2, 28]. The above cited constants were determined by nonlinear regression analysis and obtained values and correlation coefficients were given in Table 3.

As it can be seen in Table 3, the best correlation for all adsorbents was obtained with the Langmuir model.

Q_{max} values of carbonized macroalgae indicated that the adsorption capacity was found higher than that of raw macroalgae. Q_{max} values were 1.748, 1.417, 3.749 and 2.561 mg g^{-1} for UL, CF, CUL and CCF, respectively. The results indicated that the carbonization process increases the adsorption of dyes. The adsorption performance of RBBR increased approximate two times with carbonization process of macroalgae.

Since, this system is explained with the Langmuir isotherm, the determination of the equilibrium parameter (R_L) is very significant [29]. The equilibrium parameter (R_L) can be calculated by the following equation:

$$R_L = \frac{1}{1+bC_0} \quad (6)$$

where b (mg L^{-1}) is the Langmuir constant and C_0 (mg L^{-1}) is the initial dye concentration. The value of R_L shows the kind of the Langmuir isotherm to be unfavorable ($R_L > 1$), linear ($R_L = 1$), favorable ($0 < R_L < 1$) or irreversible ($R_L = 0$). Fig 3 presents the R_L values of the adsorption process at different initial dye concentrations for all adsorbents. As it can be seen in Fig 3, all of R_L values were between 0 and 1. This result was shown that the adsorption behaviors of RBBR dye onto all adsorbents were significantly favorable [2]. Table 4 shows a summary of related studies about RBBR adsorption onto different

adsorbents and their adsorption performance comparing the results of this study. Considering the previous studies about the RBBR uptake by adsorbents obtained from various sources, macroalgae samples and carbonized macroalgae underperform in RBBR dye removal.

Table 3. Freundlich and Langmuir isotherms constants

Adsorbent	Freundlich			Langmuir		
	n	K_f $(mg\ g^{-1})/(mg\ L^{-1})^{1/n}$	R^2	Qmax (mg g^{-1})	b (L g^{-1})	R^2
UL	2.834	0.338	0.849	1.748	0.112	0.940
CF	2.341	0.163	0.958	1.417	0.031	0.979
CUL	1.121	0.026	0.964	3.749	0.007	0.981
CCF	1.839	0.198	0.878	2.561	0.052	0.899

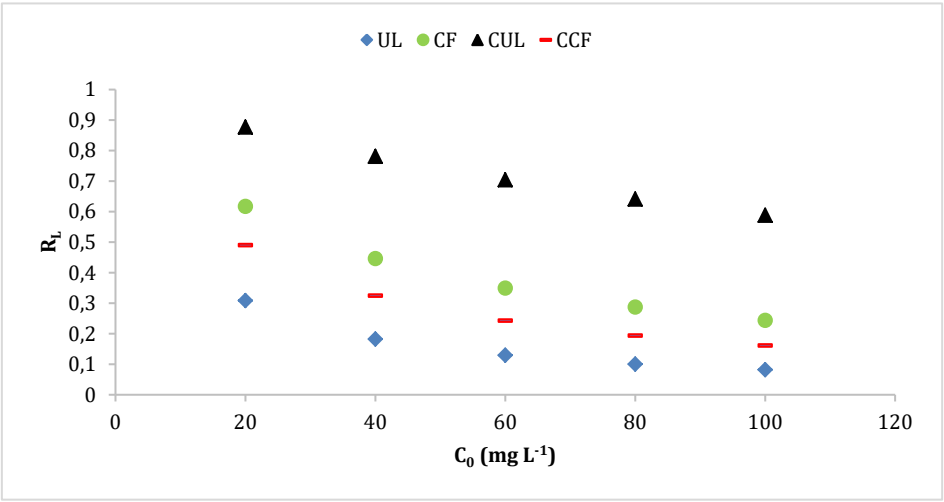

Fig 3. The equilibrium parameter (RL) of RBBR adsorption onto adsorbents

Table 4. Adsorption capacity of various adsorbents for the adsorption of RBBR

Adsorbent	Adsorption capacity, mg g^{-1} or %	pH	Ref.
Immobilized *Scenedesmus quadricauda*	48.3 mg g^{-1}	2	[30]
Jatropha curcas pods based activated carbon	95%	3	[31]
Bone char	20.6 mg g^{-1}	7.1	[32]
Sewage sludge based active carbon	33.47 mg g^{-1}	2	[33]
Peach-Palm (*Bactris gasipaes*) residue	1.8 mg g^{-1}	6.2	[34]
Poly(NOPMA)	238.10 mg g^{-1}	7	[35]
Carboxylated multi-walled carbon nanotubes	109.41 mg g^{-1}	4	[36]
P. eryngii immobilized on Amberlite XAD-4	98%	5.5	[37]
Pineapple leaf powder	96.2 %	-	[38]
Lime peel powder	95.9 %	-	[38]
Orange peel	95.72 %	-	[39]
Spent tea leaves	99.02 %	-	[39]
Carbonized sewage sludge	34.60 mg g^{-1}	3	[2]
Ulva lactuca	0.953 mg g^{-1}	3	This study
Codium fragile	0.683 mg g^{-1}	3	This study
Carbonized *Ulva lactuca*	2.113 mg g^{-1}	3	This study
Carbonized *Codium fragile*	1.997 mg g^{-1}	3	This study

4. CONCLUSIONS

RBBR adsorption from an aqueous solution by UL, CF, CUL and CCF was investigated in this study. According the obtained results, CUL showed the best adsorption performance (2.113 mg g^{-1}) while CF showed worst performance (0.683 mg g^{-1}) among the four samples. Besides, it was found that the equilibrium time was determined as 90 min for raw macroalgae and 60 min in the case of carbonized macroalgae. Adsorption kinetics were described better by the pseudo-second-order model rather than pseudo-first-order model. The best fit of equilibrium data was described by the Langmuir model for all adsorbents.

As can be seen from the results, adsorption capacities of the raw and carbonized macroalgae are not so good in comparison with the literature studies. However, adsorption capacities of these materials can be improved by activation of these materials directly, or after carbonization process. Therefore, it can be suggested that, further studies should be carried out to utilize these materials which are considered as waste, and produce new adsorbents.

REFERENCES

[1]. M. Farnane, H. Tounsadi, A. Machrouhi, A. Elhalil, F.Z. Mahjoubi, M. Sadiq, M. Abdennouri, S. Qourzal and N. Barka, "Dye removal from aqueous solution by raw maize corncob and H3PO4 activated maize corncob," *Journal of Water Reuse and Desalination*, Vol. 8, 1-11, 2017.

[2]. D. Özçimen and T. Salan, "Removal of reactive dye Remazol Brilliant Blue R from aqueous solutions by using anaerobically digested sewage sludge based adsorbents," *Chemical Industry and Chemical Engineering Quarterly*, Vol. 22(2), 167-179, 2016.

[3]. S. Kanchi, K. Bisetty, G. Kumar and M.I. Sabela, "Robust adsorption of Direct Navy Blue-106 from textile industrial effluents by bio-hydrogen fermented waste derived activated carbon: equilibrium and kinetic studies," *Arabian Journal of Chemistry*, Vol. 10, 3084-3096, 2017.

[4]. M.T. Yagub, T.K. Sen, S. Afroze and H.M. Ang, "Dye and its removal from aqueous solution by adsorption: a review," *Advances in colloid and interface science*, Vol. 209, 172-184, 2014.

[5]. G. Crini, "Non-conventional low-cost adsorbents for dye removal: a review," *Bioresource Technology*, vol. 97 (9), 1061-1085, 2006

[6]. A. Mittal, D. Kaur, A. Malviya, J. Mittal and V.K. Gupta, "Adsorption studies on the removal of coloring agent phenol red from wastewater using waste materials as adsorbents," *Journal of Colloid and Interface Science*, Vol. 337(2), 345-354, 2009.

[7]. D. Özçimen, "Evaluation of various vegetable residues by carbonization," Phd thesis, Istanbul Technical University, Istanbul, Turkey, 2007.

[8]. K. Vijayaraghavan, S.W. Won, and Y.S. Yun, "Treatment of complex Remazol dye effluent using sawdust-and coal-based activated carbons," *Journal of Hazardous Materials*, Vol. 167(1-3), 790-796, 2009.

[9]. V.K. Gupta, S.K. Srivastava, D. Mohan, and S. Sharma, "Design parameters for fixed bed reactors of activated carbon developed from fertilizer waste for the removal of some heavy metal ions," *Waste Management*, Vol. 17(8), 517-522, 1998.

[10]. D. Özçimen and A. Ersoy-Meriçboyu, "Adsorption of copper (II) ions onto hazelnut shell and apricot stone activated carbons," *Adsorption Science & Technology*, Vol. 28(4), 327-340, 2010.

[11]. A.T. Koçer, B. Mutlu and D. Özçimen, "Algal biochar production from macroalgal wastes," EURASIA Waste Management 2016, Istanbul, Turkey, 2016.

[12]. D. Özçimen. An Approach to the Characterization of Biochar and Bio-Oil, in: Renewable Energy for Sustainable Future, [S. P. Lohani (eds.)]. iConcept Press, Hong Kong, pp.41-58, 2013.

[13]. S.K. Lagergren, "About the theory of so-called adsorption of soluble substances," *Sven. Vetenskapsakad. Handingarl,* Vol. 24, 1-39, 1898.

[14]. Y.S. Ho, and G. McKay, "Pseudo-second order model for sorption processes," *Process Biochemistry*, Vol. 34(5), 451-465, 1999.

[15]. H. Freundlich, "Über die adsorption in lösungen,"*Zeitschrift für physikalische Chemie*, Vol. 57(1), 385-470, 1907.

[16]. I. Langmuir, "The adsorption of gases on plane surfaces of glass, mica and platinum," *Journal of the American Chemical society*, Vol. 40(9), 1361-1403, 1918.

[17]. R.C. Bansal, and M. Goyal, "Activated carbon adsorption," Boca Raton: CRC press, (2005).

[18]. A.T. Koçer, B. İnan, and D. Özçimen, "A Comparison of bioethanol and biochar production from various algal biomass samples and sweet sorghum energy crop," *Environmental Research and Technology*, Vol. 1(1), 43-50. 2018.

[19]. A.B. Ross, J.M. Jones, M.L. Kubacki, and T. Bridgeman, "Classification of macroalgae as fuel and its thermochemical behavior," Bioresource Technology, Vol. 99(14), 6494-6504, 2008.

[20]. S. Nanda, R. Azargohar, J.A. Kozinski, and A.K. Dalai, "Characteristic studies on the pyrolysis products from hydrolyzed Canadian lignocellulosic feedstocks," *BioEnergy Research*, Vol. 7(1), 174-191, 2014.

[21]. E. Apaydın-Varol and A.E. Pütün, "Preparation and characterization of pyrolytic chars from different biomass samples," *Journal of Analytical and Applied Pyrolysis*, Vol. 98, 29-36, 2012.

[22]. H. Haykiri-Acma, S. Yaman and S. Kucukbayrak, ''Production of biobriquettes from carbonized brown seaweed,'' *Fuel Processing Technology*, Vol. 106, 33-40, 2013.

[23]. J. Major, C. Steiner, A. Downie, J. Lehmann, and S. Joseph, "Biochar effects on nutrient leaching," *Biochar for Environmental Management: Science and technology*, 271, 2009.

[24]. E. Topsak, "Pyrolysis process effects on the structural properties of biomass and its functional group distribution," MSc thesis, Istanbul Technical University, İstanbul, Turkey, 2011.

[25]. D. Özçimen and A. Ersoy-Meriçboyu, "Removal of copper from aqueous solutions by adsorption onto chestnut shell and grapeseed activated carbons," *Journal of Hazardous Materials*, Vol. 168(2-3), 1118-1125, 2009.

[26]. O. Abdelwahab, "Kinetic and isotherm studies of copper(II) removal from wastewater using various," *Egyptian Journal of Aquatic Research*, Vol. 33(1), 125-143, 2007.

[27]. A. El-Sikaily, A. El Nemr, A. Khaled and O. Abdelwehab, "Removal of toxic chromium from wastewater using green alga Ulva lactuca and its activated carbon," *Journal of Hazardous Materials*, Vol. 148(1-2), 216-228, 2007.

[28]. F. Li and C. Ding, "Adsorption of reactive black M-2R on different deacetylation degree chitosan,"*Journal of Engineered Fibers and Fabrics*, Vol. 6(3), 25-31, 2011.

[29]. K. R. Hall, L. C. Eagleton, A. Acrivos and T. Vermeulen, "Pore-and solid-diffusion kinetics in fixed-bed adsorption under constant-pattern conditions*,"Industrial & Engineering Chemistry Fundamentals*, Vol. 5(2), 212-223, 1966.

[30]. A. Ergene, K. Ada, S. Tan, S., and H. Katırcıoğlu, "Removal of Remazol Brilliant Blue R dye from aqueous solutions by adsorption onto immobilized Scenedesmus quadricauda: Equilibrium and kinetic modeling studies," *Desalination*, Vol. 249(3), 1308-1314, 2009.

[31]. P. Sathishkumar, M. Arulkumar, and T. Palvannan, "Utilization of agro-industrial waste Jatropha curcas pods as an activated carbon for the adsorption of reactive dye Remazol Brilliant Blue R (RBBR)," Journal of Cleaner Production, Vol. 22(1), 67-75, 2012.

[32]. K.C. Bedin, S. P. de Azevedo, P. K. Leandro, A. L. Cazetta, and V. C. Almeida, "Bone char prepared by CO2 atmosphere: Preparation optimization and adsorption studies of Remazol Brilliant Blue R," *Journal of Cleaner Production*, Vol. 161, 288-298, 2017.

[33]. T. L. Silva, A. Ronix, O. Pezoti, L. S. Souza, P. K. Leandro, K. C. Bedin, K. K. Beltrame, A. L. Cazetta, and V. C. Almeida, "Mesoporous activated carbon from industrial laundry sewage sludge: adsorption studies of reactive dye Remazol Brilliant Blue R," *Chemical Engineering Journal*, Vol. 303, 467-476, 2016.

[34]. J. A. Chicatto, K. T. Rainert, M. J. Gonçalves, C. V. Helm, D. Altmajer-Vaz, and L. B. B. Tavares, "Decolorization of textile industry wastewater in solid state fermentation with Peach-Palm (Bactris gasipaes) residue," *Brazilian Journal of Biology*, Vol.78(4), 718-727, 2018.

[35]. G. Torgut, M. Tanyol, F. Biryan, G. Pihtili, and K. Demirelli, "Application of response surface methodology for optimization of Remazol Brilliant Blue R removal onto a novel polymeric adsorbent," *Journal of the Taiwan Institute of Chemical Engineers*, Vol. 80, 406-414, 2017.

[36]. C. Hua, N. Hub, X. Lia, H. Shena, H. and Y. Zhaoc, "Adsorption of remazol brilliant blue R by carboxylated multi-walled carbon nanotubes," *Desalination and Water Treatment*, Vol. 62, 282-289, 2017.

[37]. V. Yonten, M. Tanyol, N. Yildirim, N. C. Yildirim, and M. Ince, "Optimization of Remazol Brilliant Blue R dye removal by novel biosorbent P. eryngii immobilized on Amberlite XAD-4 using response surface methodology," *Desalination and Water Treatment*, Vol. 57(33), 15592-15602, 2016.

[38]. N. A. Rahmat, A. A. Ali, N. Hussain, M. S. Muhamad, R. A. Kristanti, and T. Hadibarata, "Removal of Remazol Brilliant Blue R from aqueous solution by adsorption using pineapple leaf powder and lime peel powder," *Water, Air, & Soil Pollution*, Vol. 227(4), 104-114, 2016.

[39]. Z. M. Lazim, E. Mazuin, T. Hadibarata, and Z. Yusop, "The removal of methylene blue and Remazol Brilliant Blue R dyes by using orange peel and spent tea leaves," *Journal Teknologi*, Vol. 74, 129-135, 2015.

Environmental Research & Technology, Vol. 1(4), pp. 47-51, 2018

Environmental Research & Technology

http://dergipark.gov.tr/ert

CONFERENCE PAPER

Pyrolysis of walnut shell biomass in fluidized bed reactor: Determination of optimum conditions for bio-char production

Zeynep Yildiz[1,*] Selim Ceylan[1]

[1] 19 Mayıs University, Chemical Engineering Department, 55210 Kurupelit, Samsun, TURKIYE

ABSTRACT

The pyrolysis of the walnut shell was carried out in a lab-scale continuous fluidized bed reactor at a temperature range of 400 to 600 °C. Thermogravimetric analysis technique was used to determine the thermal properties of the walnut shell. The bio-char product obtained from pyrolysis was analyzed to evaluate the effect of the pyrolysis temperature. Increasing the pyrolysis temperature to 600 °C improved the High Heating Value (HHV) and % C value of the bio-char product. These results showed that the optimum temperature value for bio-char production from walnut shell was 600 °C.

Keywords: Biomass, bio-char, fluidized bed reactor, walnut shell, pyrolysis

1. INTRODUCTION

Unlike fossil fuels such as coal, oil and natural gas, biomass samples are clean, abundant, cost-effective, CO_2-free, low-sulfur and environmentally friendly substances used for fuel production. Biomass is a sustainable resource with a faster life cycle than fossil fuels. Biomass energy is one of the fourth largest potential energy sources in the world and is considered as the energy carrier of the biomass future. At the same time, biomass accounts for more than 10% of the world's global energy demand [1, 2].

The walnut shell is an agricultural biomass waste and is that forms the shell of the walnut tree fruit. According to the TURSTAT reports, walnut production in Turkey in 2017 is approximately 210.000 tons. Walnut is an industrial agricultural product has many different application areas from confectionery to the food industry. The ratio of the inner walnut to the total walnut knee is approximately 50% (by weight). Accordingly, the approximate amount of shell is about 105 thousand tons. Although the walnut shell is a valuable waste, it is not yet widely used and is directly burned inefficiently. Therefore, it is an important issue to convert the walnut shell into products with valuable commercial potential [13, 14].

Biomass sources are evaluated in energy technology by applying various conversion processes (combustion, gasification, pyrolysis etc.) and increasing the quality of the fuel to obtain alternative biofuels (easily transportable, storable and usable fuels) [2]. One of the transformation processes applied to biomass species is pyrolysis and pyrolysis is decomposition of substances in an inert environment. Especially with biomass pyrolysis technology (bio-oil) solid (bio-char or bio-adsorbent) gas (bio-gas) liquid products are obtained [3]. The characteristics of the gas, liquid and solid products obtained from pyrolysis depend on the pyrolysis method and working conditions. Characteristics of bio-char products in pyrolysis process the duration of the reactor and temperature. One of the most important factors affecting pyrolysis is temperature. Increasing the pyrolysis temperature changes the solid product properties as it causes the thermal decomposition of hydrocarbon materials in the biomass structure. For example; long-time and low-temperature pyrolysis can achieve maximum bio-char product yield. Although there are many literature studies on the effect of pyrolysis temperature on bio-char yield, it is not easy to find suitable temperature for bio-char production. Because the optimized temperature for high bio-char production varies

Corresponding Author: zeynepyildiz.omu@gmail.com (Zeynep Yildiz)
Received 30 June 2018; Received in revised form 3 November 2018; Accepted 5 November 2018
Available Online 07 November 2018
Doi: ISSN: 2636-8498

This paper has been presented at EurAsia Waste Management Symposium 2018, Istanbul, Turkey

depending on the biomass composition and the product [3,4]. In fluid bed reactors, the effect of temperature on the bio-char product can be examined and optimum pyrolysis conditions can be improved. Such reactors are widely used in laboratory studies to describe the effect of temperature on pyrolysis behavior [5].

The aim of this study is to transform waste walnut waste in abundant quantities into solid product with fuel potential in the fluidized bed reactor by pyrolysis method which is one of the thermochemical conversion methods. The effect of temperature on the properties of the solid product obtained from the fluidized bed reactor through pyrolysis was investigated and the optimum temperature for the pyrolysis process was determined in this study. Thermal decomposition behaviors of raw walnut shell wastes were investigated using thermogravimetric analysis technique. Characterization of the bio-char product to be obtained after raw walnut shell and pyrolysis was carried by proximate analysis (Moisture, Volatile matter, Ash analysis), ultimate analysis (% C, H, N, S and O analysis) and FTIR analysis. The bio-char products obtained at different temperatures is compared and evaluated according to the fuel potential ultimate analysis and the thermal value results.

2. MATERIALS AND METHODS

2.1. Raw Samples

The raw walnut shell samples were collected from Samsun city of Turkey. The samples were rinsed with deionized water to remove surface dirt, dried in a 70 °C oven overnight, crushed, and sieved to a particle size of 63–125 μm. Functional groups of walnut shell were determined by FTIR (Fourier Transform Infrared Spectrometer) analysis techniques. Ultimate analysis (%C, H, N, and S) was performed with a CHNS-932 LECO brand analyzer while the proximate analysis (ash, volatile matter) of raw walnut shell and bio-char samples was performed in a protherm brand oven.

2.2. Thermogravimetric Analysis

Thermogravimetric analysis (TGA) was carried out using Simultaneous Differential Thermogravimetric Analyzer (DTA) equipped with a heat-flux type DTA and a TGA (Shimadzu, DTG-60, Japan; with a precision of temperature measurement ±0.1 K, DTA sensitivity ±0.1 μV and microbalance sensitivity ±0.1 μg) at heating rates of 20 °C min^{-1} under a nitrogen atmosphere with a flow rate of 80 mL min^{-1} with samples of approximately 10 mg.

2.3. Fluidized Bed Reactor

Experiments in the laboratory were carried out using a fluid bed test system and a specially designed heat-resistant reactor. For pyrolysis experiments, a total of 10 g of walnut shells were added to the sample chamber. The amount of sand used was determined to be 20 g and the nitrogen flow rate to be 300 mL min^{-1}. The pyrolysis experiments of the walnut shells were carried out for a reaction time of 60 minutes at 400, 450, 500, 550 and 600 °C (heating rate:10 °C min^{-1}). The temperature in the furnace was checked with the thermal couple in the reactor.

3. RESULTS AND DISCUSSION

3.1. Characterization of Walnut Shell

The proximate analysis, calorific values and ultimate analysis of the walnut shell are shown in Table 1 taken after drying the samples at 70 °C overnight. As seen from Table 1, walnut shell has about 74% and 5% volatile and ash content respectively. Volatile matter and ash contents of different biomass samples vary between 47.8-87.40 and 0.1-37.80, respectively [6]. According to these results, walnut shells have low ash content and high volatile content. The S and N values of the walnut shell are 1.851 and 1.117, respectively. It is important that N and S values are low because they cause environmental problems and reactor corrosion. The higher heating value of many biomass samples given in the literature is between 15-17 MJ kg^{-1} [7, 3]. The higher heating value of the walnut shell was found to be 16.68 MJ kg^{-1}. This calculated thermal value can be considered high when compared with the literature results [8, 9].

Table 1. Main characteristic properties of walnut shell

Characteristics	Raw Walnut Shell
Lignin (%) [9]	48.11
Hemicellulose (%) [9]	22.18
Cellulose (%) [9]	23.95
Proximate analysis	
Moisture (%)	5.43
Volatile matter (%)	74.00
Ash (%)	5.00
Fixed carbona (%)	15.57
Ultimate analysis	
C (%)	45.321
H (%)	5.538
N (%)	1.117
S (%)	1.851
Oa (%)	46.173
Higher Heating Value (MJ kg^{-1})	16.68

The FTIR spectrum of raw Walnut shell is shown in Fig 1. The large peak at 3391 cm^{-1} can be attributed to the stretching of primarily O-H groups. The symmetric and asymmetric stretching vibration associated with the peaks at 2985-2920 cm^{-1} of C single bond H are alkyl and aliphatic chains. The stretch of C=O in FTIR spectrum of raw walnut shell is 1623 cm^{-1}. C=O group is mainly from the acids,

aldehydes and ketones. The 1426 cm^{-1} and 1367 cm^{-1} C-H bending bands correspond to alkyl and aliphatic bending modes. The stretching associated with the peak at 1245 cm^{-1} of walnut shell material is likely indicative of C-O stretching vibration in organic acids, ketones, ethers and alcohols groups. The absorbance peak at 1043 cm^{-1} is likely to be C-O-H deformation in secondary and primary alcohols or aliphatic ethers and, lipids [6, 11].

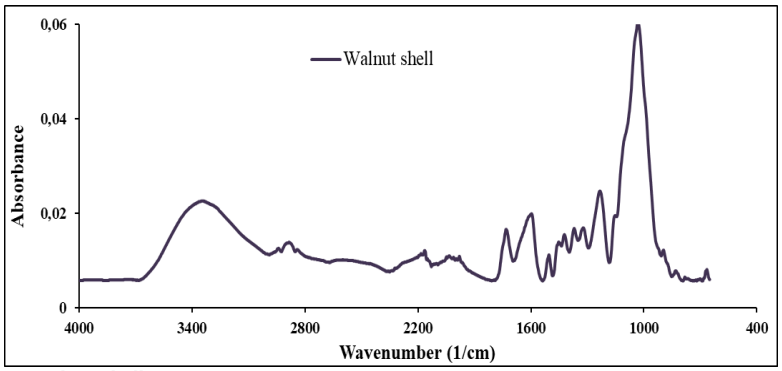

Fig 1. FT-IR spectra of raw walnut shell

3.2. Thermogravimetric Analysis

The curves of thermogravimetric analysis (TG) and differential thermogravimetric analysis (DTG) of walnut shell biomass with a heating rate of 20 °C min^{-1} are given in Fig 2.

According to the DTG curve of the walnut shell, the mass loss range can be divided into four stages due to the variable slope curves. In the first step, the decomposition of walnut shell starts at 30 °C and ends at about 110 °C. This may be due to the moisture in the structure of the walnut shell. As walnut shell biomass, all lignocellulosic materials consist of hemicellulose, cellulose and lignin. As can be seen in the DTG curve, the first decomposition starts at 199 °C and ends at 243 °C and this step indicates decomposition of hemicellulose. In the second step, the decomposition of walnut shell is between 256-311 °C, indicating that the cellulose is decomposed. The final decomposition is between 306-424 °C and the lignin component is removed from the construct. These results are consistent with the literature [10].

3.3. Characterization of Bio-char

The FT-IR analysis results of the bio-char samples obtained at different temperatures of the fluidized bed reactor are shown in Fig 3.

Aliphatic hydrocarbons belonging to alkanes in all spectra were detected at 2960-2870 cm^{-1}. It was observed that these peaks did not change as the temperature increased. The peaks at 1630 cm^{-1} were determined as C=O stretching of aldehyde, ketone and carboxylic acid compounds. These bands showed high intensity as they went out to high temperatures in the samples. The peaks seen between 2100 and 1900 cm^{-1} can be said to be Si-H stretching. These peaks showed a relatively constant density; which can be attributed to the ash content of the small sand particles that come with the char [11].

The results of the elemental analysis and the HHV value of the bio-char obtained in the fluidized bed reactor are listed in Table 2. As can be seen from the results, increasing the pyrolysis temperature increased the carbon content and reduced the oxygen value up to 600 °C. The HHV value of bio-char is the maximum value at 600 °C.

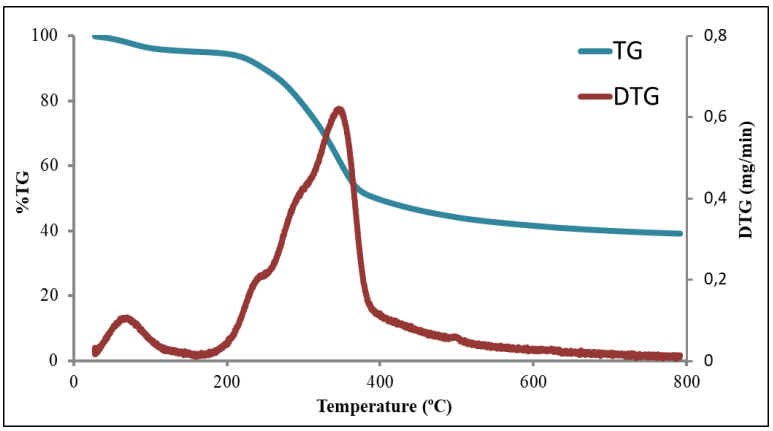

Fig 2. TG-DTG curves of walnut shell

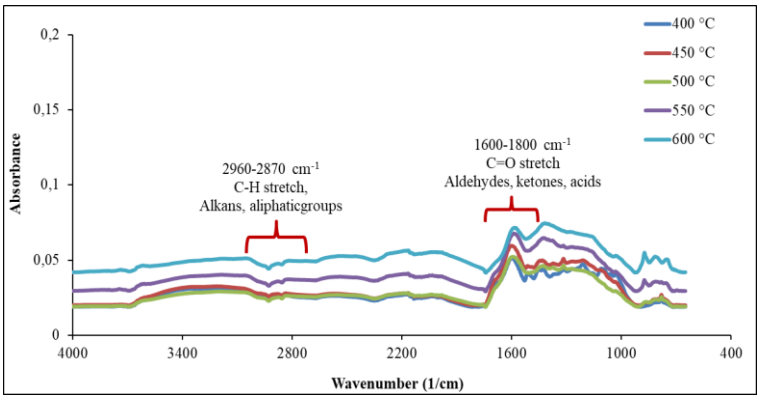

Fig 3. FT-IR spectra of bio-char samples

Table 2. Ultimate analysis of char products

Temperature (°C)	400 °C	450 °C	500 °C	550 °C	600 °C
Ultimate analysis (% wt.)					
C	57,42	59,16	62,95	64,39	73,71
H	3,95	4,42	3,63	3,09	3,02
N	1,29	1,29	1,48	1,31	1,26
S	1,86	1,85	1,98	1,93	2,03
O[a]	35,90	33,28	29,96	29,28	19,98
Higher heating value (HHV) (MJ kg^{-1}) [12]	18,65	20,38	21,13	20,96	25,68

4. CONCLUSIONS

Pyrolysis of the walnut shell biomass was carried out in the fluidized bed reactor at temperatures between 400 and 600 °C. The optimum temperature value was evaluated according to bio-char's elemental analysis and higher heating value (HHV) results. The high temperature increased the percent carbon and HHV of bio-char. With the increase in fuel properties of bio-char, the optimum temperature was determined as 600 °C.

REFERENCES

[1]. M.S. Masnadi, R. Habibi, J. Kopyscinski, J.M. Hill, X. Bi, C.J. Lim, N. Ellis and J.R Grace, "Fuel characterization and co-pyrolysis kinetics of biomass and fossil fuels," *Fuel*, Vol. 117, pp. 1204–1214, 2014.

[2]. H. Ly Vu, S.S. Kim, H.C. Woo, J.H. Choi, D.J. Suh and J. Kim, "Fast pyrolysis of macroalga Saccharina japonica in a bubbling fluidized bed reactor for bio-oil production," *Energy*, Vol. 93, pp. 1436-1446, 2015.

[3]. M. Tripathi, J.N. Sahu and P. Ganesan "Effect of process parameters on production of biochar from biomass waste through pyrolysis: A review," *Renewable and Sustainable Energy Reviews*, Vol. 55, pp. 467–481, 2016.

[4]. Y.J. Zhang, Z.J. Xing, Z.K. Duan, M. Li and Y. Wang, "Effects of steam activation on the pore structure and surface chemistry of activated carbon derived from bamboo waste," *Applied Surface Science*, Vol. 315, pp. 279–286, 2014.

[5]. D. Czajczynska, L. Anguilano, H. Ghazal, R. Krzyzynska, A.J. Reynolds, N. Spencer and H. Jouhara, "Potential of pyrolysis processes in the waste management sector", *Thermal Science and Engineering Progress*, Vol. 3, pp. 171–197, 2017.

[6]. N. Soyler, J. L. Goldfarb, S. Ceylan and M. T. Saçan, "Renewable fuels from pyrolysis of Dunaliella tertiolecta: An alternative approach to biochemical conversions of microalgae," *Energy*, Vol. 120, pp. 907-914, 2016.

[7]. M.A. Mehmood, G. Ye, H. Luo, C. Liu, S. Malik, I. Afzal, J. Xu and M. S. Ahmad, "Pyrolysis and kinetic analyses of Camel grass (Cymbopogon schoenanthus) for bioenergy," *Bioresorce Technology*, Vol. 228, pp. 18–24, 2017.

[8]. H. Karatas and F. Akgun, "Experimental results of gasification of walnut shell and pistachio shell in a bubbling fluidized bed gasifier under air and steam atmospheres," *Fuel*, Vol. 214, pp. 285–292, 2018.

[9]. B.B. Uzun and E. Yaman, "Pyrolysis kinetics of walnut shell and waste polyolefins using thermogravimetric analysis," *Journal of the Energy Institute*, Vol. 90, pp. 825-837, 2017.

[10]. S. Abhishek, P. Vishnu and Z. Dongke, "Biomass pyrolysis—A review of modelling, process parameters and catalytic studies," *Renewable and Sustainable Energy Reviews*, Vol. 50, pp. 1081–1096, 2015.

[11]. X. Yuan, Z. Shuai, B. Robert, C.K. Atul and B. Xianglan, "Fast pyrolysis of biomass and waste plastic in a fluidized bed reactor," *Fuel*, Vol. 156, pp. 40-46, 2015.

[12]. W. Hideo, L. Dalin, N. Yoshina, T. Keiichi, K. Kunimitsu and M.W. Makoto, "Characterization of oil-extracted residue biomass of Botryococcus braunii as a biofuel feedstock and its pyrolytic behavior," *Applied Energy*, Vol. 132, pp. 475-484, 2014.

[13]. K. Açıkalın and F. Karaca, "Fixed-bed pyrolysis of walnut shell: Parameter effects on yields and characterization of products," *Journal of Analytical and Applied Pyrolysis*, Vol. 125, pp. 234-242, 2017.

[14]. Available: http://www.tuik.gov.tr/ 2018.